

# Clemens Müller

# Reactive Crystallization of Terephthalic Acid towards Recycling of Poly(ethylene terephthalate)



# Bibliographical information held by the German National Library

The German National Library has listed this book in the Deutsche Nationalbibliografie (German national bibliography); detailed bibliographic information is available online at http://dnb.dnb.de.

1st edition - Göttingen: Cuvillier, 2025 authorised dissertation, Fakultät für Maschinenbau, Technische Universität Braunschweig, 2025

This publication was supported by funds from the Publication Fund NiedersachsenOPEN, funded by zukunft.niedersachsen.This work is licensed under the Creative Commons Attribution 4.0 International Licence (CC BY 4.0). https://creativecommons.org/licenses/by/4.0/

You are free to redistribute and adapt the material, even for commercial purposes, as long as the appropriate attribution is given. You must also provide a link to the licence and indicate when changes have been made. All rights to content not covered by this licence are reserved.

CUVILLIER VERLAG, Göttingen, Germany 2025 Nonnenstieg 8, 37075 Göttingen, Germany Telephone: +49 (0)551-54724-0

Telefax: +49 (0)551-54724-21

www.cuvillier.de

1st edition, 2025

This publication is printed on acid-free paper.

ISBN 978-3-68952-672-6 eISBN 978-3-68952-673-3 ORCID 0000-0002-7607-2006 DOI 10.61061/ISBN\_978-3-68952-672-6

# Reactive Crystallization of Terephthalic Acid towards Recycling of Poly(ethylene terephthalate)

Von der Fakultät für Maschinenbau der Technischen Universität Braunschweig

zur Erlangung der Würde eines Doktor-Ingenieurs (Dr.-Ing.)

genehmigte Dissertation

von: Clemens Müller geboren in: Rostock

eingereicht am: 05.03.2024 mündliche Prüfung am: 15.07.2024

Vorsitz: Prof. Dr.-Ing. Jürgen Köhler Gutachter: Prof. Dr.-Ing. Stephan Scholl Gutachter: Prof. Dr.-Ing. Matthias Kind

[...] Es handelt sich darum, alles zu leben. Wenn man die Fragen lebt, lebt man vielleicht allmählich, ohne es zu merken, eines fremden Tages in die Antworten hinein.

(Rainer Maria Rilke, 1904)

## Vorwort

Diese Arbeit entstand während meiner Zeit als wissenschaftlicher Mitarbeiter am Institut für Chemische und Thermische Verfahrenstechnik der Technischen Universität Braunschweig. An dieser Stelle möchte ich insbesondere meinem Doktorvater Herrn Prof. Dr.-Ing Stephan Scholl meinen Dank aussprechen. Ich bin dankbar für das entgegengebrachte Vertrauen, die Möglichkeit diese Arbeit zur verfassen und die wertvollen Ratschläge, die meinen wissenschaftlichen Weg geprägt haben. Zudem möchte ich mich bei Herrn Prof. Dr.-Ing. Matthias Kind für das Interesse an meinem Promotionsthema und die Erstellung des Zweitgutachtens bedanken. Darüber hinaus danke ich Herrn Prof. Dr.-Ing. Jürgen Köhler für die Übernahme des Prüfungsvorsitzes.

Des Weiteren gilt mein Dank meinen Kollegen und Kolleginnen, den Studierenden sowie allen weiteren Mitarbeitern und Mitarbeiterinnen des Instituts und der RITTEC 8.0 Umwelttechnik GmbH, welche maßgeblich zu dieser Arbeit beigetragen haben. Ihre Unterstützung, der fachliche Austausch und die kollegiale Atmosphäre haben meine Forschung und meinen Arbeitsalltag bereichert. Eine besondere Erwähnung verdienen Esther, Lars und Carsten, für ihr gemeinsames Engagement und die Zusammenarbeit am Forschungsprojekt revolPET® und den nachfolgenden Projekten.

Zudem möchte ich mich bei Nicolás und Mandy für das Korrekturlesen meiner Dissertation bedanken sowie bei meinem Hiwi Luca für die langjährige Unterstützung. Die finanziellen Mittel zur Durchführung dieser Arbeit wurden dankenswerterweise von den Bundesministerien für Bildung und Forschung (BMBF) sowie für Wirtschaft und Klimaschutz (BMWK) bereitgestellt.

Zu guter Letzt möchte, meiner Familie und meiner Verlobten Hannah, meinen besonderen Dank aussprechen. Ihr habt es mir ermöglicht zu studieren, an mich geglaubt, mich ermutigt und mir Zuspruch gegeben und so maßgeblich zum Gelingen dieser Arbeit beigetragen.

Braunschweig im März, 2024

# Kurzfassung

Die vorliegende Arbeit behandelt Untersuchungen der reaktiven Kristallisation von Terephthalsäure (TA) im Rahmen des Back-tot-Monomer-Recyclings, welches eine Möglichkeit zur Überwindung der derzeitigen Limitierungen des thermomechanischen Polyethylenterephthalat- (PET) Recyclings darstellt. Ein Ansatz ist dabei die alkalische Hydrolyse, bei welcher PET mit Natriumhydroxid selektiv in die Monomere Ethylenglykol und Dinatriumterephthalat depolymerisiert wird. Anschließend wird die TA durch Säurezugabe aus ihrem Dinatriumsalz gefällt und so zurückgewonnen.

Zur Optimierung der Fällung als Gewinnungsschritt, wurden verschiedene Betriebsparameter hinsichtlich ihres Effekts auf Kristallgröße, Filtrierbarkeit und Reinheit der TA analysiert. Dazu wurde zunächst ein Parameterscreening mit Modelllösung im Batchbetrieb durchgeführt. Hierbei führten insbesondere erhöhte Temperaturen und Essigsäureeinsatz zu größeren Kristallen und verbesserter Filtrierbarkeit. Trotz ihrer geringeren Protonierungskapazität wurde auch mit Essigsäure eine signifikante Ausbeute an TA erreicht. Anschließend wurden die Untersuchungen auf depolymerisiertes PET verschiedener Abfallfraktionen und das Aufreinigungspotential der Fällung ausgeweitet. Neben einer Verringerung der Verfärbung bei höherer Temperatur wurde auch der Isophthalsäuregehalt in TA Kristallen reduziert, was sich insbesondere bei Verwendung von Essigsäure zeigte. Dies ist insbesondere relevant, da Isophthalsäure einen entscheidenden Einfluss auf die Polymereigenschaften hat. Im letzten Teil der Arbeit wurden die Untersuchungen in einen kontinuierlichen Rührkessel überführt. Während der Fällung mit Schwefelsäure konnte so ein Wachstum der TA-Kristalle einhergehend mit einer verbesserten Filtrierbarkeit erreicht werden. Darüber hinaus induzierte eine Erhöhung des pH-Werts eine signifikante Reduktion des Isophthalsäuregehalts. Schließlich wurde ein Verfahrenskonzept für einen optimierten Fällungsschritt für TA, hinsichtlich Reinheit und Rückgewinnung abgeleitet, unter Beachtung der Notwendigkeit eines nachfolgenden Umkristallisationsschritts.

## Abstract

The present work deals with investigations of the reactive crystallisation of terephthalic acid (TA) in the context of back-to-monomer recycling, which represents a possibility for overcoming the current limitations of thermomechanical polyethylene terephthalate (PET) recycling. One approach is alkaline hydrolysis, in which PET is selectively depolymerised with sodium hydroxide into the monomers ethylene glycol and disodium terephthalate. The TA is then precipitated from its disodium salt by addition of a precipitation acid and thus recovered.

To optimize precipitation as a recovery step, various operating parameters were analysed with regard to their effect on crystal size, filterability and purity of the TA. For this purpose, a parameter screening was first carried out with model solution in batch operation. In particular, increased temperatures and the use of acetic acid led to larger crystals and improved filterability. Despite its lower protonation capacity, a significant yield of TA was also achieved with acetic acid. Subsequently, the investigations were extended to depolymerised PET of different waste fractions and the purification potential of the precipitation. In addition to a reduction in discolouration at higher temperatures, the isophthalic acid content in TA crystals was also reduced, which was particularly evident when acetic acid was used. This is particularly relevant as isophthalic acid has a decisive influence on the polymer properties. In the final part of the work, the investigations were transferred to a continuously stirred tank reactor. This induced a substantial growth of TA crystals during precipitation with sulfuric acid and improved filterability. Moreover, an increase of pH during continuous precipitation with sulfuric acid significantly reduced isophthalic acid content in TA. Finally, a conceptual procedure for an optimized precipitation step for TA regarding purification and recovery was derived, while considering the necessity for a subsequent recrystallization step.

# List of Symbols

# Latin Symbols

,	10015
A	Surface / m <sup>2</sup>
$a_{\rm i}$	Thermodynamic activity
$\mathrm{B_{i}}$	Nucleation rate / m <sup>-3</sup> ·s <sup>-1</sup>
$\mathbf{c}_{\mathrm{i}}$	Molarity / mol·L <sup>-1</sup>
G	Growth rate constant / m·s <sup>-1</sup>
ic	Number of monomers within a cluster
$k_{\rm B}$	Boltzmann constant ( $\sim$ 1.381 × 10 <sup>-23</sup> J K <sup>-1</sup> )
$\mathbf{k}_{d}$	Mass transfer coefficient / m·s <sup>-1</sup>
$K_{i}$	Dissociation/equilibrium constant/ partition coefficient
$K_{sp}$	Solubility product
$L_{\rm i}$	Size / m
$m_{\rm i}$	Mass / g
$m_{\rm i}$	Molality / mol·kg <sup>-1</sup>
$n_{\rm i}$	Molar amount / mol; number concentration / $m^{-3}$
$pK_a$	Decadic logarithm of strength of an acid
Q <sub>3</sub>	Volumetric cumulative distribution
$q_3^*$	Logarithmic volume related density distribution
R	Ideal Gas constant (~8.314 J·K <sup>-1</sup> ·mol <sup>-1</sup> )
$Re_{i}$	Impeller Reynolds number
$S_{\rm i}$	Supersaturation
T	Temperature / K
$t_{i}$	Time / s
$u_{tip}$	Circumferential velocity / m·s <sup>-1</sup>
V	Volume / m³
$\mathbf{x}_{\mathbf{i}}$	Particle diameter equivalent / µm
$Y_{i}$	Yield

# **Greek Symbols**

Volumetric shape factor, ion species fraction
Surface shape factor
Chemical potential / J·mol <sup>-1</sup>
Interfacial tension crystal/liquid / N·m <sup>-2</sup>
Activity coefficient
Gibbs free energy / J·mol <sup>-1</sup>
Contact angle / °
Stoichiometric factor
Density / kg·m <sup>-3</sup>
Residence time

# Indices

crit	critical
a	activity based
c	concentration based, crystal, cluster
aq	aqueous
hom	homogeneous
S	solid
V	volume
std	standard
exp.	experimental
*	saturated
conti	continuous
Depoly	depolymerization

# Abbreviations

lobreviations	
4-CBA	4-Carboxybenzaldehyde
AR	Acid radical
BCF	Burton-Cabrera-Frank
BHET	Bis(2-hydroxyethyl) terephthalate
BMR	Back-to-monomer recycling
CNT	Classical nucleation theory
COD	Chemical oxygen demand
DMAc	N, N-Dimethylacetamide
DMF	Dimethyl formamide
DMSO	Dimethyl sulfoxide
DMT	Dimethyl terephthalate
DST	Disodium terephthalate
EG	Ethylene glycol
HPLC	High Performance Liquid Chromatography
IA	Isophthalic acid
IAS	Intentionally added substances
IV	Intrinsic viscosity
LCA	Life cycle assessment
MSMPR	Mixed suspension- Mixed product removal
NIAS	Non-intentionally added substances
PA	Precipitation acid
PE	Polyethylene
PET	Poly(ethylene terephthalate)
pН	pondus Hydrogenii (latin)
POM	Bottles placed on market
PP	Polypropylene
PSD	Particle Size Distribution
PTA	purified Terephthalic Acid
PX	p-Xylene

rPET	recycled Poly(ethylene terephthalate)
rpm	Revolutions Per Minute
rTA	recycled Terephthalic acid
SCR	Super clean recycling
SEM	Scanning electron microscopy
SSP	Solid state polycondensation
TA	Terephthalic acid
vPET	virgin Poly(ethylene terephthalate)

# Content

V	orwort		
K	urzfassung	Ţ	II
A	bstract		V
L	ist of Syml	bols	V
C			
1	Introdu	action	1
	1.1	Problem Formulation	1
	1.2	Scope and Approach	2
2	Crysta	llization Fundamentals	4
	2.1	Supersaturation	4
	2.2	Nucleation	<i>6</i>
	2.3	Growth	10
	2.4	Reactive Crystallization	13
	2.5	Product Quality in Reactive Crystallization	15
	2.5.1	Crystal Size Distribution	15
	2.5.2	Purity	
3	State o	of the Art	19
	3.1	PET Synthesis and Recycling	21
	3.1.1	PET Polycondensation	21
	3.1.2	Thermomechanical PET Recycling	22
	3.1.3	Back-to-Monomer Recycling	25
	3.2	Terephthalic Acid	31
	3.2.1	Synthesis by p-Xylene Oxidation	31
	3.2.2	Polymorphism and Morphology	32
	3.2.3	Precipitation from Alkaline Solution	35
	3.2.4	Solubility	39
	3.2.5	Impurities and Purification in BMR	41
	3.2.6	Alternative Precipitation Acids Potential	47
	3.2.7	Influence of pH on Speciation and Supersaturation	48
	3.3	Systematic Approach of this Work	51
4	Experi	mental	53
	4.1	Equipment and Procedures	53

	4.1.1	Description of Laboratory Setup	53
	4.1.2	Batch Precipitation Procedure	54
	4.1.3	Continuous Precipitation Procedure	55
	4.1.4	Experimental Scope	58
	4.2	Materials	61
	4.2.1	Reactants for Precipitation Experiments	61
	4.2.2	Analytical	62
	4.2.3	Dosage Quantity of Precipitation Acids	63
	4.2.4	PET Reactants	64
	4.3	Analysis	65
	4.3.1	Particle Size Measurement	65
	4.3.2	Filterability	65
	4.3.3	Morphology	67
	4.3.4	Concentration Measurement	
	4.3.5	Hazen Colour Index	68
	4.3.6	Isophthalic Acid Content	68
5	Batch	Precipitation of Terephthalic Acid	69
	5.1	Screening of Optimal Parameters in Model System	69
	5.1.1	Effect of Temperature and Precipitation Acid	70
	5.1.2	Reactant Dispersion	
	5.1.3	Extended Screening of Alternative Precipitation Acids	79
	5.2	Application to PET Reactants	85
	5.2.1	Purification Potential	85
	5.2.2	Validation of Temperature and Precipitation Acid Influen	ce90
6	Transf	er to Continuous Operation	94
	6.1	Precipitation Acids Comparison	94
	6.2	Variation of Throughput	101
	6.3	Reactant Concentration and Dispersion	105
	6.4	Start-up and pH Effect	
	6.4.1	Variation of Start-up	111
	6.4.2	pH Variation	
	6.5	Precipitation Concept	118

7 Conclu	usion and Outlook	126
7.1	Conclusion	126
7.2	Outlook	129
References.		131
8 Appen	ndix	145
8.1	Appendix A – General	145
8.2	Appendix B – Experimental	
8.3	Appendix C – Batch Operation	148
8.4	Appendix D – Continuous Operation	
8.4.1	Start-up	154
8.4.2	pH Variation	
8.4.3	Precipitation Concept	158
	Vitae	
	ications	
Student con	tributions	162

## 1 Introduction

#### 1.1 Problem Formulation

Polyethylene terephthalate (PET) stands out as a showcase for recycling within the realm of plastics, notably with its widely recognized PET bottle recycling initiatives. As of 2020, approximately 97% of all PET usage, excluding PET fibres, was allocated to the packaging sector in Europe. Within this market, bottles accounted for 70% while trays comprised 20%. Despite the sizable volume of 4.6 million tonnes of rigid PET packaging, only 49% was collected and sorted for recycling in 2020. However, despite these encouraging collection figures, the actual recycled content in PET bottles reached only 17% by the same year. Simultaneously, there has been a growing demand from both industries and consumers for high-quality recycled PET (rPET). Additionally, out of the total PET recycling input, only 54% exits recycling facilities as rPET suitable for high-viscosity applications, and a mere 27% of this is approved for food contact.

To increase these rates, the European Parliament has passed its directive on single use plastics, which among other things, obliges manufacturers to use at least 25 % of rPET in new bottles.<sup>3</sup>

In addition to enhancing collection and sorting methods to bolster the supply and quality of rPET, mechanical recycling faces significant challenges. Apart from dealing with contaminated input streams, the thermal and chemical degradation of PET polymer during reprocessing limits its mechanical recyclability. On one hand, the tensile strength of rPET diminishes with each cycle due to polymer chain scission. Conversely, the polymer's colour darkens and becomes more yellow with increasing recycled content. Furthermore, additives and the inclusion of foreign polymers can substantially alter its properties, thereby limiting its reusability. Consequently, new technologies for PET recycling are necessary to overcome these challenges and utilise yet unrecyclable PET waste as a valuable resource.

Back-to-monomer recycling (BMR) emerges as a promising approach under current investigation to restore the properties of virgin PET from previously unrecyclable PET feedstocks such as brittle bottles, multi-layered trays, or even synthetic polyester fibres. While various reaction pathways like alcoholysis, aminolysis, or hydrolysis are being explored, these technologies share a common goal of breaking down PET into its fundamental monomeric building blocks. This targeted depolymerization process liberates contaminants, colorants, and other by-products that can subsequently be treated and removed.<sup>9</sup>

Among these, the approaches using hydrolysis are of special interest as they

produce terephthalic acid (TA) and ethylene glycol (EG), the reactants for direct esterification to PET. <sup>10,11</sup> Since TA is practically insoluble in water, it remains as solid after neutral and acidic hydrolysis making it practically impossible to be separated from the reaction residue. <sup>12</sup> While this can be overcome through mixing in alkaline solution leading to the respective alkali salt of TA, this step can be skipped by directly using alkaline hydrolysis. Biermann and Brepohl et al. depolymerized a PET dual layer in less than one minute and up 97 % yield by using sodium hydroxide. <sup>13,14</sup> The EG and TA precursor disodium terephthalate (DST) were dissolved in water and underwent filtration for solids removal.

However, regardless of the depolymerization pathway, the consecutive recovery of TA from DST demands sodium replacement, which is commonly conducted through acidification using strong acids, like sulfuric or hydrochloric acid. 12,13,15,16 Due to the nature of chemical reactions between liquids leading to a sparely soluble crystalline product like TA, the reaction induces high supersaturations. Thus, more TA is present in the liquid phase than possible in thermodynamic equilibrium. In order to restore equilibrium, TA instantly precipitates as fine crystals. These crystals complicate downstream processing and differ substantially from the industrial standard purified TA (PTA). In order to successfully recover and reuse terephthalic acid, its properties regarding its reapplication as one monomer for PET polycondensation must meet industrial specifications to close the loop using BMR. 17

# 1.2 Scope and Approach

Despite the significant potential of the depolymerization pathway, the TA crystallization from DST solution is still not fully developed. To date, only a limited number of studies have been dedicated on investigating this step. Among these, Lee et al. follow a one-step approach by using an organic solvent mixture in batch precipitation leading to a final recycled TA (rTA) suitable for repolymerization. Wu et al. precipitated rTA first and subsequently recrystallized the crude TA in an organic solvent by cooling crystallization. However, the rTA of these studies does still not possess PTA properties. Moreover, the use of organic solvents instead of water for PTA purification increases downstream efforts. Nevertheless, the separation of synthesis and final product purification and design is a sensible approach. 10,19

Hence, this thesis focuses exclusively on the first step: the advantageous and straightforward recovery of TA through precipitation. The understanding of this first step is of critical relevancy to exploit this technique in its full potential.

#### Introduction

Therefore, the present work aims for identification of process parameters to (e.g. temperature, precipitation acid type) which increase TA crystal size and improve filterability. Based on the demand for a process with a straightforward applicability in order to be industrially implemented, a standard stirred tank reactor setup is used throughout this work.

The investigation starts with screening in a model reactant system and progresses to depolymerized waste PET reactants containing impurities. Among PET impurities, particularly isophthalic acid (IA), a TA isomer, requires precise control over its integration into rTA crystals. Thus, alongside assessing decolourisation potential, process parameters are examined with regard to their efficiency in reducing IA content in rTA. Furthermore, with focus on operating costs, productivity and scale-up, a continuously operated precipitation step is developed, subsequently. Moreover, continuous operation can improve crystallization behaviour by reducing supersaturation and naturally providing crystal seeds.

Finally, a precipitation concept is proposed, emphasizing the benefits that can be achieved through TA precipitation, while recognizing the necessity for a subsequent recrystallization step.

In conclusion, this research work represents a significant advance for PET circularity, by providing practical and innovative approaches on improving TA purity, recovery and processability. Precipitated rTA could be used directly in polycondensation in mixtures with PTA. Regarding pure rTA application, this research can be a starting point for consecutive developments for rTA recrystallization. Alternatively, rTA can be used as feedstock for existing PTA purification plants, whose capacity utilisation will be reduced in circular PET economy.

The results shown are the product of publicly funded research work conducted in collaboration with RITTEC 8.0 Umwelttechnik GmbH. Thus, the research project revolPET was financially supported by the German Federal Ministry of Education and Research (Grant No. 033R193A-F) while the project reform-2-rePET was funded by the German Federal Ministry for Economic Affairs and Climate Action (Grant No.16KN082926.)

The following chapters introduce the fundamental relations of the determining factors and processes regarding crystallization. They aim to provide an overview about the driving force of crystallization and the effects leading to solid formation and subsequent growth. The information within is given on a descriptive level rather than calculative. A detailed insight including the mathematical aspects, model approaches and theories on crystallization fundamentals can be found in Mersmann, Mullin and Myerson.<sup>22–24</sup>

## 2.1 Supersaturation

Given a defined set of conditions (e.g. temperature, pressure), supersaturation describes the state of a solution containing a higher amount of solute than in thermodynamic equilibrium. The supersaturated solution regains its equilibrium state by formation of a solid phase. Therefore, supersaturation is the fundamental driving force and essentially necessary for crystallization. In strict terms, the supersaturation is a simplification aimed at addressing the difference in chemical potential  $\mu$  between the solute component in solution and its crystalline state, which is responsible in the formation of a new solid phase, as expressed in Equations 2-1 and 2-2.

$$\Delta \mu = \mu_{solution} - \mu_{crystal} = RT \cdot ln \left( \frac{a_{solution}}{a_{crystal}^*} \right)$$
 2-1

$$\frac{\Delta \mu}{RT} = ln\left(\frac{a_{i,solution}}{a_{i,crystal}^*}\right) = ln\left(S_a\right)$$
2-2

An exact expression of supersaturation requires the knowledge of the effective concentrations  $a_i$  (activities), which are not always known in industrial applications. Therefore, a simplified practical approximation of the dimensionless supersaturation ratio S is given by Equation 2-3 in terms of molarity (c) and molality (m).<sup>22</sup>

$$S_c = \frac{c}{c^*} \text{ or } S_m = \frac{m}{m^*}$$
 2-3

It presumes activity coefficients to be 1 (ideal) and differs substantially from activity-based supersaturation ratios. Regarding the dependencies (e.g. temperature) of the solubility limit, supersaturation can be induced by several ways e.g. by cooling, solvent removal or drowning out. These procedures share the mutuality of a reasonable solubility of the target solute in the liquid phase. Instead, concerning reactive crystallization or precipitation, supersaturation is induced by a chemical reaction, e.g.  $A_{(aq.)} + B_{(aq.)} \rightarrow C_{(s)}$ . Thus, the sparingly soluble target solute C is produced as soluble reactants A and B are contacted. For description of the supersaturation ratio for these systems an expression in dependence of the concentration solubility product  $K_{SP}$  (saturated state) is appropriate and shown in Equation 2-4.

$$S_{c} = \frac{c_{AB}}{c_{AB}^{*}} = \frac{\left(c_{A}^{\nu_{A}} \cdot c_{B}^{\nu_{B}}\right)^{\frac{1}{\nu_{A} + \nu_{B}}}}{K_{SP}} \text{ with } K_{SP} = \left(c_{A}^{\nu_{A}} \cdot c_{B}^{\nu_{B}}\right)^{*}$$
 2-4

However, as for the supersaturation ratio based on molarities and molalities, the use of concentrations instead of activities is limited to low concentrations for realistic approximations. The necessary activity coefficients can be approximated by thermodynamic models e.g. extensions of the Debye-Hückel equation like the Bromley equation<sup>25</sup> or UNIFAC models in addition to empirical approaches by Meissner.<sup>22,26</sup> For details on these activity coefficient approaches and their calculations it may be referred to Zemaitis et al. as well as Luckas and Krissmann.<sup>26,27</sup>

Nevertheless, the given Equation 2-4 describes the fact that a low solubility leads to high supersaturation values. Additionally, the velocity of the chemical reaction leads to a fast build-up of the supersaturation that cannot be depleted by molecular growth.<sup>28</sup> Instead a high number of small nuclei is formed in order to reduce supersaturation.<sup>29</sup> This phenomenon to so called homogeneous nucleation (see 2.2) leads to reactive crystallizations being complex and difficult to control.<sup>22,24</sup>

#### 2.2 Nucleation

The starting point for crystallization is the formation of solid nuclei representing the smallest arrangement of a number of molecules being able to exist. Prerequisite to this stochastic process is a system in non-equilibrated supersaturated condition which is the driving force for reduction of supersaturation by aggregation. This condition is described as metastable zone whose width depends on the respectively applying nucleation mechanisms.<sup>23</sup> The classification of the different nucleus formation mechanisms is displayed in Figure 2-1.

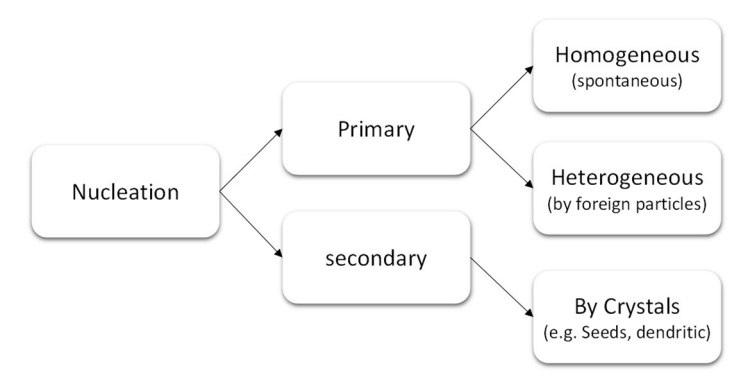


Figure 2-1 Basic mechanisms of nucleation, adapted from Mullin and Myerson. <sup>22,23</sup>

Spontaneous nucleation from particle free solution is referred to as homogeneous nucleation. If foreign matter (e.g. dust, foreign surfaces) is present in an otherwise crystal free solution, heterogeneous nucleation occurs. These two are grouped as primary nucleation mechanisms and require high supersaturations. Under the presence of crystals of the same kind suspended in solution, secondary nucleation comes into effect, requiring significantly lower supersaturations.

The origin of theories on homogeneous nucleation are early works on droplet nuclei forming from supersaturated gas,<sup>30</sup> which was extended in early works from Becker and Döring<sup>31</sup>, and Turnbull and Fisher <sup>32</sup> to derive in the classical nucleation theory (CNT). Despite ongoing research, until today experimental verification of theoretical predicted nucleation rates has not been achieved, due to the complex interplay of influencing factors and measurement limitations.<sup>33–35</sup> In the following the fundamental understanding behind the CNT will be presented. For extensive calculative approaches on the estimation of nucleation rates it may

be referred to the work of Mersmann and Mullin.<sup>22,24</sup> For an overview on non-classical nucleation theory it may be referred to Myerson.<sup>23</sup>

Starting point for this perspective is a metastable solution without foreign particles nor impurities. Prerequisite for a new phase to develop is the formation of an interface, requiring additional enthalpy in the system. This new interface appears as the result of single molecules spontaneously approximating and joining due to local density and concentration differences. Despite the reversibility of this event, at sufficiently high supersaturation the birth of these embryos surpasses their decay and eventually leads to the formation of larger units. The build-up of these clusters leads to an increase in interfacial tension  $\gamma_{CL}$  between crystal and surrounding liquid. In parallel, this cluster formation process releases free volume-enthalpy  $\Delta G_V$ .

Figure 2-2 displays the free surface and volume enthalpies and their sum, the total enthalpy  $\Delta G$  over the nucleus size, L, increase in free surface enthalpy  $\Delta G_A$ .

As the positive free surface enthalpy is proportional to the square of the nucleus

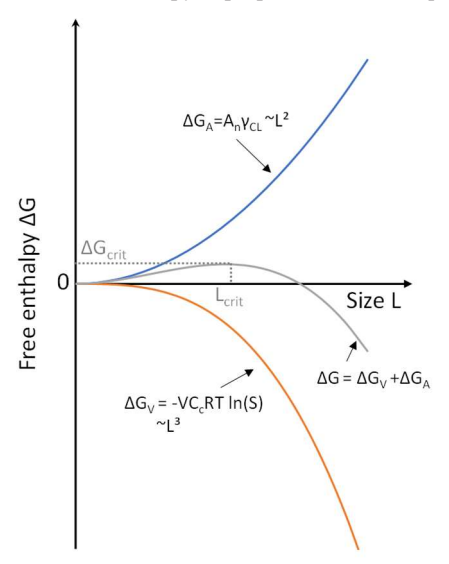


Figure 2-2 Free enthalpy over nucleus size L, adapted from Mersmann.<sup>24</sup>

size whereas the negative free volume enthalpy is proportional to nucleus size cubed, their sum features a maximum value  $\Delta G_{crit}$  at a critical size,  $L_{crit}$ . For a spherical particle this critical size can be calculated by Equation 2-5, with  $k_B$  as the Boltzmann constant and the temperature T. Nuclei being smaller than this critical size decompose while nuclei being larger can continue to grow.

$$L_{crit} = \frac{4 \cdot \gamma_{CL}}{k_R \cdot T \cdot \ln S}$$
 2-5

In the following, a CNT approach on calculation of the homogeneous nucleation rate  $B_{hom}$  is presented, as displayed in Equation 2-6. It is based on three fundamental factors which are shortly introduced subsequently.

$$B_{hom} = n_{crit} \cdot k \cdot Z$$
 2-6

The first factor is the number concentration of critical clusters  $n_{crit}$  which, assuming random collision of molecules can be described through a Boltzmann distribution, with  $n_0$  being the number concentration of monomers in supersaturated solution (Equation 2-7).

$$n_{crit} = n_0 \cdot e^{-\frac{\Delta G_{crit}}{k_B \cdot T}}$$
 2-7

The rate at which these clusters can cross the thermodynamically stable barrier is represented by the impact coefficient k which is displayed in equation 2-8, as derived by Mersmann and Kind.<sup>24,36</sup> It additionally depends on the surface area  $A_c$  of a cluster and the diffusion coefficient  $D_{AB}$ .

$$k = \frac{3}{4}n_0^{\frac{4}{3}} \cdot D_{AB} \cdot A_c$$
 2-8

At last, the Zeldovich factor Z is introduced in Equation 2-9 to account for the probability that a cluster reaching the critical diameter continues to grow. It represents the imbalance between equilibrium and steady state distribution as the clusters constantly cross the critical barrier.<sup>24</sup> Within this equation,  $i_c$  displays the number of monomers contained in a critical cluster.

$$Z = \sqrt{\frac{\Delta G_{\text{crit}}}{3 \cdot \pi \cdot k_B \cdot T \cdot i_c^2}}$$
 2-9

Generally, homogeneous nucleation is dominating at high supersaturations common for reactive crystallization and precipitation and displays a maximum

rate. However, under industrial conditions it is accompanied by heterogeneous and secondary nucleation.<sup>24</sup>

Nucleation under presence of foreign surfaces is described as primary heterogeneous nucleation. Their presence can reduce the activation barrier of nucleation which depends on the contact angle  $\Theta$  between the surface and the clusters prior to nucleation. <sup>23,24</sup> Therefore, with respect to the wetting behaviour three cases can be distinguished. If no wetting of liquid on the foreign surface occurs ( $\Theta = 180^{\circ}$ ), nucleation is not affected and can be regarded as homogeneous. A partial wetting ( $180^{\circ} > \Theta > 0^{\circ}$ ) reduces the surface excess energy and thus a lower overall free excess energy is required for nucleation compared to homogeneous nucleation. For the theoretical case of complete wetting ( $\Theta = 0^{\circ}$ ), the activation barrier for nucleation is reduced to an extent as if parent crystals were present in supersaturated solution. <sup>22,23,37</sup>

However, nucleation under the presence of crystals of the same species differs from the previously introduced primary nucleation and is referred to as <u>secondary nucleation</u>. The underlying mechanism is explained by several theories mainly aiming to describe the connection between nuclei and parent crystal. While theories on the effect of fluid shear exist as well, in the following only mechanisms based on dendritic crystals and contact nucleation will be introduced closer. High supersaturations as present in precipitation processes lead to the formation of needle and dendritical structures. Due to their mechanical instability, parts of these structures can break and the resulting fragments provide new surface for nucleation. On the contrary, in contact nucleation the physical impact between the crystal and a stirrer, reactor wall or other crystals results in surface damage. This surface defect provides a site for nucleation in addition to the lose fragments broken off the crystal.<sup>23</sup>

With regard to industrial applications and conditions (e.g. presence of dust, bubbles, rough surfaces) pure homogeneous nucleation displays a rare phenomenon and heterogeneous nucleation is more common.<sup>22</sup> Additionally, formation of crystals during crystallisation leads to their direct presence in a reactor inducing secondary nucleation. It displays the dominating nucleation mechanism in continuous or seeded crystallization processes, as it requires substantially lower supersaturations compared to primary nucleation.<sup>23</sup>

#### 2.3 Growth

Crystal growth is the second phase that follows after initial nucleation and is often described by the linear growth rate as the increase of particular crystal face over time. Due to its complexity, this process is still not fully understood today.<sup>22–24</sup> The single fundamental steps necessary for crystal growth can be summarized as follows. Considering a supersaturated bulk solution, the contained solvated ion or molecules must first diffuse through the diffusion-boundary- and adsorption layer. This is followed by a surface diffusion to the integration site. In case of a solvated species, desolvation follows in order for the unit to be integrated into the crystal lattice. Finally, the released solvent molecules diffuse through the diffusion-boundary- and adsorption layer back into the bulk media.<sup>22</sup> Depending on the respective crystallization process, growth can be either controlled by the diffusion or integration (reaction) process. This growth pathway and the respective driving forces are depicted in Figure 2-3, according to Mullin.<sup>22</sup>

For low supersaturations crystal growth is controlled by the integration of new ions or molecules into the crystal lattice. This integration is significantly influenced by the roughness of the crystal surface. Thus, a suitable energetically

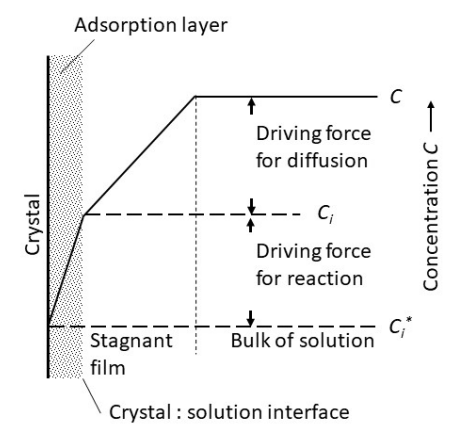


Figure 2-3 Driving forces in solution crystallization with regard to concentration, adapted from Mullin.<sup>22</sup>

favourable site features a maximum number of adjacent faces for a growth unit to attach to. There are several theories trying to explain the origin of these kinks and steps like the BCF model (Burton-Cabrera-Frank). It assumes that defects inside

the crystal lattice lead to a screw like dislocation on the crystal surface. This spiral can provide a constant number of steps for growth at low supersaturations. Under these conditions, growth is assumed to be limited by the diffusion of a growth unit on the crystal surface to the integration site. The polynuclear model displays the opposite approach with growth to happen only because of surface nucleation. Thus, a new surface layer is only formed due to coverage by sufficient individual nuclei. This approach is extended by the birth and spread model which also considers growth of nuclei for forming a new surface. These last-mentioned models also display valid theories for higher supersaturations. <sup>23,24</sup> However, these theories primarily focus on the integration process. Instead layer diffusion becomes the limiting factor for growth at high supersaturations and fast integration reactions (typical for precipitations). This is due to the surface becoming rougher and eliminating limitations for building units to find an integration site for growth.

Consequently, the rate of diffusion determines the speed of growth. Therefore, next to general diffusivity dependencies like molecule diameter or liquid viscosity, layer thickness and concentration are target factors for growth. <sup>22,24</sup> This is also displayed by Equation 2-10 for the growth rate of diffusion controlled growth according to Mersmann. <sup>24</sup>

$$G = \frac{\beta}{3 \cdot \alpha} \cdot k_d \cdot \frac{(c - c^*)}{\rho_c}$$
 2-10

Within, the factors  $\alpha$  and  $\beta$  represent the volumetric and surface area shape factor respectively while  $\rho_c$  stands for the density of the crystal.  $k_d$  describes the mass transfer coefficient which can consist of diffusive and convective contributions. Therefore, Figure 2-4 shows general operating parameters and their effect on linear growth rate.

As an increased specific power input leads to a higher relative particle velocity, the thickness of the effective film for mass transfer decreases. The resulting

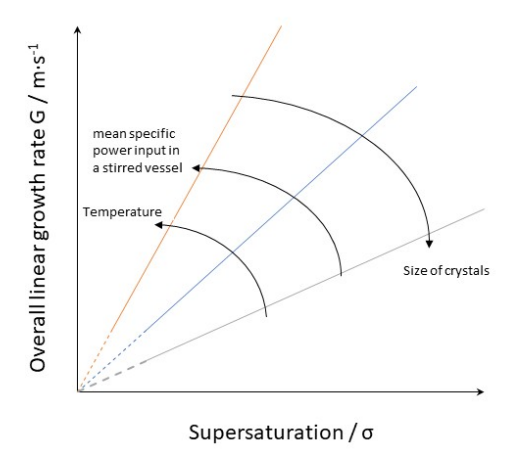


Figure 2-4 Influence of operating conditions on diffusion controlled growth, adapted from Mersmann.<sup>24</sup>

increase in mass transfer continues until full suspension in a stirred reactor is reached. Further increase in agitation would lead to disadvantageous aeration.<sup>22</sup> The effect of temperature positively influences the mass transfer as well as the integration reaction.

The latter can also lead to a change in behaviour for integration controlled systems being diffusion controlled at higher temperatures.  $^{24}$  Additionally, particle size as the result of growth can have an influence on growth rate as well. For example small crystals (< 1  $\mu m$ ) have a higher tendency to dissolve (Gibbs-Thomson effect), which results in their apparent supersaturation and therefore growth rate to be reduced.  $^{22,23}$  However, this tendency of small crystals to dissolve can also lead to growth due to Ostwald Ripening since dissolution creates supersaturation which is reduced through growth on larger crystals. Regarding size dependent growth of larger crystals, occurrence of lattice defects and thus integration sites increases, leading to an increased growth rate.  $^{23}$ 

Finally, it is to mention that other studies propose growth rate dispersion as explanation for apparent size dependent growth. One approach assumes that theoretically identical crystals under identical conditions merely grow at different yet individually constant growth rates. Alternatively, it is assumed that the

average growth rate is the same for identical crystals considering indefinite time. However, as it varies over time, the observed growth rate over the course of an experiment varies as well. For the sake of completeness, aggregation as a group of processes during which single particles merge and form larger particles should be mentioned as well.<sup>23</sup>

## 2.4 Reactive Crystallization

Reactive crystallization represents a special case in crystallization. For evaporative, cooling and antisolvent crystallization, liquid-solid phase transition of the already existing target product is achieved by changing the physical properties of the solution. For reactive crystallization instead, crystallization is induced by a chemical reaction forming the target species. In case of sparingly soluble products this is also referred to as precipitation.<sup>24</sup>

This is commonly obtained by mixing of two soluble reactants that simultaneously and rapidly react and crystallize into a product, which itself is sparely soluble in the solvent. As a consequence, reactive precipitation is generally more complex and difficult to control as it is based on competing sub steps. On one hand, it depends on the chemical reaction leading to the target product with its individual kinetics, which provokes supersaturation. This generation of supersaturation defines the nucleation and crystallization behaviour on the other hand. Both parts substantially depend on mixing in order to contact the reactants and product units for solids formation. The combination of low product solubility and high reaction rate between soluble reactants induces high supersaturations that significantly affect the properties of the final product.<sup>38</sup> Therefore, precipitation products are especially affected by primary nucleation mechanisms leading to a high number of nuclei and small crystals between 0.1 µm and 100 µm.<sup>23</sup>

This interplay between growth and nucleation defining mean crystal size is qualitatively depicted in Figure 2-5. As growth rate dominates at low supersaturations, it leads to a maximum crystal size. However, with increasing supersaturation the impact of the nucleation rate exceeds the linear growth rate. As a consequence, mean crystal size drops steeply.

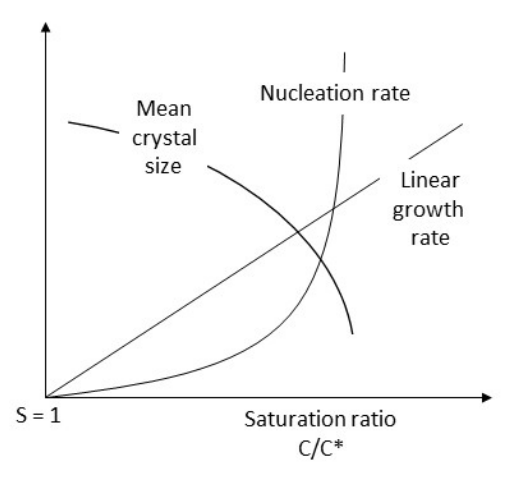


Figure 2-5 Interplay of crystal size, nucleation rate and linear growth rate in dependence of supersaturation, adapted from Tung. <sup>39</sup>

## 2.5 Product Quality in Reactive Crystallization

While the nature of precipitation is advantageously exploited in production of pigments or particles in the nanometre range, the opposite is desired in terms of processability (e.g. filterability) for a majority of products. <sup>28,39,40</sup> Thus, in the following, an overview on the operational parameters that control supersaturation and consequently improve crystal size and processability is presented. It is followed by operational strategies targeting crystal purity with regard to the respective impurity incorporation site. In congruence with the objectives of this work, the respective parameters are assessed regarding the perspective of industrial applicability. Therefore, precipitation approaches based on T-mixers, with high supersaturations and small mixing times are excluded from the following statements, which instead focus on stirred tank reactors.

# 2.5.1 Crystal Size Distribution

Generally, low supersaturations are desired in crystallization processes as they promote the crystal growth over the nucleation thus preventing the generation of fine crystals, which predominates at higher supersaturation. This facilitates the production of a coarse crystalline product with a narrow crystal size distribution, as usually aimed.<sup>39,41</sup>

Due to their nature, sparingly soluble products get rapidly supersaturated during formation which significantly complicates process control. Considering supersaturation (Equation 2-4) of a barely soluble substance with a small solubility product, two objectives can be derived in order to reduce and control supersaturation. Thus, on one hand, the (apparent) concentration of reactants should be reduced and on the other hand solubility of the product should be increased.<sup>29</sup> While being sparingly soluble, the solubility of the precipitation product can be temperature dependent, and therefore, it can be increased by changing the process temperature at which reactants are mixed. Additionally, the solubility of a substance and its temperature behaviour is completely dependent on the applied medium (pure single solvent or solvent mixtures). However, regarding reactive precipitation, the insoluble product is formed of at least two reactants that are liquid initially. Thus, the solvent should be able to favour dissolution of reactants and product, but also its separation through a change of process conditions. Therefore, the selection of solvent must adhere to a rational approach to achieve a crystal product with the intended crystal size distribution, all while ensuring its suitability for the crystallization process, whether it involves cooling or evaporation. Moreover, the solvent often affects the resulting crystal

habit (e.g. inhibit growth of a specific face), a property that cannot be overlooked, due to its impact in the product properties.<sup>24</sup> In addition, solubility can also be affected by impurities, that either lead to consecutive reactions that change the entire nature of the system or directly change the solubility of any of involved substance.<sup>22,24</sup>

Regarding reactant concentration, several studies have proven the positive effect of a reduced concentration favouring production of larger crystals. This was shown for example for precipitation of benzoic acid or salicylic acid.<sup>42,43</sup> However, from an industrial perspective, direct dilution leads to an additional effort with respect to equipment size (e.g. pumps, vessels) and for general downstream processing (e.g. waste solvent treatment). Instead, increased mixing can induce a "diluting effect", when considering a commonly used stirred tank reactor in a semi-batch set-up. In the ideal case, mixing leads to an even distribution of reactant molecules in the reactor volume and avoids local supersaturations at the dosing position.<sup>42–45</sup> In addition mixing directly promotes mass transfer (e.g. thinner diffusive layer<sup>22</sup>) and thus promotes the availability of units for crystal growth at the integration site. In combination with the reduced supersaturation, this leads to significantly larger crystals.<sup>29</sup> However, systems for which nucleation is limited by mixing time (e.g. calcium sulfate<sup>41</sup>), the opposite effect can be induced.

Regarding systems that react beneficially on mixing, next to energy dissipation, impeller type or baffles, the interplay with reactant dosing must be considered. This includes, the feed position (e.g. on surface, on impeller), dosing speed and time, number of feeds or feed opening diameter. In an optimal setup the reactants would be slowly fed through a high number of afar distributed feed pipes with a small diameter directly into the zone of maximum energy dissipation. <sup>42,45</sup> However, the effect of mixing and energy dissipation can only be exploited up to a certain individual maximum. By exceeding this maximum, collisions and attrition can induce secondary nucleation which in consequence reduces the crystal size. <sup>42</sup>

On the contrary, secondary nucleation can also be exploited intentionally through seeding in order to circumvent homogeneous nucleation due to high supersaturations. A suitable addition of seeds (namely: size, amount, location) can provide surface for depletion of supersaturation by growth instead of homogeneous nucleation. These seeds can also be provided by means of product recirculation or in a continuous reactor setup. Thus, next to the mere advantage of continuous production (capacity, time, energetically) the process itself can provide seeds for secondary nucleation and low yet constant supersaturations (assuming sufficient mixing). <sup>29,38,39</sup> However, these conditions are only the case

for reactors operating in a "mixed suspension mixed product removal" (MSMPR) mode, which favours the generation of coarser crystals. Alternative tubular reactors create high supersaturations and very short mixing times, that have the opposite effect.<sup>38</sup> Regardless of the operational mode or condition the mere residence time of a crystal in suspension influences size as well. More time for depletion of supersaturation and effects like Ostwald ripening (see 2.3) can increase particle size.<sup>29</sup> For details beyond this short and simplified overview on improving size of precipitated crystals it can be referred to McDonald et al., Myerson et al. and Mersmann and Kind.<sup>23,29,38</sup>

# 2.5.2 Purity

Next to the control of crystal size, crystallization represents a process that facilitates purification of the crystalline product. However, as mentioned in the previous chapter, impurities can also affect solubility and thus crystal habit and size. While impurities can also be present or added intentionally, the following chapter does only focus on measures to improve crystal purity regarding the recovery of a pure single target substance.

Crystal impurities can be classified according to their location in or on the crystal and by their development and origin. A crystal with an evenly distributed foreign molecule or atom inside the crystal lattice (interstitial or substitutional) is called a liquid solution and can appear for chemically similar substances. Impurities can also undergo surface adsorption with subsequent incorporation into the crystal, similar to processes during crystal growth. Therefore, favourable incorporation sites are also favourable integration and growth sites represented by crystal defects. At last, impurities can be also included in the crystal (inclusions) or adhere to the surface of the crystal as a consequence of insufficient washing (e.g. solvent, mother liquor). This effect can be especially pronounced for small or dendritical crystals, as they provide a larger specific surface. 22,23

While sufficient washing provides a direct strategy to improve crystal purity for adhering impurities after crystallization by displacing the impurities from the crystal and mother liquor interstices, different strategies are necessary to reduce incorporated impurities during the crystallization process. Regarding solid solutions the difference in solubility between impurity and target substance displays a strategy to be exploited. Thus, by increasing the solubility of the impurity relative to the target species, the partition coefficient of the impurity increases towards the liquid phase. This effect requires a suitable solvent but can also be induced by benefitting from a different temperature dependent solubility between both substances. Additionally, an overall reduction of the concentration

of the solution can reduce the share of incorporated impurities.<sup>23</sup> A different approach focusses on a steric hindering of incorporations by complex assisted crystallization. Its central idea is selective binding of the impurity molecule with a complexing agent. This has successfully been applied for cases in which target and impurity molecule have different functional groups but also for structural isomers.<sup>23</sup> Thus, in a study by Pons-Sieperman et al. 4-nitrophenol was purified from 3-nitrophenol through addition of 3-Aminobenzoic acid. This complexing agent provided a hydrogen bond acceptor and donator site and had the highest molecular mass of the investigated agents which they assumed as prove for its steric inhibition effect. They reached an impurity incorporation reduction of up to 89 % which positively depended on the amount of complexing agent. However, this additive was also incorporated into the crystal to a small amount consequently representing an impurity itself.<sup>46</sup>

Considering inclusions in crystals, their formation can occur during (primary) or after growth (secondary inclusions). While secondary inclusions are understood to form in cracks as the result of capillary forces, primary inclusions are still not fully understood.<sup>22,23</sup> However, experiments on adipic acid appear to prove the theoretical approaches stated by Mullin. Due to different growth rates of different crystal faces in addition to the faster growing edges, voids form and are overgrown during growth leading to inclusions. 22,47 This effect is reduced for smaller crystals and can be controlled by small growth rates through reduced supersaturation.<sup>22,23,47</sup> However, occlusions of solvent or washing liquid can also form during subsequent drying of a crystalline product. Given sufficient species solubility, fast evaporation of solvent during drying can induce a crystal layer to form at the exterior trapping residual solvent inside. Being especially present for small crystals, this effect can be prevented by slow drying at low temperatures.<sup>39</sup> In conclusion, it can be deduced that operating parameters that reduce supersaturation (e.g. concentration, stirring rate, solubility) can similarly reduce the amount of impurities incorporated in the crystal.

### 3 State of the Art

The investigation in this work covers the reactive precipitation of terephthalic acid (TA) from its alkaline DST solution. This alkaline solution is the result of a BMR process by alkaline hydrolysis. It displays an alternative to thermomechanical PET recycling to approach the recycling of challenging PET containing materials that cannot be recycled so far (e.g. multi-layered and undersized PET).

The following chapters are intended to classify this research work on TA precipitation and its necessity within the field of PET recycling whose lifecycle is simplistically schematised in Figure 3-1.

The first step in a PET lifecycle is its synthesis via polycondensation (3.1.1) which with regard to BMR simultaneously represents the repetitive final step to recover PET. After synthesis, the PET is adjusted to its respective application, processed repeatedly and exposed to various contaminants.<sup>2,4</sup>. This history of the PET material substantially defines the necessary effort for its recycling, where each step contributes contaminants which must be handled during recycling.

However, with regard to strongly coloured, additive-enriched or mixed polymer feedstocks, existing thermomechanical recycling technologies (chapter 3.1.2) have already reached their limits.<sup>49,50</sup> This represents the opportunity for chemical recycling processes and within, especially BMR processes which are introduced in section 3.1.3.

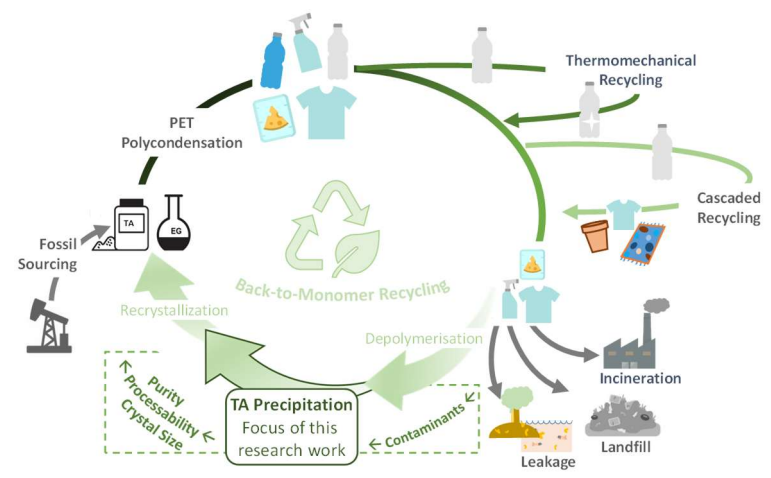


Figure 3-1 Overview and classification of the present research work within the PET lifecycle, adapted from Biermann.<sup>48</sup>

#### State of the Art

However, the products of BMR must meet the requirements for subsequent reapplication and polycondensation. In terms of the crystalline TA monomer, this comprises a high purity product with a specific particle size and morphology leading to a desired rheological behaviour.<sup>20</sup> Therefore, chapter 3.2 presents the common pathway regarding fossil PTA production as well as approaches for recovery and purification of rTA.

Nevertheless, this research work does not target the final adjustment of the rTA properties for polycondensation after recycling, as it is considered a consecutive step. Instead, it aims for the optimization of the precipitation for rTA recovery in order to ease processability and reduce impurities. Therefore, section 3.2.3 introduces current studies and

approaches regarding the optimization of the precipitation step. As this is affected by the quality of the raw PET reactant<sup>17</sup>, chapter 3.2.5 emphasizes the complexity of the PET product ("waste") regarding the variety of possible contaminants, which must be handled by a recycling process. Finally, these challenges together with the requirements on a rTA product are merged to a methodical approach (3.3) to identify the possible advantages that can be exploited by the TA precipitation step.

### 3.1 PET Synthesis and Recycling

The following sections introduce the common PET manufacturing process and different technological approaches for PET recycling considering their individual applicability and potential regarding different feedstock requirements.

### 3.1.1 PET Polycondensation

The production of virgin PET (vPET) is industrially approached via two different methods. Historically, trans-esterification of dimethyl terephthalate (DMT) with EG used to be the preferred process since only DMT purification by distillation could provide sufficient monomer quality for polycondensation. However, the development of improved catalysts for synthesis and purification methods for TA, see also 3.2.1, lead to the now domination direct esterification, explained in the following. Holling the synthesis and purification in the following.

At first solid TA and liquid EG are mixed to form a slurry (molar ratio e.g. 1: 1.25) and subsequently reacted to build Bis(2-hydroxyethyl) terephthalate (BHET) and water as by-product. This esterification is conducted at approximately 250 °C and 5 bar to promote TA solubilisation in EG.<sup>4</sup> In the consecutive step, the prepolymer of PET is formed under vacuum and temperatures up to 280 °C in order to remove by-product water.<sup>51</sup> While initial esterification is self-catalysed by TA. the formation of the polymer relies on the use of catalysts commonly based on antimony.4 This pre-polycondensation reaction is proceeded until a mean oligomeric chain length of 30 repetitive units is reached.<sup>51</sup> Afterwards polycondensation is continued and temperature is increased up to 300 °C in order to remove the initial molar excess of the EG monomer. This is necessary as EG tends to react to diethylene glycol under these conditions, which significantly alters PET properties, thus, its formation must be controlled.<sup>4,52</sup> The polycondensation is continued up to a mean chain length of approximately 100. However, regarding bottle grade PET, values of more than 150 repetition units are necessary. This is accomplished in a subsequent solid state polycondensation (SSP) step. During SSP low molecular PET is held at elevated temperatures of up to 240 °C for up to 25 h until the desired molecular weight and thus intrinsic viscosity is reached (e.g. 0.7 g/dL - 0.85 dL/g for bottle grade PET<sup>11</sup>).<sup>51</sup> Within the presented synthesis process of PET homo polymer itself, incorporation of comonomers forming copolymers in order to alter PET properties is widely applied. With regard to bottle grade PET and food packaging in general, especially isophthalic acid (IA) is a commonly used co-monomer to slow down PET crystallization (steric inhibition, see also 3.2.5). 51-53 This is primarily desired as only amorphous PET is transparent whereas semi-crystalline PET is white or opaque.<sup>11</sup>

# 3.1.2 Thermomechanical PET Recycling

The thermomechanical recycling of PET refers to several steps aiming to restore a save and stable polymer suitable for reuse in its original application. With regard to PET in plastic packaging this recycling is widely applied for the omnipresent PET bottle. In order to maintain a constant quality and a low level of contamination of the feedstock, the PET bottles are kept in a closed-loop e.g. by means of deposit return systems.<sup>2</sup> This feedstock of bottles made from PET monomaterial is subsequently sorted, screened, shredded, washed, re-extruded and blow moulded into new preforms and bottles. However, this mechanical recycling is limited to a maximum of five to six cycles for a bottle due to thermal degradation and contaminants which severely reduce physical PET properties like tensile strength.<sup>4,54,55</sup>

Additionally, an increase in recycled content crucially influences optical properties of PET (e.g. haze, yellowing) despite the strong influence of the quality and purity of the used rPET itself.<sup>8,56,57</sup> Therefore, optimistic future scenarios assume a mixture of 75 % high quality rPET and 25 % vPET to be realistic for indefinite mechanical recycling.<sup>2</sup> While this proves the limits of thermomechanical recycling, it also emphasizes the necessity of BMR processes for achieving a complete recycling rate without vPET provision.

Figure 3-2 shows the results of a case study on PET bottle circularity in Europe.

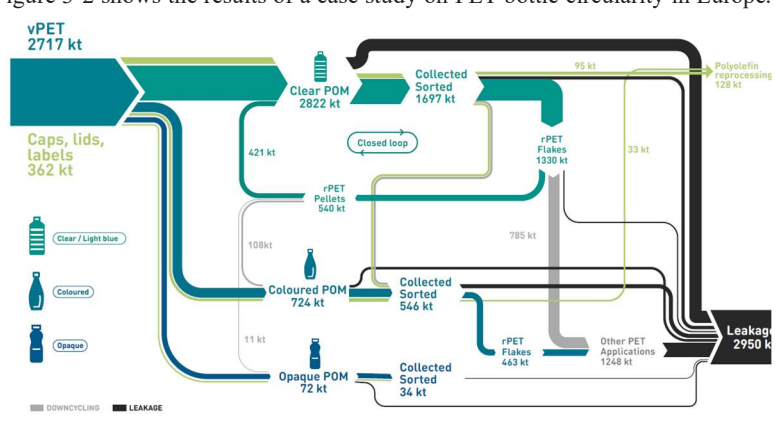


Figure 3-2 Current state (2022) of European PET-bottle mass flows. 50

The closed loop recycling of clear bottles placed on market (POM), symbolizing

e.g. the result of the deposit return systems cycles only about 15 % rPET. While an additional 4 % is being fed to coloured and opaque POM, 32 % rPET are downcycled to other PET applications and more than 40 % are lost directly.

However, in comparison to coloured and opaque POM which are limited to a single use, clear POM represent a rather positive example. These numbers emphasize the need for recycling solutions for PET end-of-life applications where practically every POM eventually ends up.

The limits of mechanical recycling are a product of the interplay between polymer degradation through the recycling process in addition to its catalysis by degradation products and contaminants. <sup>6,51,54</sup> The first step in mechanical recycling, regarding a well sorted PET flake fraction as input material, is (hot) washing with caustic soda and detergents. As any remaining water promotes undesired hydrolysis of the polymer, PET flakes are subsequently dried. In a conventional setup, these cleaned flakes are now fed into an extruder with a vacuum unit for removal of volatile components especially acetaldehyde. <sup>2,54</sup> However, after melt filtration and pelletizing the resulting rPET does not possess sufficient quality for reapplication as a bottle yet.

Therefore, several processing methods have been developed next to additives and admixture of vPET. <sup>2,8,51</sup> These processes are referred to as "super clean recycling" (SCR) processes. <sup>54,58</sup> Among these, partial depolymerization of the PET flake surface displays one approach. By coating the flake surface with sodium hydroxide and heating to a temperature above 150 °C, a minimum of 10 µm of the flake surface are hydrolysed to DST and EG. Thus, migrated contaminants are released and subsequently removed by washing together with soluble EG and DST. A different method decontaminates PET flakes at temperatures ranging from 180 to 230 °C for up to 2 h under vacuum or inert gas atmosphere. The applied temperature allows for contaminants to diffuse out of the polymer. Its application on thin flakes comes with the advantage of reduced distance and time for diffusion of contaminants compared to pellets. While the energy demand and the residence time are comparably low for these two SCR processes, the intrinsic viscosity (IV) does not increase as desired since low molecular weight compounds remain in the polymer.

This challenge is overcome by SSP, adapted from the PET manufacturing process, presented in the previous chapter.<sup>58</sup> While this process has been considered too slow and expensive for industrial application initially, it is now widely applied.<sup>51,58</sup> SSP is usually performed on pellets at temperatures between 180 and 230 °C for 6 to 20 h in batch or continuously operated reactors. Regarding contamination, the larger diffusion distance of pellets compared to flakes is compensated through longer residence times.<sup>51,58</sup> Next to this decontaminating

#### State of the Art

effect, SSP improves the IV and restores the polymer chain length which is supported by the catalyst remaining in the PET after initial polycondensation. It provides more time for diffusion of low molecular substances (e.g. water, EG) in the polymer matrix. Thus, also water that is newly reacted during SSP is shifting the polycondensation reaction equilibrium towards the polymer. For this reason, SSP is always applied when a long chain length and high IV are needed. However, with regard to realistic sorting qualities of PET, contamination with degradation catalysts like polyvinylchloride or polyamides cannot be completely avoided, making indefinite thermomechanical recycling impossible. 2

For the sake of completeness, a different SCR process based on highly pure PET material shall be mentioned as it applies glycolysis, a BMR method, in conventional PET manufacturing. In a parallel recycling plant, high quality PET flakes (no contaminations, no colourants) undergo a glycolytic depolymerization. The resulting mixture of PET oligomers possesses a composition comparable to the pre-polymer during the polycondensation process, mentioned in the previous chapter (3.1.2). Therefore, this mixture is applied as an alternative feed for the subsequent melt-phase condensation step. Typical values in industrial application report an addition of 10 - 30 % of rPET. Nevertheless, since contaminants cannot be removed within this process, the introduced material has to meet vPET quality with regard to purity.<sup>58</sup>

### 3.1.3 Back-to-Monomer Recycling

In order to overcome the limits of mechanical recycling when using PET feedstock, alternative recycling approaches can be classified into their respective target output with regard to the PET life cycle.

Thus, Figure 3-3 shows an overview of the different recycling approaches and the application of their products in order to close the loop for PET recycling.

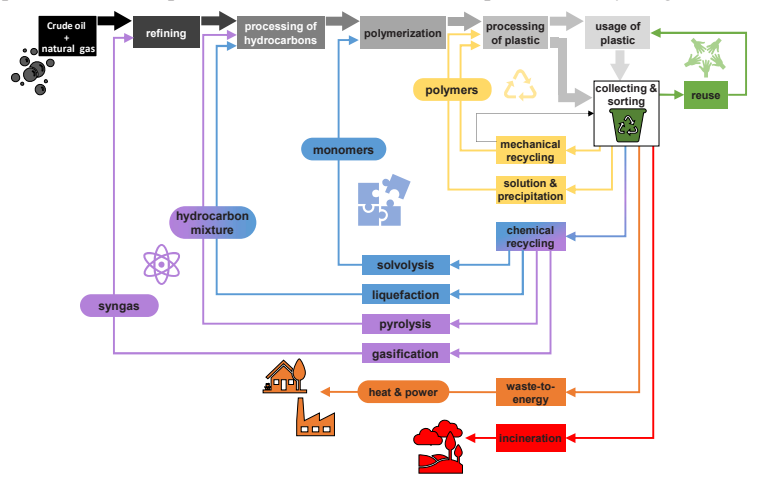


Figure 3-3 Simplified plastic lifecycle and classification of recycling technologies with regard to respective input and output streams, colour code from green to red refers to qualitative effort for plastic reapplication, adapted from Brepohl et al..<sup>49</sup>

Generally, the size of the displayed cycles can be interpreted as the effort necessary for reuse of PET product. Thus, by direct reuse (green) and methods maintaining polymer the polymer matrix (yellow), the smallest individual effort is needed. Regarding chemical recycling (blue/purple), a general classification of recycling effort is not possible as the approaches and their products differ substantially. Initially, chemical recycling has primarily been connected with pyrolysis or gasification processes requiring high temperatures and pressures. The products of these processes are syngas or complex mixtures of hydrocarbons similar to crude oil from fossil sources. The necessary purification of these mixtures in order to reach polymeric grade purities is nearly impossible.<sup>59</sup> Additionally, the products of these processes represent early precursors in the crude oil process chain towards a final product. Instead, chemical recycling that

#### State of the Art

produces monomers (= BMR) builds on the selective breakage of polymer chains into their defined monomeric building blocks. On one hand, additives and contaminants are released from the polymer matrix and can be eliminated by different separation techniques. On the other hand, the selectively separated monomers can be used directly for new production of polymers in virgin quality.<sup>49,59-61</sup> Thus, BMR represents the consequential consecutive step to recycling, when thermomechanical and polymer-structure maintaining approaches come to their limits. There are different methodical approaches regarding BMR of polycondensates.

- 1. Aminolysis or ammonolysis by addition of aqueous amine (ammonia) solutions yielding amides (mainly under research focus).<sup>59,60</sup>
- 2. Methanolysis uses methanol to produce DMT and EG. DMT can be purified more easily by distillation than TA and used to be the standard PET monomer. Industrial application for various PET feedstocks is currently focused by Loop Industries and Eastman chemical company. To date, methanolysis is reported to be the only industrially accomplished chemical PET recycling path. 62
- Glycolysis applies EG for depolymerization resulting in the PET monomer Bis-hydroxyethyl terephthalate and oligomers of similar structures. The process relies on mono-layered PET and is currently under development by Ioniqua Technologies and Garbo.<sup>7,63</sup>
- 4. Hydrolysis can be conducted in neutral acidic or alkaline environment and can also be catalysed enzymatically. These methods eventually produce TA and EG monomers for direct polycondensation to PET. Several companies follow this approach, e.g. RITTEC 8.0 Umwelttechnik, gr3n or carbios.<sup>60,64</sup>

Due to the direct applicability of monomers and the broad range of possible feedstocks hydrolysis (4) and especially alkaline hydrolysis represent promising procedures.<sup>65</sup> An overview about different studies and current technological approaches on alkaline hydrolysis is presented in the following chapter.<sup>17</sup>

### 3.1.3.1 Alkaline Hydrolysis

A BMR approach studied extensively is offered by selective alkaline hydrolysis producing EG and an alkali terephthalate salt, as a TA precursor (Figure 3-4). It possesses several general advantages in comparison to acidic and neutral hydrolysis processes. On one hand, alkaline hydrolysis allows for simple separation of solid impurities due to the aqueous solubility of the reaction products TA-salt and EG.

Figure 3-4 Stoichiometric reaction equation of alkaline hydrolysis of PET with sodium hydroxide.

Instead, neutral and acidic hydrolysis produce solid TA directly, which has to be dissolved in order to separate it from solid residuals. On the other hand, alkaline hydrolysis does not produce oligomeric reaction products as the alkaline reaction partner selectively attacks the ester binding, in contrast to neutral hydrolysis. Additionally, neutral hydrolysis requires a significantly higher pressure and temperature, as it is reported to be most effective on PET in its molten state. 62,63,66,67

In view of the above, the following section focuses on the most advantageous approaches based on alkaline hydrolysis with studies investigating process parameters, different feedstocks or catalyst variations.

Kosmidis et al. hydrolysed PET with the help of a phase transfer catalyst in aqueous sodium hydroxide solutions of 5 wt.-% up to 15 wt.-% at temperatures between 70 °C and 95 °C. Despite the mild conditions, they achieved TA yields exceeding 90 %. With regard to yield and reaction time they found that a high sodium hydroxide concentration and small PET particle size at high temperatures promoted depolymerization best. <sup>68</sup>

Cosimbescu et al. took an organic co-solvent approach for depolymerization of mixed PET waste under low temperature conditions. While varying the PET chip size and sodium hydroxide concentration like Kosmidis et al. they added EG or ethanol to an aqueous sodium hydroxide between 20 wt.-% to 30 wt.-%. They observed similar parameter effects like Kosmidis et al. for chip size while hydroxide concentration appeared to be irrelevant at applied concentrations.

However, the application of ethanol resulted in yields of up to 95 % within 2 h for mixed PET waste in a simple laboratory flask set up at a temperature of 80 °C.  $^{69}$  Karayannidis et al. focused on the influence of reaction time and depolymerization temperature in aqueous sodium hydroxide reaching almost 98 % yield after one hour at 200 °C, the highest temperature tested. They compared the procedure to depolymerization in nonaqueous 2-methoxyethan-1-ol with potassium hydroxide at 120 °C and reached a yield of more than 80 %.  $^{70}$ 

Tournier et al. engineered an enzyme being able to depolymerize PET aiming for an increased productivity. In their best experimental setup, they converted more than 90 % PET within 10 h at 72 °C. During their experiments they had to maintain a slight alkaline pH by constantly adding sodium hydroxide in order to avoid enzyme inhibition by acidification of the produced TA. <sup>16,64</sup> Therefore, their approach applies stoichiometric amounts of sodium hydroxide and is considered most similar to alkaline hydrolysis as well.

Ramopoulus et al. presented a continuously operated industrial scale microwave reactor for alkaline PET hydrolysis. The reactor consists of glass tubes in which Archimedean screws transport the reaction media. More details on the holistic approach including this microwave reactor design for alkaline hydrolysis approach are presented by Crippa and Morico with the DEMETO technology. They report a yield of 98 % in less than 30 minutes for alkaline hydrolysis with additional use of ethylene glycol.

A similar approach is reported by Biermann and Brepohl using a twin screw extruder two continuously depolymerize PET and Polyethylene (PE) dual layer packaging with solid sodium hydroxide. 14,72 Within an average residence time of 1 min, the reach degrees of depolymerization of up to 97 %. Together with the usage of industrially available (standard) and scalable equipment this approach represents significant advantages compared to the previously mentioned studies. 14,72 Since the PET reactants used within the present work were depolymerized by this technology, it is extensively described in the following chapter.

# 3.1.3.2 revolPET® Technology

The PET reactants used throughout this work originate from an approach on alkaline hydrolysis, patented by Rittee 8.0 Umwelttechnik GmbH and first reported by Biermann and Brepohl et al..<sup>14,72</sup> Its central idea is the continuous depolymerization of so far unrecyclable PET waste fractions like the common PET/PE packaging compound. Its PET content is selectively hydrolysed to DST and EG while PE stays inert and can be separated subsequently as solids.

A simplified flow chart of the process is displayed in Figure 3-5.

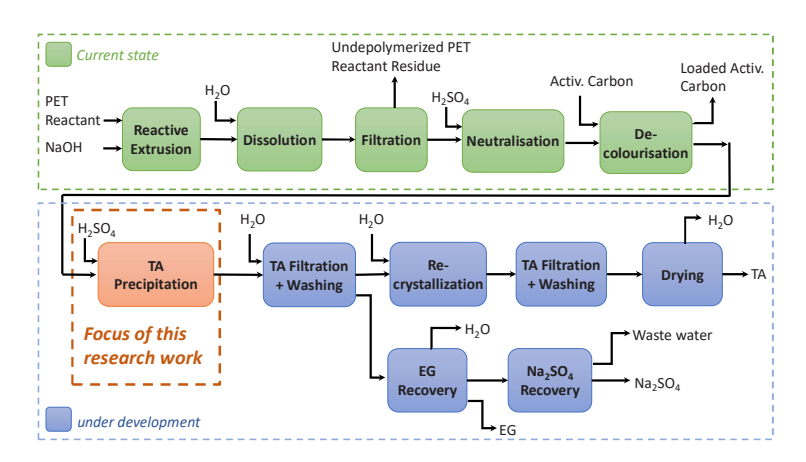


Figure 3-5 Simplified flow chart of the revolPET® process, colour code refers to current state of development of the pilot plant.

In detail, the apparatus used for depolymerization is a twin-screw extruder ZSE 27 MAXX by Leistritz Extrusionstechnik GmbH with a main feeder for waste PET material (e.g. flakes, pellets) and a side feeder for solid sodium hydroxide. The reaction zone of the extruder is initially heated to process temperature between 130 °C and 160 °C. Due to the exothermal reaction, heating is not required but cooling during continuous operation. As a result of an average residence time of 60 s and injection of cold water to partly dissolve the DST solids, thermal runaway is not an issue. Furthermore, a lower reaction temperature reduces coloured impurities in the final TA product.<sup>73</sup> Despite its short residence time, the process reaches degrees of depolymerization of up to 97 %.<sup>14,15</sup> At the current state of development, depolymerization is performed at a throughput of 6.96 kgpet/h.

After depolymerization the partially dissolved reaction mixture is mixed with sufficient deionised water to completely dissolve the DST (~130 g/L max.<sup>74</sup>). Afterwards, the undissolved solid residue containing unreacted PET, foreign polymers, pigments or fibre is removed by means of filtration up to a limit of 45 nm.

This coloured but practically particle free solution is referred to as PET reactant throughout this work. In contrast to the process displayed in Figure 3-5, this solution is not purified further prior to conducting the precipitation experiments in this work, in order to stress and identify the purification potential of the

precipitation. However, within the revolPET® process this solution is treated with regard to dissolved and colour forming impurities by an activated carbon treatment. The resulting transparent and colourless solution is acidified with sulfuric acid leading to instant precipitation of TA with a Hazen colour index > 10 in line with industrial specification. By means of filtration the TA product is washed and separated from its mother liquor containing the second monomer EG and the sodium salt of the precipitation acid residue.

However, at the current state of development precipitation of TA leads to disadvantageously small crystals that significantly inhibit TA recovery by filtration and its washing. Furthermore, in contrast to the continuous depolymerization, TA precipitation is performed in batches leading to a reduced productivity. Additionally, PET packaging commonly contains the TA comonomer IA which cannot be removed through the current purification step using adsorption. Therefore, next to optimizing the crystal size (and processability) as well as a transfer to continuous operation, especially the separation of colourless IA (3.1.1 and 3.2.5) is targeted in this research work.

Regarding the mechanically dehumidified TA after filtration, two possible routes are under current consideration. As precipitated TA crystals significantly differ in their size and morphology from large and rounded purified TA (PTA) crystals, their reapplication as a drop-in product could require recrystallization, prior to drying. In the opposite case of industrial suitability regarding precipitated TA processability, it can be dried directly.

Regarding the recovery of the second monomer EG, at the current state of development, different technologies are still under consideration (e.g. rectification, membrane-based processes). Thus, only partial concentration by evaporation of water in the mother liquor is conducted at the pilot plant scale so far. The recovered water from the distillate can be reused for the dissolution step of the depolymerization product.

Additionally, the mother liquor contains significant amounts of sodium sulfate by-product ( $^{\sim}0.9~g_{Na2SO4}/g_{TA}$ ). Therefore, different crystallization approaches are currently under consideration in order to recover the salt and recirculate the water.

## 3.2 Terephthalic Acid

The huge worldwide demand of polyester fibre and PET packaging has led to a constant growth of production of TA (1,4-benzene dicarboxylic acid [100-21-0]), putting it among the top ten organic chemicals produced globally. The following chapters give an introduction into the decisive properties of the dicarboxylic acid with regard to its synthesis from p-xylene and purification but also subsequent polycondensation. Next to introducing the solubility data of TA reported in literature, its morphological appearance originating from the industrial purification process is displayed. Additionally, the alternative production approach through precipitation after alkaline hydrolysis is presented. It is concluded with the challenges and chances regarding the precipitation process and the specific impurities of the PET feedstock.

### 3.2.1 Synthesis by p-Xylene Oxidation

The growing demand for PET in packaging, textile or technical applications was the main driver for an increase of p-xylene (PX) production representing the main precursor for PTA synthesis. Therefore, from year 2000 until 2020 the annual PX production capacity has more than tripled from 20 to more than 70 mio. tonnes. <sup>76</sup> The raw material for PX production mainly consists of C8-aromatic isomers (ethyl benzene, o-, m-, p-xylene) whose close boiling points complicate separation by distillation. Therefore, the main supply of PX is produced by the simulated moving bed (adsorption based) Parex<sup>TM</sup> process. <sup>76</sup>

In a similar manner global production of PTA is mainly based (up to 76 % in 2018) on the Amoco process which is being introduced in the following. <sup>10,77</sup> For an extended insight into the reaction mechanisms of the synthesis it is referred to the review by Tomás et al.. <sup>78</sup> Generally, the process is split in two consecutive parts – synthesis and purification. In the first stage PX is oxidised at temperatures between 180 °C to 220 °C using air as oxygen source under pressures from 15 bar to 30 bar. The reaction is homogeneously catalysed by salts of Co(II) and Mn(II) mixed with a bromide source in aqueous acetic acid and exceeds yields of 95 mol%. Despite this nearly complete oxidation of the methyl groups, the resulting crude TA is contaminated with partly oxidised intermediates (Figure 3-6).

$$H_{3}C$$
 $O=C$ 
 $O+O_{2}$ 
 $O+O_{2}$ 
 $O+O_{2}$ 
 $O+O_{3}$ 
 $O+O_{4}$ 
 $O+O_{5}$ 
 $O+O_{5}$ 

Figure 3-6 Simplified reaction of PX to TA and intermediates p-toluic acid and 4-CBA (from left to right).

Next to a variety of coloured low concentrated by-products, especially the presence of critical amounts of 4-carboxybenzaldehyde (4-CBA) demand a subsequent purification step. 79 As 4-CBA possesses only one carboxylic group for esterification, it acts as chain terminator in the polycondensation process and drastically reduces chain length and stability of the final polymer.<sup>78</sup> The purification process uses hydrogenation to reduce 4-CBA to p-toluic acid next to reduction of yellow and other impurities. However, as structurally similar substances to TA like 4-CBA are incorporated in the crystal matrix, crude TA must be dissolved completely in order to access these impurities. At temperatures exceeding 260 °C at least 15 wt.-% of crude TA are dissolved in water under presence of excess hydrogen and a highly selective fixed Palladium catalyst. In a subsequent cascade of crystallizers, the temperature is reduced stepwise by flash evaporation of water which induces crystallization of TA. Due to the significantly enhanced solubility of the reduced impurities (e.g. p-toluic acid) in comparison to TA, these remain in the mother liquor and are filtered off. The resulting purified TA displays a white (hazen colour index < 10) powder with less than 25 ppm of 4-CBA. 10,80 Since this PTA is used for PET synthesis, it equally represents the raw material for BMR processes. Consequently, rTA is based on a highly purified bulk chemical displaying a promising opportunity regarding the necessary purification effort in BMR.

# 3.2.2 Polymorphism and Morphology

The importance of the crystalline appearance of commercially available TA is motivated by its behaviour in PET synthesis. As the single molecules of TA and EG co-monomer are alternating in the PET chain, their molar ratio during synthesis must preferably be as close to one as possible.<sup>21</sup> Regarding weight ratio,

this results in a mixture of approximately 70 % solid TA with 30 % EG (volume ratio 60/40 TA/EG<sup>20</sup>). In order to reach a flowable and polymerizable mixture, the resulting slurry viscosity must be below 3.5 Pa·s. It is to mention that the slurry viscosity cannot be adjusted by adding surplus EG exceeding a molar ratio of 1.4, as undesired condensation of EG molecules to diethylene glycol reduces polymer stability (see also 3.1.1).<sup>21</sup> Therefore, in order to achieve these requirements, TA crystals with a rounded morphology and a low specific surface area are applied, as these have been evidenced as the only way to keep the desired molar ratio and viscosity in the PET synthesis.<sup>20</sup>

Several studies have been conducted to connect the molecular arrangement (in the crystal structure) and crystallization behaviour of commercially available TA to its macroscopic appearance. 81–84 To date, the existence of three different polymorphs of TA has been reported, with triclinic polymorphs I and II and the monoclinic polymorph III. This chapter will focus on polymorph I and II as their transition is reported to be responsible for the rounded morphology developing under industrially relevant conditions. For further information on the third polymorph, it may be referred to the publications by Sledz et al. and McKinnon et al. 84,85

Difficulties in classification of the TA polymorphs have led to inconsistencies in nomenclature of these in the literature. As a consequence, the classification on the polymorphs by Bailey and Brown, Gerasimov et al. and Träger and Jostmann is the reverse to Davey et al. and later publications, which is used hereafter. <sup>20,81–83</sup> Generally, polymorph II is reported to be more stable at room temperature with a transition from II to I between 75 and 100 °C. This transition is completed at temperatures above 150 °C where the majority of crystals are represented by polymorph I. <sup>82</sup> Figure 3-7 displays a simplified two-dimensional arrangement of single TA molecules in their respective crystal lattices.

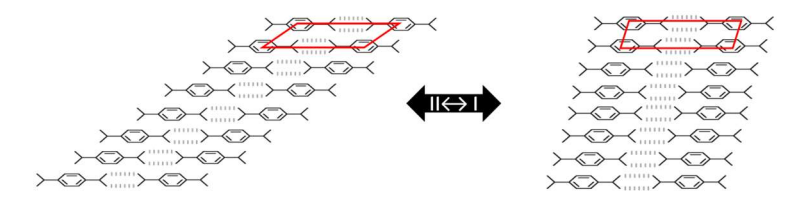


Figure 3-7 Molecular arrangement of TA polymorph I and II, adapted from Davey et al..<sup>81</sup>

Both polymorphs consist of chains of TA molecules connected through hydrogen bonds between their carboxylic groups. The difference between form I and II is

the angular arrangement between TA molecule chains. While the aromatic benzene rings in adjacent layers of form I are almost directly in line, they are shifted in form II and alternate with the carboxylic groups. This leads to a rhombic shape of single form II crystals and a rather rectangular shape of form I in equilibrium. Although being metastable at room temperature commercially available PTA is reported to be commonly found as polymorph I. This polymorph features a tendency towards crystal twinning allowing for apparent growth by merging in lateral direction of its needle axis. Davey et. al revealed this microstructure of parallel needles inside PTA by cutting single rounded crystals with a microtome knife.

They assumed a mechanical stabilisation of the otherwise unstable polymorph I by adherence of adjacent needle twins making a morphological transformation impossible. In their experiments, recrystallization of twinned polymorph I crystals was only achieved under presence of p-toluic acid. Additionally, they concluded that the high temperature and pressure conditions of industrial purification process in combination with high supersaturation lead to twinned form I crystals. The original facetted surface could turn into the rounded morphology as the result of abrasive forces during production (Figure 3-8).

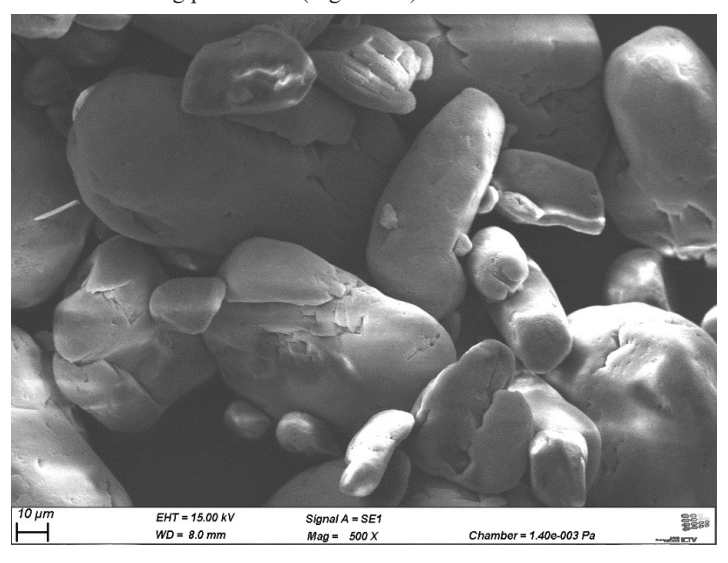


Figure 3-8 SEM image of purified terephthalic acid.

Regardless of the polymorph they observed that the direction of growth is not along the hydrogen bonded chains but normal to these.<sup>81</sup> In accordance with earlier work on adipic acid, they assume that the strong binding of water molecules to these carboxylic groups inhibit an extension in this direction. Instead, the desorption of water molecules from these sites would rule lateral growth.<sup>86</sup> For general comparison, a particle size distribution of PTA crystals is displayed in the Appendix (Figure 8-1).

# 3.2.3 Precipitation from Alkaline Solution

This chapter comprises the recent developments and investigations on TA precipitation in BMR processes towards adjustment and optimization of its properties. A detailed description of the TA precipitation chemistry is presented in section 3.2.6. Apart from recycling approaches, precipitation of TA from its alkaline salt has also been reported in other fields with a different focus. Thus, in the 1950ies the so called "Henkel process" for production of TA used hydrochloric acid for precipitation of TA from dipotassium terephthaltate.<sup>87</sup> A different source of DST solution are effluents from polyester fibre manufacturing and dying plants. They apply sodium hydroxide to modify (partly depolymerize) the PET surface in order to achieve a silky touch and improved colour durability. The objective by TA precipitation through acidification is wastewater treatment by reducing the chemical oxygen demand (COD).<sup>88,89</sup>

To date, with regard to alkaline hydrolysis, the majority of publications focusses on advantageous and innovative depolymerization, showing the

growing attention on alkaline hydrolysis. These studies apply precipitation of TA in order to proof feasibility of their respective depolymerization concept for BMR. Apart from purity analysis, no evaluation of TA crystal quality and the industrial applicability is reported. <sup>12,16,68–71</sup>

In contrast, only a few studies have been published so far with a research focus on the recovery of TA by precipitation. 17,18,90

A short overview of these studies and their parameters is given in Table 3-1. In the following, a detailed description of the different approaches is presented. The DST reactant used by Wu et al. originated from wastewater of polyester fibre plants. However, they aimed for the recovery of high purity TA meeting industrial specifications instead of mere reduction of COD (see also 3.2.5). Therefore, they divided their process into two parts to enhance TA solubility and overcome supersaturation issues. <sup>19</sup> In their first recovery step, they precipitated TA at 80 °C with sulfuric acid directly from wastewater. They reported a mean crystal size of

#### State of the Art

less than 10  $\mu$ m and a purity of 80 %. In order to improve crystal size and purity they applied a cooling crystallization step.

Table 3-1. Overview of research studies focussing TA precipitation.

Procedures	PET reactant	Solvent	Precipitation Acid	Tempera- ture Range	Ref.
Precipitation + Recrystallization	Waste- water	Water/ EG + DMAc	Sulfuric acid	30 °C - 80 °C	19
Precipitation (Cubic dosing)	Bottle flakes	Water/ EG + DMSO	Sulfuric acid	25 °C - 75 °C	18
Precipitation (two-steps)	PET waste	Water	Sulfuric acid	50 °C - 95 °C	91
Precipitation	Waste- water	Water	Sulfuric acid	30 °C - 70 °C	90

Hence, crude TA was dissolved and recrystallized in N, N-Dimethylacetamide (DMAc) from 70 °C to 30 °C with varying cooling rates (0.78-1.88 K/min). Generally, the enhanced solubility in DMAc led to higher purity and significantly larger TA crystals. They found that the slower applied natural (not linear) cooling rates were able to produce crystals larger than 100 μm. Especially, the rate of 1.18 K/min resulted in enlarged crystals with a narrow size distribution. Microscope pictures showed a rod-like structure of TA crystals. The visually assessed aspect ratio appeared to be more equant-shape in comparison to precipitated needle-like TA. However, a disadvantage of using DMAc was a maximum yield of 86 % due to residual TA at 30 °C in the solvent. Additionally, with regard to food packaging of rPET from rTA, the toxicity of DMAc might limit its application.

Lee et al. used aqueous sodium hydroxide to depolymerize mineral water bottles. <sup>18</sup> However, instead of depolymerization their main focus was to tailor a TA that directly meets industrial specifications after a one step process. Therefore, they combined several approaches for increasing TA solubility and reducing

supersaturation during precipitation. On the one hand, they introduced dimethyl sulfoxide (DMSO) as co-solvent being completely miscible with water. In order to avoid precipitation of DST by addition of DMSO, they premixed it with their precipitation acid (PA), sulfuric acid. Additionally, they dosed the DST solution after depolymerization into the crystallizer containing DMSO and the PA. As a result, solubility for TA during TA formation was enhanced and antisolvent crystallization of DST avoided. Furthermore, they precipitated at elevated temperatures up to 75 °C to promote TA solubility and implemented a cubic dosing technique to minimise supersaturation. For this technique, a single feed of DST solution was dosed in 10 equal amounts but different intervals of time. These intervals got shorter over course of the experiment and describe a cubic function. The intention behind this cubic dosing technique is avoidance of excess initial nucleation while promoting growth on existing TA crystals as the precipitation advances. In order to increase the reduced yield due to solubility losses to DMSO solvent, they proceeded with a cooling crystallization step in between two feeding steps. An additional heating and cooling cycle at the end of the experiment could only improve crystal morphology and processability, in terms of filterability, slightly. The results of their approach lead to a rounded TA morphology and improved filterability evaluated by the pressure drop and depending drying time. However, regarding crystal size, the microscopic analysis revealed a maximum of 20 μm while the average crystal appeared to be smaller than 10 μm. In addition, the use of DMSO comes with the downside of a reduced yield, reduced DST solubility, and a solvent mixture leading to additional downstream effort stressing process economics. Regarding solvent recycling, the proximity to the EG boiling point (197 °C for EG vs. 189 °C for DMSO) could complicate its technical application. 92 Additionally, its decomposition temperature (190°C) is rather low and unfortunately catalysed by acids. Nevertheless, their cubic dosing approach as a batch procedure could be transferred to a continuous procedure in a reactor cascade.

A similar approach was targeted by Yazaki et al. who invented an entire depolymerization process in continuous operation. With regard to precipitation they used a cascade of two reactors with sulfuric acid as PA, of which the first reactor was held at a constant pH of 6 and the second at target pH 2 to 4. The PA was fed through the hollow shaft of the stirrer, in order to reduce concentration peaks of the PA upon dosing by improved mixing. Additionally, they mixed the PA prior to dosing with mother liquor after the second crystallizer, diluting the PA without additional solvent. A subsequent classifier was used to separate and recycle small crystals to the first reactor. However, according to Yazaki et al., these crystals were dissolved and did not serve as seeds. Next to these instrumental

measures, they also crystallized at elevated temperatures up to  $85\,^{\circ}$ C, which significantly improved processability of TA. An analysis of the polymorphic state crystallized in the transition range was not performed, although the temperature hence the rounded morphology could not be correlated to polymorph II.  $^{91}$ 

A recent investigation by Marlena et al. focussed on precipitation of TA from polyester weight reduction waste water. In a first step they precipitated TA with sulfuric acid from purified solution (activated carbon). After washing and drying this crude TA was dissolved in sodium hydroxide followed by a semi-batch precipitation. Therefore, they precipitated TA from a 0.06 M DST solution in batch mode which served as bulk media and did not contain EG. Its condition was adjusted to the desired target pH of 3, 4 or 5 and a temperature between 30 °C to 70 °C. During the subsequent semi-batch precipitation, they fed a secondary DST solution of varying concentrations (max. 0.5 M) simultaneously to sulfuric acid (0.5 M) into the bulk media. In their experimental variations feeding time (duration), feeding rate, stirring rate and temperature hardly affected the particle size distribution of TA. Instead target pH and DST concentration influenced crystal size most. Especially a pH of 3 showed an interesting behaviour as its initially smaller mean crystal size of approximately 4 µm increased significantly to 10 µm after 30 minutes of constant stirring. A pH of 4 lead to larger mean crystal size initially and dropped steeply afterwards to a similar size as pH 5, which remained constantly low. Increasing DST concentration to 0.5 M led to a mean crystal size of 9 µm instead of 3 µm for 0.1 M and 0.3 M. They concluded with a TA purity analysis that met PTA purity characteristics apart from ash content.90

Summarizing these approaches with regard to the resulting TA crystals, it can be derived that none of the procedures leads to a TA similar in size and morphology to PTA. This is in agreement with the expectations on a precipitation process producing a large number of crystals with a small size due to high supersaturations (except from the recrystallization approach by Wu et al.<sup>19</sup>). With regard to reducing supersaturation, the most promising parameters in these studies target a solubility increase through elevated temperatures and alternative solvents. Second, a controlled reactant dosing and distribution should be mentioned. All in all, the given information is scarce and TA crystal size is hardly being analysed nor related to its processability characteristics like filterability. Sulfuric acid is used throughout these studies without alternative PAs being applied. However, as significant amounts of low value sodium sulfate are being produced (3.1.3.2), consideration of alternative PAs could promote overall process economics and sustainability (3.2.6) as the salt by-product changes.<sup>16</sup> Furthermore, the applied modes of operation are to batch and semi-batch procedures, disregarding the

potential of continuous processes.

Therefore, this research work targets the identification of operational parameters including alternative PAs during precipitation on TA crystal size. Its effect regarding an improved TA processability will be evaluated by measuring filterability.

In addition to batch precipitation, finally, a continuous operation is focussed as it can provide significant advantages (e.g. reduced supersaturation, secondary nucleation, productivity) but also a consistent continuation of a continuous depolymerization step.

## 3.2.4 Solubility

The solubility of TA and its structural isomers has been part of several investigations due to its relevance in industrial applications and its crucial role in its crystallization process. From the vast number of possible solvents in which the solubility of TA has been studied, here is revisited its solubility on solvents that are directly involved in its synthesis and purification - specifically acetic acid, water and their mixtures (see also 3.2.1). Additionally, the solubility of the TA co-monomer isophthalic acid (IA) is reviewed as its reduction by precipitation displays a central aim of this work (3.1.1 and 3.1.3.2).

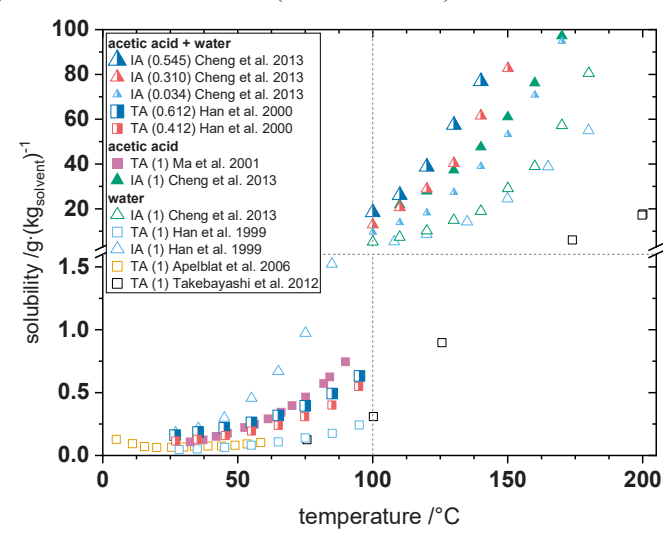


Figure 3-9 Solubilities of terephthalic and isophthalic acid in water and (aqueous) acetic acid. 93-98

Therefore, Figure 3-9 shows a selection of literature data on TA and IA solubility in both solvents. In order to support visualisation, the y-axis is split and scaled differently for the respective "low" (<1.5 g/kg) and "high" (>15 g/kg) solubility regions. IA is displayed by triangles whereas squares are used for TA, while respective fillings and symbol sizes represent solvent and concentration respectively.

Generally, the data shows that both dicarboxylic acids are sparely soluble at temperatures below 100 °C with TA being significantly less soluble in either solvent. Thus, solubility at around 75 °C is approximately 1 g/kg for IA is instead of only 0.1 g/kg for TA. However, TA solubility is significantly improved in aqueous and pure acetic acid for which data is presented below 100 °C. On the contrary, values for TA solubility below 60 °C in pure acetic acid are lower compared to the more concentrated acetic acid mixture.

A similar effect is revealed for IA in a solvent containing acetic acid shown at temperatures exceeding 100 °C. Thus, IA solubility in more concentrated aqueous mixtures surmounts pure acetic acid above 100 °C. This effect can be attributed to the maximum solubility effect as predicted by the Scatchard-Hildebrand Solution theory.<sup>99</sup> All in all, the solubility data provides the necessary fundamentals for understanding the industrially common high temperature TA crystallization (3.2.1) as well as the investigated low temperature precipitation (3.2.3). Thus, the low TA solubility comes with the downside of high temperatures and pressures for complete dissolution (purification step) of reasonable amounts. On the other side, the strong temperature dependence of solubility allows for subsequent flash crystallization with no need for additional solvent evaporation and almost complete TA recovery. While complete yield is a significant advantage when precipitating TA in water, its low solubility promotes nucleation due to high supersaturations (3.2.3). However, in addition, its increased solubility in acetic acid is a promising starting point for the application of an alternative precipitation acid to lower supersaturation (3.2.6).

With regard to the increased solubility of IA contamination in realistic feedstocks it can be deduced that increased temperatures can favour TA precipitation over IA. In a similar manner this selectivity can be increased even more upon application of acetic acid as PA. This effect could be even more pronounced considering that IA is added in small amounts to PET.

### 3.2.5 Impurities and Purification in BMR

The purity of rTA is challenged by contaminants of various sources that primarily accumulate indirectly during the usage of PET. Among these, insoluble contaminants (e.g. pigments) can be separated by simple means of solid-liquid separation. This is because of the target substances DST and EG after alkaline hydrolysis being water soluble. However, instead BMR is challenged by colorants (non-pigment) and other water soluble impurities emanating from every possible user in the supply chain. <sup>62</sup>

These can be classified into four different groups that can be critical in terms of monomer processability, consumer safety or legislation as displayed in Table 3-2.

Table 3-2. Possible impurities and their sources in PET and rTA<sup>100</sup>

Group	Source	<b>Short Description</b>	Examples	
1		By-products of p-		
	Fossil synthesis	xylene oxidation,	4-CBA, p-toluic	
	(3.2.1)	critical for PET	acid	
		manufacturing		
2	PET Manufacturing (3.1.1)	IAS for polycondensation	Antimony catalyst, isophthalic acid-	
3	Application	IAS to tailor and	Residues of	
		restore rPET properties	foreign polymers,	
		(production and post	ink, glue, metals,	
		production)	flame retardants	
4	Usage, recycling and collection	post-consumer residues	Bisphenol A,	
		after usage, non-	foreign polymeric	
		intentional contact	degradation	
	and confection	through mixed	products, food	
		collection	residue	

These groups refer the moment of occurrence of the impurity in the lifecycle of TA and PET respectively.

Generally, BMR is based on PET which is made from highly purified TA, hence critical impurities from fossil synthesis pose a theoretical risk for rTA only (Group 1).

Next to these critical contaminants, three general sources remain as displayed in Table 3-2. The impurities of group 2 are intentionally added substances (IAS) which are used during PET manufacturing by polycondensation except for EG

and TA (process described in 3.1.1). Within this process, foreign substances are represented by metal catalysts mainly antimony and co-monomers like IA or 1,4 cyclohexanedimethanol. On one hand, parts of EG are replaced by cyclohexanedimethanol in the polymer chain which promotes toughness, clarity and solvent resistance of the final PET. On the other hand, up to 5 % of total TA mass is commonly replaced by IA which is added in order to steer PET crystallisation behaviour and thus processability and transparency, especially desired in food packaging and drinking bottles. On a molecular level this can be explained by the angular carboxylic group of IA that interferes with the parallel orientation of the polymer chains (Figure 3-10). Si,101

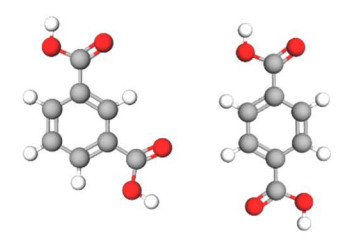


Figure 3-10 Molecular structure of and IA (left) and TA (right). 102

Despite the intentional addition of these substances in order to facilitate polycondensation and alter polymer properties, they cannot be disregarded as impurities in a BMR process.<sup>7,70</sup> On one hand they can degrade, as seen for haze caused by antimony in PET recycling<sup>57</sup>, or participate in disadvantageous side reactions. On the other hand, they could stay inert and accumulate upon addition of more catalyst or co-monomer during re-polycondensation.

As for IA, its structural similarity with TA (Figure 3-10), leads to coprecipitation with TA after acidification of the alkaline hydrolysis product.<sup>68,70</sup> As already small amounts of co-monomer suffice to affect the polymer properties, their dosage must be controlled during manufacturing.<sup>6,7,101</sup> In addition to technical issues, the legal perspective of an obligatory registration of recycled monomeric mixtures must be considered (e.g. European REACH directive).<sup>103</sup> Therefore, a central objective of this research work is the identification of precipitation process parameters that allow for reducing IA content in rTA.

While the contaminants of group 2 comprise a manageable number of substances which eases their identification, group 3 on application and use is significantly larger in consequence of the variety of PET applications. Technical additives have two general objectives: maintaining (e.g. antioxidants, heat stabilisers) or

extending (e.g. flame retardants, antimicrobials) polymer properties. <sup>100</sup> As these substances tend to migrate out of the polymer matrix during mechanical recycling they can pose a risk for consumer safety. Furthermore, application tailored packaging often consists of layers of different polymers in order to combine individual advantages and improve overall packaging performance (e.g. low weight, increased food shelf life). <sup>104</sup>

Considering, the substances from group 2 and 3, to date 885 chemicals (incl. monomers) are registered in the positive list of the European commission for plastic materials intended for food contact. Although, not all of these substances will be used in PET packaging, the sheer number already emphasizes the challenges for purification its verification in BMR. Furthermore, this number refers to food contact additives and will be even larger in technical PET applications.

The last group 4 of contaminants comprises substances originating from usage or collection. This includes for example polyvinylchloride that can depolymerize into hydrochloric acid or polycarbonate leaching Bisphenol A or any organic matter. In terms of foreign polymers, the impurities of this group coincide with tailored packaging made of different polymers (group 3).

Finally, the substances of all groups can degrade during use or depolymerization and could potentially participate in consecutive reactions, adding up to even more possible contaminants. <sup>100</sup> Nevertheless, a save recycling of PET is possible and already widely applied, as displayed in section 3.1.2 regarding the drinking bottle feedstock. This is the result of the closed loop (bottle to bottle) recycling limiting the number of possible contaminants while preserving the polymer matrix.

As mentioned before, the contaminant groups in Table 3-2 are ordered according to their time of appearance in a PET lifecycle. This order is reversed when any kind of recycling is applied. For instance regarding BMR, additives that were initially fixed in the polymer matrix are released during depolymerization and can now add a risk to consumer safety or to polycondensation. <sup>15,100</sup> Therefore, several research groups investigated purification of recycled monomers from alkaline hydrolysis to produce rPET and prove its quality and harmlessness in laboratory and pilot plant scale. <sup>15,16,106</sup>

The research group around Karayannidis et al. depolymerized post-consumer-bottle flakes, common in thermomechanical PET recycling by alkaline hydrolysis. The monomeric rTA contained about 2 wt.-% of IA which they did not consider as impurity. They did not perform any purification treatment apart from filtration, rTA precipitation and a consecutive methanol washing step. The repolymerized PET featured an IV of 0.54 dL/g which is similar in comparison to the results by Franco et al.. Is Instead of bottle flakes, they depolymerized flakes

of PET/PE dual layer trays. They used alkaline hydrolysis with sodium hydroxide as a method, first published by Brepohl and Biermann et al. 14 They recovered both PET monomers EG and rTA which they subsequently used for polymerization of rPET. They performed an additional purification step to remove soluble impurities before precipitating TA. The rTA contained an IA content of 1.4t wt.-% and EG was purified via distillation after rTA recovery. With an IV of 0.599 dL/g their PET possessed a comparable value to vPET (IV = 0.606) which they prepared from PTA and virgin EG. They also held the industrial standard in terms of the measured Hazen colour index being below 10. At last, they tested for nonintentionally added substances (NIAS) in an external institute proving the suitability of their rPET for food contact.<sup>15</sup> A similar investigation was conducted by Kirstein et al. applying the depolymerization approach which was used by Franco et al.. <sup>106</sup> Instead of packaging, they depolymerized mixed polyester textiles of red, blue and black colour. Next to the unknown composition of the polyester mix, it contained a white lining fibre of non-PET origin. They applied an adsorptive treatment prior to precipitating rTA and a separation of EG by distillation as mentioned for Franco et al.15 before. The rTA purity met the industrial specifications apart from an IA content below 0.5 wt.-%. They were able to successfully repolymerize their recycled monomers to PET, despite having EG of antifreeze grade quality. Next to characterizing their rPET by IR spectra, they sent PET in for NIAS analysis The results proved their rPET to be suitable for food contact despite its non-food textile origin. 106

An enzyme-catalysed depolymerization approach was applied by Tournier et al., also using sodium hydroxide. 16 They pre-amorphized and micronized PET residue from post-consumer bottle flakes. Before precipitating TA, they purified the DST solution with activated carbon. In contrast to the aforementioned studies, Tournier et al. implemented an additional recrystallization step for rTA at 250 °C which could explain the absence of IA in their rTA. With a colour index of 2.9, their rTA met the industrial specifications and was subsequently polymerised with virgin EG. The PET polycondensation was followed by a SSP leading to a higher IV of 0.75 dL/g compared to the previous studies. 16 Using recrystallization to avoid incorporation of chemically similar substances into TA crystals was already introduced in the PTA purification step in section 3.2.1. With regard to TA purification in BMR this approach was mentioned by Crippa and Morico suggesting a stepwise crystallization. 6 Such a two-step crystallization process was used by Cheng et al. who precipitated TA from alkali reduction wastewater of polyester plants, as introduced in 3.2.3.19 For recrystallization, they used DMAc as an alternative solvent with improved TA solubility at mild temperatures. The application improved crystal size and purity which they proved by IR

spectroscopy and HPLC analysis. Additionally, they claimed a successful benchscale polycondensation which proved the resulting PET to be of sufficient quality. 19 A comparable feed of alkali weight reduction wastewater was used by Liu and Chen with the objective of recovering highly purified rTA.<sup>89</sup> They applied coagulation sedimentation with aluminium sulfate and adsorption with activated carbon. They evaluated the purification effect of these methods by measuring rTA ash content, thermogravimetry and light transmittance at 340 nm. They found that adsorption and coagulation generally improve purity individually but their combined effect is most effective. 89 This investigation was continued by Liu et al. focusing on determination of optimal parameters for activated carbon treatment. 107 They found that at least 4 g/L of active charcoal were necessary to reach a high transmittance at 340 nm. They stated that purified TA could be precipitated into larger crystals compared to impurified TA through REM imaging and laser diffraction measurement. At last, they successfully repolymerized a mixture containing 30 % rTA with an IV of 0.61 dl/g.<sup>107</sup> Although applying neutral instead of alkaline hydrolysis of virgin PET fibres, the study by Quartinello et al. contains an interesting purification approach in connection to the previously mentioned work by Tournier et al.. 16,108 Since neutral hydrolysis produces oligomeric by-products, subsequent enzymatic depolymerization of these residual oligomers was applied for purification. 108 Their studies on neutral hydrolysis of PET fibres were continued by Valh et al..<sup>12</sup> Instead of enzymatic depolymerization they dissolved the rTA product in sodium hydroxide and removed residual oligomers by filtration of the DST solution. Equal to the product of alkaline hydrolysis they precipitated rTA by acidification with hydrochloric acid. This rTA substituted parts of virgin PTA in their subsequent repolymerization experiments, of which no further details are revealed. 12 A similar purification approach was applied by Slapnik et al..<sup>109</sup> They were supplied with rTA from textile PET which was depolymerized by a partner using alkaline hydrolysis. In a first step they re-dissolved the crude rTA in sodium hydroxide to subsequently remove insoluble impurities by filtration like Valh et al. 12 In the next step, they applied adsorption by activated charcoal and precipitated the rTA with acetic acid. Afterwards, this rTA was dissolved in boiling DMAc and recovered by cooling crystallization similar to the recrystallization by Cheng et al.<sup>19</sup> They also used the transmittance at 340 nm to compare the purity of TA like Liu et al..<sup>107</sup> Afterwards, in different batches purified and crude TA were successfully repolymerized in laboratory scale with virgin EG. Thermograms from differential scanning calorimetry proved the significantly higher quality of the purified TA. Additional Fourier-transform infrared spectroscopy indicated the presence of unreacted TA in PET polymerised from crude rTA. They concluded that their purification step successfully reduced polymerization inhibiting compunds. <sup>109</sup> These examples show the feasibility of BMR for different feedstocks from pure PET and bottle flakes to highly contaminated wastewater and coloured polyester textiles. The purification approaches, often active charcoal adsorption, suffice in improving rTA purity to be re-polymerized and partly reapplied. Among these, especially the NIAS investigations by Kirstein et al. and Franco et al. stand out, as they recycle a complex feedstock to food grade momoners. <sup>15,106</sup>

However, while rTA is precipitated in all of these approaches, the individual effect of the precipitation with its process parameters on rTA purification is not considered at all. Additionally, co-monomer IA is not considered a critical impurity in the cited literature, yet it significantly influences PET properties. Consequently, it is necessary to determine the effect of the precipitation on IA content in rTA in order to provide strategies for its separation. Thus, the purification potential of the precipitation step will be centrally focussed within this work.

Regarding the analytical methods for determination of impurities, it is evident that individual determination of substances is hardly being performed (only NIAS). This can be reasoned as a result of the sheer number of possible substances which can impossibly be individually determined. Therefore, UV/vis spectroscopy displays a common approach within these studies, either as transmittance at 340 nm or for purity determination by colour. The latter is especially relevant since impurities in TA are known to provoke discolouration at already very low levels. For this reason, the Hazen colour index of PTA and PET is a widely applied in PET manufacturing analytics and a substantial quality parameter for BMR. Ta,79,110,111 Within this work, the Hazen colour index therefore serves as sensitive measure for the purification effect of the precipitation step. Additionally, IA will be determined by high performance liquid chromatography (HPLC) according to a method developed by Biermann.

## 3.2.6 Alternative Precipitation Acids Potential

Considering BMR generally, its advantages regarding infinite recycling cycles without quality losses and removal of contaminants already make it a promising technological concept for PET circularity. However, in a life cycle assessment (LCA) study by Paschetag et al. regarding the revolPET® technology, the sulfuric acid used as PA was found to contribute substantially to the environmental impact in several categories e.g. ecotoxicity and terrestrial acidification. They recommend a full recovery and return to the value chain, in order to avoid disposal and negative impact of waste sodium sulfate. For this reason, any BMR process applying rTA precipitation will automatically be producer of the associated PA salt. Tournier et al. stated that the recycling of 100,000 t of PET with their process produces 60,000 t of sodium sulfate, which would make up for 0.28 % of its world market.

Consequently, the considerate choice of a PA with regard to its respective salt could significantly improve the ecological footprint and equally affect process economics regarding a high value PA salt. For the sake of completeness, it shall be mentioned that direct electrolysis can offer an alternative approach to avoid salt waste. 114,115 However, regarding to acidification of rTA, among other issues electrode blocking and low yield is reported, questioning its industrial applicability. 116-118 Instead, a full in-process circularity approach was taken by Crippa and Morico. 6 They precipitated rTA with hydrochloric acid which allowed for subsequent chlorine-alkali electrolysis as a well-established technology. In consequence sodium hydroxide solution for depolymerization and hydrochloric acid for precipitation can be recycled within their process.<sup>6</sup> Apart from the approaches on strong acids, the use of weak acids can display a feasible alternative for TA precipitation regarding higher value by-products like sodium acetate or citrate. However, for theoretically complete recovery of TA during precipitation, the amount of PA must be synchronized with regard to two separate reactions neutralisation excess sodium hydroxide and displacement of the sodium ions in DST. Disregarding acid strength, this can be summed up as a total molar amount of hydronium ions by the PA being equal to the total presence of sodium ions. As the provision and thus concentration of hydronium ions can be measured by the pH value, similar processes are often referred to as pH-shift crystallizations. For these processes the target species is produced in dependence of the maximum yield and the influence of the individual acidification agent is usually not considered/of interest. 62 However, with regard to sparely soluble target substances like TA, product formation involves product removal by precipitation. Therefore, the dissociation of the PA is affected by the low product solubility.

The interdependence of the two reaction equilibria of this pH shift precipitation is visualised in Figure 3-11 for TA.

Figure 3-11 General reaction scheme of TA precipitation from DST with simplified equilibrium of a PA (AR = Acid radical)<sup>17</sup>

Due to high local supersaturations and therefore instant precipitation for TA it can be assumed that product removal by TA precipitation rules equilibrium  $K_R$ . A similar effect is induced regarding the dissociation equilibrium of the PA. As the hydronium ions displace the sodium ions in DST, TA precipitates and the amount of hydronium ions in  $K_R$  is reduced. This shifts the equilibrium  $K_a$  towards its dissociated species. This effect is minor for strong acids like sulfuric acid that independently dissociate nearly completely but gains influence for weaker acids like acetic acid for which equilibrium is naturally shifted towards the undissociated species. In consequence, the provision of hydronium ions by the PA represents the main factor affecting yield, which itself is affected by a product removal. This allows for consideration of weaker PAs regardless of their actual acid strength or the final pH during addition.<sup>17</sup>

In consequence, weak acids extend the variety of suitable PAs which opens up opportunities a more sustainable and economical process, eventually promoting the general position of BMR as a complementary technology for plastics circularity.<sup>49</sup>

# 3.2.7 Influence of pH on Speciation and Supersaturation

Next to the previously described product removal due to low aqueous TA solubility, the effect of the pH on supersaturation shall be examined closer in the following chapter. Considering an aqueous solvent, TA dissociates into protons and different species of its terephthalate ion according to the respective dissociation constants Ka1 and Ka2. These constants are commonly found as pKa

values, representing the negative decadic logarithm of these dissociation constants. The two TA dissociation equilibria can be described with the two corresponding laws of mass action displayed in Equations 3-1 and 3-2.

$$K_{a1} = \frac{[H^+][HTA^-]}{[H_2TA]}$$
 3-1

$$K_{a2} = \frac{[H^+][TA^{2-}]}{[HTA^-]}$$

Considering mass conservation, the following Equation 3-3 can be derived.

$$TA_{total} = [TA^{2-}] + [HTA^{-}] + [H_2TA]$$

These expressions eventually lead to  $\alpha$  as a Factor describing the fraction of the respective species as a function of proton concentration and thus pH.

$$\alpha_{H_2TA} = \frac{[H^+]^2}{[H^+]^2 + K_{a1}[H^+] + K_{a1}K_{a2}}$$
 3-4

$$\alpha_{HTA^-} = \frac{K_{a1}[H^+]}{[H^+]^2 + K_{a1}[H^+] + K_{a1}K_{a2}}$$
 3-5

$$\alpha_{TA^{2-}} = \frac{K_{a1}K_{a2}}{[H^+]^2 + K_{a1}[H^+] + K_{a1}K_{a2}}$$

Plotting these functions over the pH leads to the subsequent Figure 3-12 showing the TA species distribution over the pH. Additionally, the course of supersaturation over pH is included.

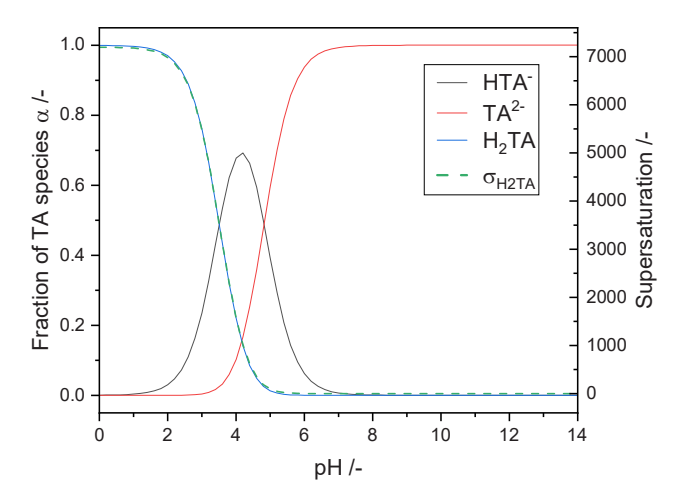


Figure 3-12 Fractions of TA species calculated using a pKa<sub>1</sub> of 3.51 and pKa<sub>2</sub> of 4.51 and concentration-based supersaturation for 0.62 mol/L DST and 3 mol/L sulfuric acid at 36 °C.

At pH values above 7, only ionic terephthalate (TA2-) is present, while below a pH value of 5, the proportion of fully protonated TA (H2TA) increases until a pH value of 1 is reached, at which H2TA is the only species present. Between pH 1 and 7 the partially deprotonated hydrogen terephthalate (HTA-) species occurs, reaching its peak around a pH of 4.2. Its two intersections with the courses of H2TA and TA2- are at the pH values that equal the respective pKa. Focusing on the formation of the target species H2TA by precipitation, it can be derived that elevated pH values above 1 reduce the fraction of sparely soluble H2TA that can be formed. Taking the example of adding a PA to an alkaline DST reactant which results in a pH of 3, according to Figure 3-12 about 75 % of H2TA and 25 % of the HTA- species is being formed.

Regarding Supersaturation under these conditions, this reduces the concentration in the enumerator in equation 2-4 proportionally to the fraction of H2TA species at a given pH as shown be the green dashed line. This dependence is represented by the parallel course of the concentration-based supersaturation to the course of the H2TA species. In consequence, pH control can promote control of supersaturation and therefore precipitation.

Nevertheless, this represents a theoretical example neglecting local mixing deficiencies and thus local pH peaks which lead to higher local supersaturations. In consequence, due to the sparingly soluble nature of TA instant precipitation can temporarily and locally occur. Additionally, as stated in the previous chapter,

the low solubility of TA can affect the dissociation equilibrium of weak PAs. This can lead to an underestimation of the formation of a H2TA at elevated pH conditions as more PA molecules dissociate than indicated by the pKa.

## 3.3 Systematic Approach of this Work

The objective of this work is the development of a concept for precipitation of TA from DST. The incentive is based on the essential recovery of rTA after alkaline hydrolysis of PET as one approach among several in BMR. Due to the more recently aroused interest in BMR, precipitation of TA has only been looked at in a couple studies so far (3.2.3). Among these, the approaches on optimization of the crystallization step apply an additional recrystallization step, introduce mixtures of organic solvents and operate in batches. To date, only two studies were published that focus on the optimization of the precipitation step, of which only one applies pure water as solvent. <sup>18,90</sup> However, high supersaturations during TA precipitation commonly lead to small crystals with a challenging processability behaviour, demanding for an efficient recovery of TA after depolymerization.

Therefore, the objective of this work is the development of a precipitation process with focus on a simple and direct transferability to an industrial BMR process. Therefore, a stirred tank reactor setup for precipitation is used, as a standard industrial precipitation vessel naturally leading to reduced supersaturations. Experimental starting point are parameter studies without additional solvents but water in a model reactant system of PTA dissolved in sodium hydroxide solution forming aqueous DST.

In batch operation, the most influencing process parameters are identified and their potential is evaluated with regard to a large TA crystal size, yield and advantageous processability by fast filtration (without losses).

In the second step, the identified key parameters are applied in the same batch setup but using various depolymerization products. These real depolymerized waste fractions contain the second monomer EG in addition to impurities from PET application (post-consumer/ production). Next to the validation of the influence of these substances on rTA precipitation, the purification potential of the precipitation is evaluated. Thus, the potential of precipitation as a purification step regarding undesired discolouration and especially IA-content is investigated. Finally, following the continuous depolymerization approach of the revolPET® process<sup>14,15</sup> TA precipitation is transferred to a continuous operation and analysed in further parameter studies. With focus on a straight forward and qualitatively advantageous implementation in a revolPET® pilot plant, finally an operational

#### State of the Art

precipitation concept is proposed. Since preparatory purification of PET reactants and subsequent recrystallization of rTA is essential for drop-in specifications, this work concludes with an outlook for future development and research.

# 4 Experimental

# 4.1 Equipment and Procedures

### 4.1.1 Description of Laboratory Setup

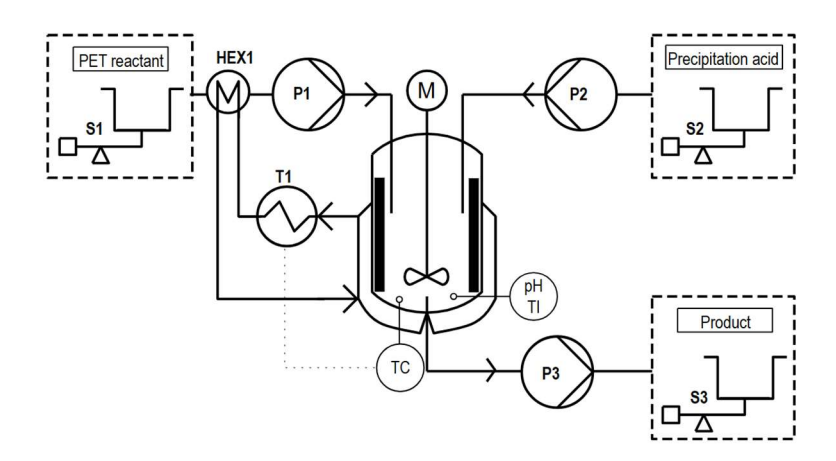


Figure 4-1 Scheme of experimental setup for continuous operation, an image of the setup is displayed in the Appendix Figure 8-2.

The setup of the precipitation experiments is displayed in Figure 4-1, which contains the equipment for batch and continuous operation. The precipitation was conducted in a 2 L (1 L filling volume, height 110 mm) double jacketed glass crystallizer with 4 baffles. Process temperature was measured inside the crystallizer by a resistance type temperature sensor (Pt100) and controlled by means of a thermostat (T1, CC-205B, Peter Huber Kältemaschinenbau SE, Germany). An indirect cooling circuit was established by using a separate thermostat (cryostat R20 CS, Lauda, Germany). The dosing of the PAs was performed by a peristaltic pump P2 (Ismatec, Switzerland) through a tube with 2 mm inner diameter and the position of the dosing nozzle located directly (5 mm) above the stirrer. The necessary quantity of acid being dosed was controlled with a digital scale (S2, HCB 2202, Adam Equipment Co. Ltd., UK). Distribution and mixing of the reaction media were performed using a 65 mm four-blade propeller ("elephant ear") at different stirring rates between 150 and 600 rpm by means of an overhead stirrer (HT-50DX, Witeg Labortechnik GmbH, Germany). For

control of the crystallization process a pH-probe (pH, tecLine HD, Jumo GmbH & Co. KG, Germany) with an integrated PT1000 was used.

During continuous operation the setup was extended by two additional peristaltic pumps (503u, Watson-Marlow, UK) denoted as P1 for the PET reactant and P3 for the product suspension. The outlet of the PET reactant of pump P1 was located directly above the stirrer. In order to maintain a constant temperature in the crystallizer, the PET reactant flow was preheated by a plate heat exchanger (HEX1) before entering the reactor. Furthermore, two digital scales (Signum, Sartorius, Germany) were used to measure PET reactant (S1) and product mass (S2). The inlet tube of P3 was located 10 mm above the reactor bottom withdrawing mixed suspension and avoiding tube blockage by sedimentation.

## 4.1.2 Batch Precipitation Procedure

For the batch experiments, 1 L of model or respective model or PET reactant with a defined DST concentration (Table 4-3) was filled into the described glass crystallizer and heated to the desired process temperature under constant stirring. After reaching the respective target temperature, the PA was dosed at a constant dosing rate. It was varied during specific parameter screening experiments and otherwise set to 30 mL/min, corresponding to a dosing velocity of 0.16 m/s and a Reynolds number of Re = 320 at the nozzle outlet. The dosing volume (mass) of PA was defined in accordance with section 4.2.3, neglecting individual acid strength (equimolar addition) and thus pH. Afterwards the suspension was cooled to 36.5 °C and analysed on filterability (4.3.2). In addition, the crystal size was measured directly from suspension samples. The suspension was subsequently washed and the crystalline rTA from PET reactants was additionally analysed on purity regarding colour index (4.3.5) and IA content (4.3.6).<sup>17</sup> All experiments were conducted as duplicates, if not stated differently in the text.

Example of experimental batch procedure: 1 L of model PET reactant containing 21 g/L DST and an excess of 0.4 g/L sodium hydroxide is heated to 65 °C. After reaching the target temperature, 41.2 g of sulfuric acid with a mass concentration 0.25 gacid/gtotal are dosed at 30 mL/min with the peristaltic pump P2. This amount is sufficient to protonate the terephthalate ion to form terephthalic acid and neutralize excess sodium hydroxide (4.2.3). Afterwards the suspension is cooled to 36.5 °C. During the entire experiment stirring rate is maintained at 300 rpm.

## 4.1.3 Continuous Precipitation Procedure

The general reactor setup of the continuous precipitation procedure can be described as a MSMPR crystallizer. Before starting the continuous operation, the reactor content (1 L) was preheated to the desired target temperature and held constant during the experiments. The subsequent initialization of the precipitation was varied in dependence of the reactor starting content as shown in Table 4-1.

Table 4-1. Crystallizer content and respective initialization procedures at start-up.

	PET reactant (A)		Water (B)		
First step	Batch precipitation	only P2	Continuous precipitation	P1, P2, P3 start directly	
Second step	Continuous precipitation	Start of P1 and P3			

For case A (standard procedure) the reactor was initially filled with PET reactant of a defined DST concentration. The first step is a batch precipitation (Start P2) by acid addition to the chosen target pH with a constant dosing rate as described in the previous section. Afterwards, P1 and P3 are started as well. For case B, the crystallizer does not contain DST solution and consequently no batch precipitation is performed initially. Instead, continuous precipitation begins directly by starting P1, P2 and P3.

Thus, the PET reactant and PA are diluted by the aqueous reactor content. During the continuous process the level inside the crystallizer was monitored visually and controlled manually by adjusting the flow of product pump P3. Likewise, the pH was measured with a pH probe and controlled by changing the flow of the acid pump P2. The initial acid flow was estimated according to section 4.2.3 and manually adjusted to reach and maintain the desired target pH. Manual adjustment was especially relevant as lower yield of depolymerization (Y<sub>Depoly</sub>) induced underestimation of the PA demand. This was due to low UV/vis detected DST but high undetected sodium hydroxide concentration. Figure 4-2 displays the trends of pH, temperature and proportionate acid addition of an exemplified experiment with PET reactant for start-up (case A).

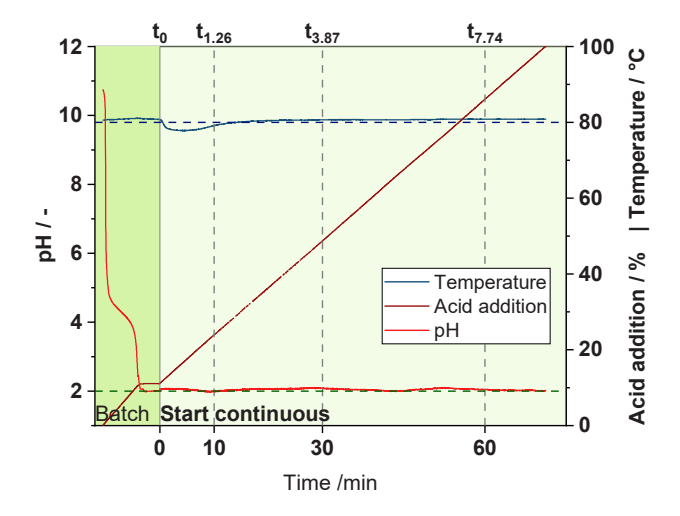


Figure 4-2 Exemplified trends of pH, temperature and acid addition over time during continuous operation.

The continuous operation was performed with 9 L of PET reactant (+1 L at start) of a defined concentration. For long-term experiments the triple amount ( $\sim$ 27 L) was used under otherwise identical conditions. The experimental duration is dictated by the larger mass flow of P1 (P3) ruling the residence time. In order to compare experimental samples for different residence times  $\bar{\tau}$ , the samples were taken after the same multiple of the dimensionless residence time  $\Theta$  with  $t_{i,exp.}$  in Equation 4-1 representing the actual experimental time.

$$\Theta = \frac{t_{i,exp.}}{\bar{\tau}}$$
 4-1

The resulting actual moments of sampling in dependence of the respective residence time are shown in Table 4 2. All experiments were conducted as duplicates, if not stated differently in the text.

Table 4-2 Actual and standardized sample time for different residence times

Dimensionless	residence time $oldsymbol{artheta}$	$\mathbf{t}_0$	t <sub>1.26</sub>	t3.87	<b>t</b> 7.74	t <sub>9</sub>
Residence time $\bar{\tau}$ / min	Approximate volume flow* P1/P2/P3 mL/min	Act	ual sam <sub>l</sub>	oling tin	ne $t_{i,exp.}$ /	min
3.5	61/3.2/64.2	0	4.3	13.3	26.6	31
7.9 (standard)	121/6.2/127.2	0	10	30	60	70
15.7	277/ 14.3/ 291.3	0	20	60	120	140

<sup>\*</sup>Mass flows of pump P2 and P3 represent example estimations considering DST content of 26.6 g/L,  $Y_{depoly} = 0.9$  and sulfuric acid as PA with 0.25  $g_{acid}/g_{total}$ . Change of Volume due to solid forming reaction is neglected for P3 and calculation of  $\bar{\tau}$ .

Example of continuous experimental procedure: 1 L of model PET reactant containing 26.6 g/L DST and an approximate excess of 1.1 g/L sodium hydroxide (assuming  $Y_{depoly}$  of ca. 0.95) is heated to 80 °C. After reaching the target temperature, sulfuric acid with a mass concentration 0.25 gacid/gtotal is dosed at 30 mL/min with pump P2. In parallel the pH is controlled with a pH probe to assure the target pH of 2 being reached. As the final amount of sulfuric acid for precipitation is based on an estimation of  $Y_{depoly}$  the actual dosed amount can differ from this calculation (4.2.3). In example instead of 54.9 g, 57.9 g sulfuric acid are dosed to reach the target pH (Y<sub>depoly</sub> of ca. 0.9). Using equation 4-4 and the target residence time of 7.9 min, the approximate mass flow of acid pump P2 for the continuous is calculated (7.3 g/min). The approximate mass flow of the PET reactant pump P1 for the continuous experiment is 121 g/min. Before starting the continuous procedure, the first sample to is taken, representing the batch precipitation. Afterwards, pumps P1, P2 and P3 are started. Over the course of the experiment flow of pump P3 is manually adjusted to maintain a constant level at 1 L filling volume in the reactor. Likewise pump P2 is manually adjusted when pH is starting to drift more than 0.15 one sided of the target pH. Samples during the continuous experiment are taken in accordance with Table 4-2. During the entire experiment stirring rate is maintained at 300 rpm. After 70 min the last sample is taken and the experiment is stopped. The samples are left to cool and analysed subsequently.

## 4.1.4 Experimental Scope

In the experiments of this work, different parameters were varied which, according to chapter 2.5, have an influence on the quality properties, crystal size, purity and processability of the precipitated TA. Therefore, in the first part, several process parameters were screened using a model reactant system to avoid influences on crystal size or processability of impurities. Subsequently, investigations were continued on real depolymerized PET waste, allowing an additional evaluation of the purification potential of the precipitation step. Finally, the setup is transferred to continuous operation during which the most advantageous parameters of the batch experiments were applied while opening up new possible parameters. Table 4-3 contains the scope of the parameter variations of the conducted experiments. Further details regarding the respective reactants and PA is displayed the following chapter 4.2.1.

Table 4-3 Experimental parameters.

	Parameter	Variation
	Model Reactant-	21 g <sub>DST</sub> /L
	concentration	(~ 0.1 mol/L)
ch	Precipitation acid	CH <sub>3</sub> COOH; H <sub>2</sub> SO <sub>4</sub> , HCl, H <sub>3</sub> PO <sub>4</sub> ,
Bat		(COOH)2, Citric Acid
del	CH <sub>3</sub> COOH concentration	7.7 wt%– 98.5 wt%
Model Batch	Temperature	$8^{\circ}\text{C} - 90^{\circ}\text{C}$
	Stirring rate	150 RPM- 450 RPM
	Acid dosing speed	6 mL/min – 54 mL/min
	PET Reactant concentration	26.6 g <sub>DST</sub> /L (~ 0.13 mol/L)
çh	PET reactant	PET light blue, PET/PE, Undersized
3ate		PET
PET Batch	Precipitation Acid	CH <sub>3</sub> COOH; H <sub>2</sub> SO <sub>4</sub>
PE	Acid concentration	25 wt%
	Temperature	$60^{\circ}\text{C} - 90^{\circ}\text{C}$

	PET Reactant concentration	26.6 g <sub>DST</sub> /L- 75.9 g <sub>DST</sub> /L
		(0.13 ~0.36 mol/L)
S	PET reactant	PET light blue, PET/PE
10 <b>n</b>	Precipitation Acid	$CH_3COOH, H_2SO_4*,$
continuous	H <sub>2</sub> SO <sub>4</sub> concentration	*(25 wt% - 96 wt%)
	Temperature	80 °C
PET	Residence Time	$3.5 \min - 15.7 \min$
Ы	Stirring rate	300 RPM; 600 RPM
	Start-up content	Water, Seed crystals, Reactant
	Target pH	2 - 4

Additionally, a scope of the supersaturation based on calculations of the maximal concentrations (Equation 2-4) is presented in Figure 4-3. It assumes a complete dissociation of the PA, disregarding dissociation equilibria.

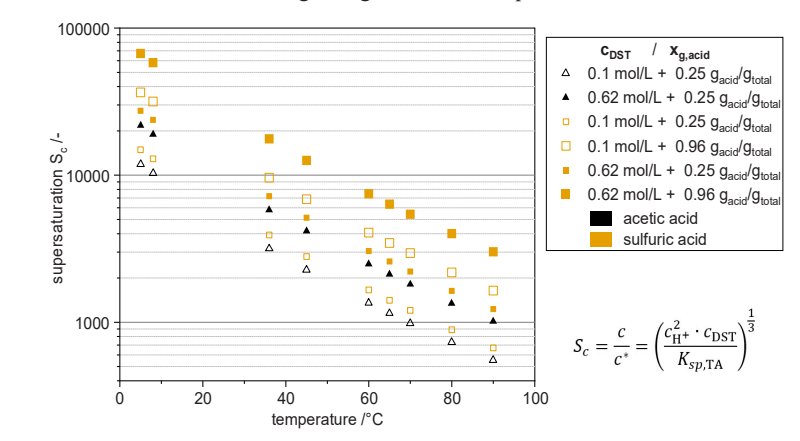


Figure 4-3 Maximal supersaturation based on concentrations<sup>29</sup> over precipitation temperature, 0.62 mol/L refers to DST solubility limit<sup>74,120</sup>, solubility product  $K_{SP,TA}$  was calculated using solubility correlation by Han et al.<sup>96</sup>.

For calculation of the solubility product K<sub>SP,TA</sub>, a TA solubility correlation by Han et al. is applied. <sup>96</sup> Moreover, 0.1 mol/L of DST refers to the concentration applied during model system experiments whereas 0.62 mol/L refers to the approximate DST solubility limit around 140 g/L below 100 °C. <sup>74,120</sup> Together with the PA concentrations of 25 wt.-% (standard concentration) and 96 wt.-% the displayed supersaturations are stretched over several orders of magnitude in dependence of temperature. However, as these are based on (maximal) concentrations and not

## Experimental

activities, their range overestimates the supersaturations under realistic conditions. This overestimation would be particularly pronounced for weak acetic acid. Nevertheless, the diagram clearly emphasizes the influence of temperature on solubility and consequently supersaturation.

#### 4.2 Materials

# 4.2.1 Reactants for Precipitation Experiments

The following table contains the reactants used for preparation of the model reactant and the used PAs. The concentrations of the respective PAs applied in the experiments were prepared on mass basis by dilution with deionised water. Thus, all displayed percentages refer to weight- % (wt.-% =  $g_{substance}/100~g_{total}$ ). Where applicable, PAs were diluted to the target concentration of 25 wt.-% before usage, unless stated differently.

Table 4-4 Chemical substances used as reactants in precipitation experiments.

Substance (concentration)	Manufacturer	Purity
Terephthalic acid (solid)	Acros Organics	≥ 99 %
Isophthalic acid (solid)	Sigma Aldrich	≥ 99 %
Sodium hydroxide (solid)	Carl Roth	≥ 98 %
Sulfuric acid (25 %; 96 %)	Carl Roth; Sigma Aldrich	≥ 98 %
Acetic acid (99.7 %)	Sigma Aldrich	≥ 99.85 %
Oxalic Acid (solid)	Sigma Aldrich	≥ 98 %
Orthophosphoric acid (25 %)	Carl Roth	≥99 %
Hydrochloric acid (25 %)	Carl Roth	≥99 %
Citric acid (solid)	Carl Roth	≥ 99.5 %

#### Experimental

# 4.2.2 Analytical

The substances contained in Table 4-5 were applied during purity analysis of rTA. This comprises suitable solvents to facilitate rTA liquid analytics as well as reagents for chromatographic analysis as described in section 4.3.6

Table 4-5. Chemical substances for analytical purposes.

Substance	Manufacturer	Purity	
Dimethyl formamide	Carl Roth	≥ 99.8 %, p.a.; ACS	
Orthophosphoric acid (85 %)	Carl Roth	≥ 99 %, p.a.	
Ammonia solution (25 %)	Carl Roth; Thermo Fisher scientific	≥ 99 %, p.a.	
Acetonitrile	VWR	≥ 99.9 %; HPLC Grade	

# 4.2.3 Dosage Quantity of Precipitation Acids

The dosage quantity of the respective PA can be calculated using Equation 4-3 derived from molar balance in Equation 4-2.

This equation is used for the examination on yield and pH effect for the different

$$n_{Na^+} = n_{NaOH.excess} + 2 \cdot n_{DST} = n_{PA} \cdot z_{H^+PA}$$
 4-2

$$m_{PA} = \frac{\left(2 + \nu_{NaOH,excess}\right)}{Y_{Depoly}} \cdot \frac{m_{DST}}{M_{DST}} \cdot \frac{M_{PA}}{Z_{H^+}} = n_{Na^+} \cdot \frac{M_{PA}}{Z_{H^+,PA}}$$
 4-3

PAs in Section 5.1.3.1 (model reactant with  $Y_{Depoly} = 1$ ). With regard to PET reactants, the yield of depolymerization has to be considered, since complete PET conversion cannot be reached. Additionally, sodium hydroxide is added stoichiometrically with regard to the PET material input and its amount is not adjusted to the PET content of the polymeric material. Therefore, the mere measurement of DST concentration by UV/vis spectroscopy (4.3.4) does not suffice for determination of PA dosage quantity. In other words, TA precipitation from a PET reactant with a low DST concentration and low depolymerization yield requires the same amount of PA for a high yield depolymerization with the same throughput. The influence of varying concentrations of sodium hydroxide of PET reactants was targeted by a manual adjustment of the pH to the desired target value during the experiment.

A close approximation and validation of the PA mass flow during continuous operation was additionally adopted from the initial batch precipitation ("titration"). By using the PA quantity during the Batch start-up (case A) and the expected residence time with regard to the DST flow, the PA flow could be estimated applying Equation 4-4.

$$\dot{m}_{PA,conti} = \frac{m_{PA,Batch}}{\tau_{f(\dot{m}_{DST,conti})}}$$
 4-4

#### 4.2.4 PET Reactants

The PET reactants used within this work were produced through the revolPET® process. A detailed description of the depolymerization procedure for production of the PET reactants is found in Section 3.1.3.2. The provided PET reactants varied in their degree of depolymerization and thus DST concentration. In order to maintain constant experimental conditions, the reactants were diluted to the desired target DST concentration with demineralized water prior to precipitation (4.1.4). Table 4-6 provides a short overview on the applied PET reactants and their original supply prior to depolymerization by RITTEC 8.0 Umwelttechnik GmbH.

Table 4-6. Overview of the original application and source of the used PET reactants.

PET	Original application	Source	
reactant			
PET light blue	blue/colourless mono layer PET, washed and shredded bottle flakes, used in bottle recycling, post- consumer	Source One GmbH	
PET/PE	Dual layer of PET with PE, colourless cuttings of food trays, post-production	W.u.H. Fernholz GmbH & Co. KG	
Undersized PET	Lightly blue coloured, mono layer PET, sieve residue (< 2 mm) of bottle recycling, post-consumer	Veolia environmental services S.A	
Model reactant	Made from PTA		

The model reactant used for comparative reasons was produced by dissolving TA in aqueous sodium hydroxide solution. Sodium hydroxide was used at a hyper stoichiometric factor of 2.1 moles per mole TA in order to ensure complete dissolution. For the initial parameter screening studies, a reference concentration of  $\sim$ 21 g<sub>DST</sub>/L equalling 0.1 mol/L for the model reactant was used.<sup>17</sup>

# 4.3 Analysis

The following section contains the conducted analytical procedures for evaluation and preparation of the precipitation experiments and reactants. The first group presents the analytical equipment and procedures used for determination of processability correlated parameters crystal size, morphology and filterability. The second group comprises tools and procedures for determination of yield and TA purity in terms of colour index and IA content.

#### 4.3.1 Particle Size Measurement

Particle size was determined using a laser diffraction spectrometer with wet dispersing unit by (Helos Kr + Quixel, Sympatec GmbH, Germany). Due to the alkalinity of tap water which partially dissolved TA crystals, measurements were performed in deionised water. Ultrasound was applied for 15 s to homogenize sample conditions while avoiding crystal breakage. Analysis and calculation of particle size was done by proprietary software (Windox 5, Sympatec GmbH, Germany) in accordance to the Fraunhofer diffraction model. Despite the limits of the model in terms of particle size, it is reported to be more applicable to needle shaped crystals. Thus, it has to be considered that the measurement results refer to an equivalent mean particle diameter of a sphere, while precipitated TA possesses a pronounced needle or rod shape. Therefore, measured distributions can appear wide or bimodal as they represent varying dimensions (e.g. length and width) of a non-spherical needle crystal. 17,122

For presentation of the resulting broad distributions the logarithmic volume-related density  $q_3^*$  and cumulative distributions as functions of the equivalent mean particle diameter x are used. For the density distribution it is assumed that the logarithm of the particle size and not the particle size itself is expected to be normally distributed.<sup>17</sup> In order to display the time dependent courses of the continuous precipitation experiments, the 10 %, 50 % and 90 % quantiles (= wt.-% for constant product density) of the volumetric cumulative distribution  $Q_3$  are used, also known as  $x_{3,10}$ ,  $x_{3,50}$  and  $x_{3,90}$ .

# 4.3.2 Filterability

Filtration of TA suspension was performed using a 750 mL stainless steel vacuum suction strainer with a filtration area of 56 cm $^2$ . A polypropylene (PP) filter cloth (PPD3143, Markert Filtration GmbH, Germany) with 19  $\mu$ m mesh openings was

inserted as filter media. 123 Vacuum was supplied by a vacuum generator (VP20-150 H, Sommer-Technik GmbH, Germany) and initially set to 500 mbar vacuum pressure by leak air valve adjustment.

The setup is displayed in Figure 4-4. It was adopted from an industrial setup used for testing and design of belt and pressure filters. 124

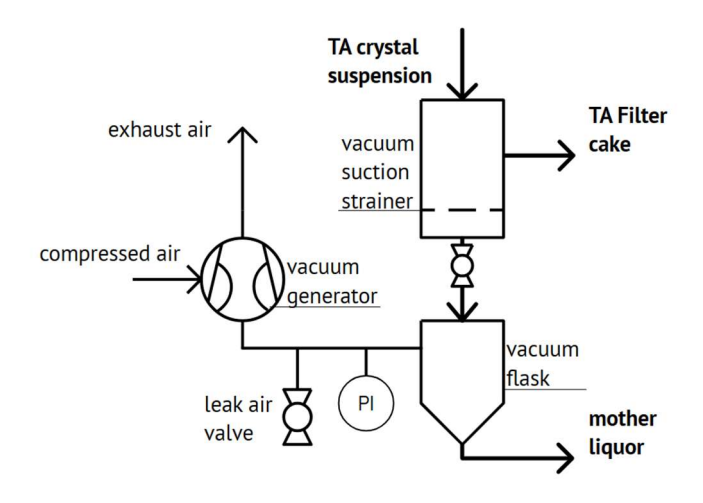


Figure 4-4 Vacuum suction strainer setup for filtration time determination.

The time for filtration was determined for 500 mL of suspension in batch experiments and 200 mL for continuous experiments. At the start of the filtration time measurement, the valve below the strainer was opened. Stop watch time was stopped when solid filter cake appeared at the bottom and slightly contracted towards its centre. Subsequently, the filter cake was washed twice, each time applying 200 mL distilled water. Due to the manual procedure, unwanted cracks in the filter cake could not always be avoided. Although, the filter cloth was washed between experiments and rinsed regularly with sodium hydroxide solution, partial blockage of the filter probably occurred. In consequence, exact filtration time can be partially compromised and must only be compared (absolute values) within an experimental series.

In order to compare filtration times for different PAs with different TA yields inducing different filter cake mass, the filtration time is normalized with the yield of the respective PA at equimolar addition shown in Equation 4-5 (5.1.3.1).

$$normalized filtration time = \frac{filtration time}{equimolar Yield_{PA}}$$
 4-5

This normalization puts a potentially faster filtration time due to less crystal mass into perspective with a slower filtration of a high yield PA.

# 4.3.3 Morphology

The results of the laser diffraction measurements refer to the equivalent diameter of spherical particles. These differ substantially from needle shaped TA crystals and demand for qualitative verification. Therefore, scanning electron microscopy (SEM) was performed (Evo LS 25, Carl Zeiss AG, Germany) to visually analyse the TA crystals. The crystals were separated from mother liquor first, then washed and slurried in deionised water in order to remove residual acid residue salt and DST. Afterwards, a drop of the slurried suspension was placed on SEM Sampling plates and dried prior to microscopy.

#### 4.3.4 Concentration Measurement

Measurements were performed with a UV-spectrometer (Specord 210 Plus, Analytik-Jena GmbH & Co. KG, Germany). Particle free samples were transferred in UV-capable glass cuvettes with 10 mm light path length and measured at 270 nm. The corresponding calibration data for DST dilutions between  $6\cdot10^{-4}~g_{DST}/L$  and  $8\cdot10^{-2}~g_{DST}/L$  is shown with its linear fit in the Appendix, Figure 8-3.

This method was applied for determination of initial DST content and adjustment to the desired concentration of depolymerized PET reactants (Equation 4-6).

absorbance 
$$(270 \text{ nm}) = 9.5524 \cdot c_{DST} - 0.005$$
 4-6

Yield of precipitated TA ( $Y_{TA}$ ) was determined by measuring the residual DST  $c_{DST,residual}$  concentration in the mother liquor of the filtered samples, using Equation 4-7 with the initial DST concentration  $c_{DST,initial}$ .

$$Y_{TA} = 1 - \frac{c_{DST,residual}}{c_{DST,initial}}$$
 4-7

#### 4.3.5 Hazen Colour Index

The Hazen colour index was adopted as quality parameter from industrial PET and PTA manufacturing. It is used as a general approach on determination of the degree of rTA impurification. Values below 10 meet the industrial specifications and imply a practically white TA. <sup>125</sup> Samples exceeding a colour index of 10 possess an undesired yellow discolouration. In order to determine the colour index, the washed rTA samples were dried at ca. 70 °C until weight remained constant. The dry rTA was subsequently homogenized with a mortar. 0.5 g of the resulting powder were dissolved in 10mL of 2 mol/L (2 N) ammonia solution or dimethyl formamide (DMF) and centrifuged to separate undissolved solid residues. <sup>14,102,106,110</sup> Transmission measurements were performed between 360 nm and 830 nm with a spectrometer (Specord 210 Plus, Analytik-Jena GmbH & Co. KG, Germany). Automatic calculation of the Hazen colour index was conducted with proprietary software (Aspect UV Analytik-Jena GmbH & Co. KG, Germany) in accordance with ASTM5385-05 and ASTM-E-313.

## 4.3.6 Isophthalic Acid Content

In order to determine the IA content in TA, the samples prepared in the previous section 4.3.5 were diluted with ultrapure water by 1:25. The subsequent analysis was performed with an HPLC (ULTIMATE 3000, Thermo Fisher scientific, US), equipped with a UV detector (240 nm) and a reversed Phase column (Gemini 3u C18 110A, Phenomenex Ltd., Germany). The eluent consisted of 82 % phosphoric acid ( $c_{H3PO4} = 1.01 \text{ g/L}$ ) and 18 % acetonitrile with a flow rate of 0.4 mL/min. Column temperature was set to 35 °C  $^{106}$  and total measurement time 25 min. Retention time of TA was 3.4 and IA 4.3 min under these conditions. The linear fit used for determination of the IA content is displayed in the Appendix in Figure 8-4.

# 5 Batch Precipitation of Terephthalic Acid

In the first part of this investigation a model reactant system is used, consisting of purified TA dissolved in sodium hydroxide to form an aqueous DST solution. This particular reactant is employed for parameter screening in batch operation. This allows for identification of the most influencing parameters on TA precipitation independent from reactant provision by depolymerization and impurities. Hence, in accordance with section 2.5, solvent properties through varying temperature and PA as well as reactant concentration, stirring rate and dosing strategies affecting dispersion are focused as target parameters in controlling supersaturation. The efficacy of the parameters is evaluated regarding large TA crystal size and good filterability, representing central TA quality features within this work. Subsequently, parameters with the highest potential are applied on precipitation in (real) PET reactant systems.

# 5.1 Screening of Optimal Parameters in Model System

Parts of the results presented in this chapter have been published in the ACS journal of Industrial and Engineering Chemistry Research.<sup>17</sup> A significant part of the experimental work and raw data originates form the master thesis by Carina Heck.<sup>126</sup>

## 5.1.1 Effect of Temperature and Precipitation Acid

In accordance with literature for the first experiments, sulfuric acid as a strong protonation agent was chosen as reference precipitation acid (PA). As dilution of reactant concentration leads to large process streams, instead TA solubility increase was targeted for reduction of supersaturation. Despite the low absolute TA solubility below 100 °C (see 3.2.4), its significant relative increase by factor ~3 can equally reduce supersaturation. Thus, as displayed in Figure 4-3, concentration-based supersaturation is reduced from ~4000 to ~600 for sulfuric and similarly acetic acid between 36.5 °C and 90 °C.

This influence of TA precipitated with sulfuric acid (0.25 g<sub>acid</sub>/g<sub>total</sub>) from aqueous DST solution according to the method described in 4.1.2 was determined. Figure 5-1 shows the cumulative volume-related particle size distribution (PSD) Q<sub>3</sub> of TA precipitated at temperatures between 36.5 °C and 90 °C.

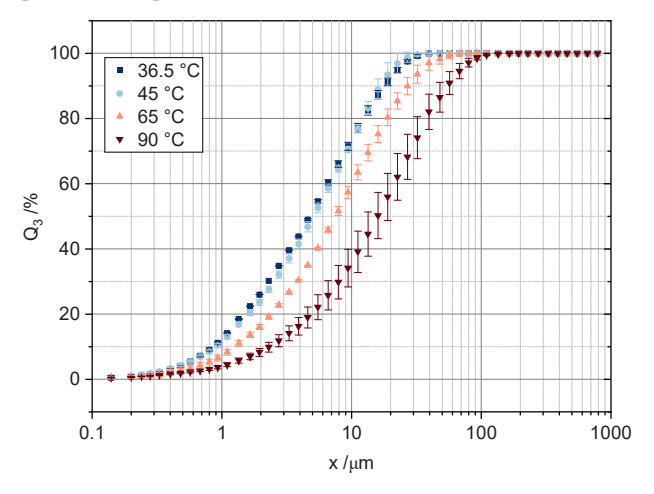


Figure 5-1 Volume-related cumulative PSD of TA after precipitation with sulfuric acid at different temperatures. 17

In accordance with increasing temperature, the particle diameter equivalent x increases as well, being a prove for the effect of an increasing solubility of TA with temperature on crystal size. Thus, supersaturation is reduced, leading the system to lower nucleation rates, which reduce the formation of excessive fine material, characteristic of higher nucleation rates. <sup>29</sup> Thus, while at 36.5 °C about 70 % of the crystal population are smaller than 10  $\mu$ m, for 90 °C it is only 35 %. Moreover, the crystal growth predominates over the nucleation and is fostered by a faster diffusive mass transport due to the temperature increase. <sup>127</sup> The  $x_{3,10}$ 

values increase from  $0.8 \,\mu m$  to  $2.3 \,\mu m$ ,  $x_{3,50}$  from  $4.6 \,\mu m$  to  $16 \,\mu m$  and  $x_{3,90}$  values  $18 \,\mu m$  to  $57 \,\mu m$ . In consequence, a reduction of supersaturation by  $80 \,\%$  leads to a similar increase of quantile values by factor 3.

Another effect between solubility and particle size can be retrieved from the almost identical 36.5 °C and 45 °C curves, as solubility remains almost constant in this region (Figure 3-9). Instead the 65 °C and 90 °C distributions widen and show larger crystal sizes. <sup>17</sup> The effect of temperature on the crystal size of TA is significantly more pronounced in comparison to a study reported by Marlena et al. who varied temperature between 30 °C and 70 °C in a similar setup. <sup>90</sup>

As introduced in 3.2.6, the low solubility of TA represents a quasi-removal of the crystalline reaction product which consequently affects the dissociation equilibrium of weaker PAs. Thus, the application of weak acetic acid, as PA and simultaneous solubility enhancer represents an interesting alternative. Following the previously shown results for sulfuric acid, the same procedure was applied for precipitation with acetic acid. The respective results are shown in Figure 5-2 for temperatures between 8 °C and 90 °C.

The distributions show an even more pronounced effect of temperature compared to sulfuric acid. The acetic acid distributions are clearly separated and show a

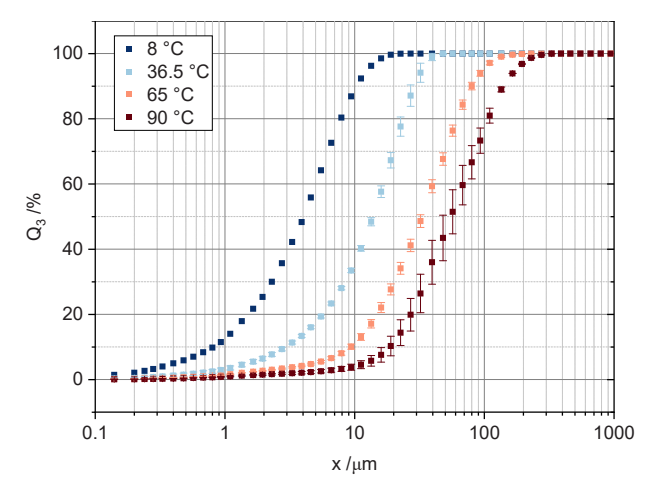


Figure 5-2 Volume-related cumulative PSD of TA after precipitation with acetic acid at different temperatures, 8 °C acetic acid represents single measurement only. 17

distinct temperature influence. Thus, for 36.5 °C about 40 % of the population

consist of fines smaller 10  $\mu$ m, while for 90 °C, it is less than 10 %. Additionally, the width of the distributions, the absolute difference between the  $x_{3,10}$  and  $x_{3,90}$  quantiles increases significantly, from 27  $\mu$ m at 36.5 °C to 117  $\mu$ m at 90 °C. This indicates a more pronounced longitudinal growth of the TA needles, as shown in Müller et al..<sup>17,122</sup> Thus, in addition to a reduced supersaturation growth rate increases with temperature as well. The separate effects of temperature and supersaturation were shown by Mullin and Osman for nickel ammonium phosphate.<sup>128</sup> At moderate but constant supersaturations, the increase in growth rate due to increased temperature contributed significantly to an increase in crystal size. Likewise, a reduction of supersaturation from 5 to 1 at constant temperature almost doubled mean crystal size. As both effects are simultaneously exploited on TA here, their results appear reasonable.

Figure 5-3 shows SEM images at 1000 x magnification for TA precipitated with both acids at 90 °C. While maintaining an overall needle-shape with visible steps, TA crystals obtained in acetic acid are also about 10 times thicker and longer than the ones obtained by sulfuric acid.

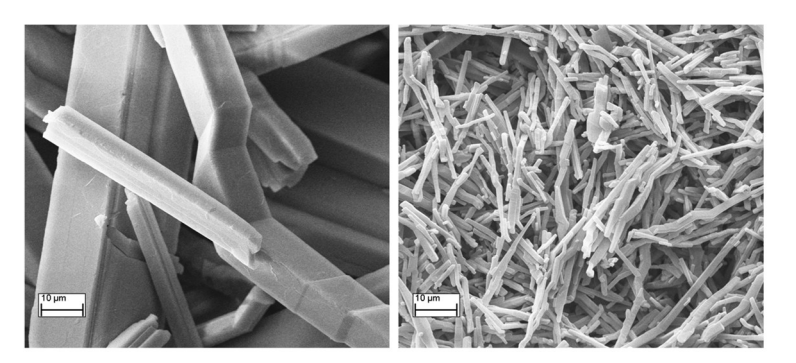


Figure 5-3 SEM images of TA precipitated with acetic (left) and sulfuric acid (right) precipitated at 90 °C.

The significant difference in crystal size is induced by temperature leading to enhanced TA solubility and consequently reduced supersaturation through acetic acid. While this reduces nucleation rate and the generation of fines, the elevated temperature additionally promotes diffusive mass transport and thus crystal surface growth. 127 These differences in crystal appearance are also visible in the crystallization behaviour when adding the PA during experiments. For sulfuric acid, dosing instantly results in formation of white precipitate and initial flocculates. Instead, dosing of acetic acid shows a significant induction time with a gradually increasing turbidity as crystallization advances. This shows that the

initial concentration of freely available hydronium ions is too low to form clearly visible amounts of TA crystals as weak acetic acid remains undissociated. This retarded hydronium ion provision reduces the effective supersaturation and is subsequently affected by the mentioned quasi-removal of the TA product.

From a processability perspective these differences in crystal size are also reflected by the filtration behaviour. Figure 5-4 shows the respective normalized filtration times in dependence of the respective precipitation temperature and acid. The results do not contain the data for 8°C acetic acid, as it could not be filtrated successfully due to the displayed 90 % of fines. As precipitation experiments were conducted with equimolar PA addition, the TA crystal mass for acetic acid is ~20 % lower than for sulfuric acid (see yield in 5.1.3.1). As these differences in

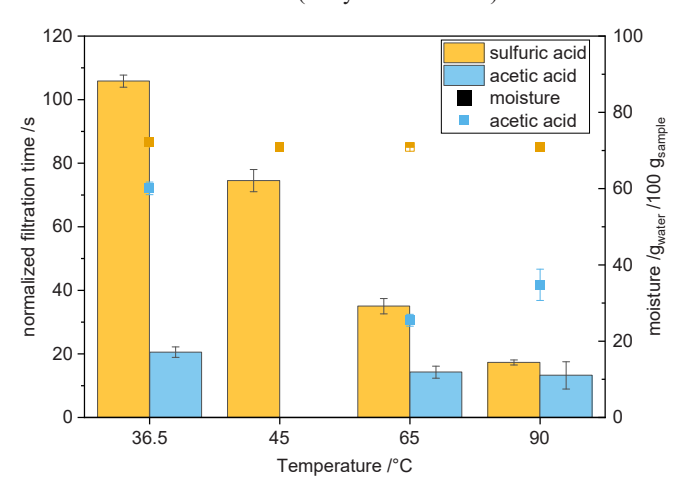


Figure 5-4 Normalized filtration times and residual cake moisture of TA precipitated with sulfuric and acetic acid at different temperatures.

yield promote apparently shorter absolute filtration times for acetic acid, they were normalized with the yield of the individual PA ( $Y_{acetic} \sim 0.78$ ;  $Y_{sulfuric} \sim 1$ ) as explained in 4.3.2. Nevertheless, the main contributor for filtration time is the significant difference in crystal size.

Thus, at 36.5 °C TA obtained by sulfuric acid contains about 70 % of fines compared to 40 % for acetic acid. At 90 °C sulfuric acid passes the 40 % limit which is also reflected by similar filtration times to acetic acid at 36.5 °C. Nevertheless, for sulfuric acid, filtration times decrease as precipitation temperatures increase. Accordingly, a relative decrease in supersaturation by

factor  $\sim$ 5 induces 5 times shorter filtration between 36.5 °C and 90 °C. It can be deduced that the reduction of fines primarily contributes to the reduction in filtration time. Additionally, as the decrease in filtration time also continues for 36.5 °C and 45 °C, it proves the sensitivity of filterability as a quality parameter, since almost no differences in PSD could be observed in this region.

This was also shown by Lee at al. who precipitated TA with sulfuric acid and additionally using DMSO as a co-solvent. 18 Despite similar crystal sizes for their 25 °C and 60 °C experiments the specific cake resistance was almost halved for the higher temperature.

Regarding acetic acid, the almost proportional relation between filtration time and temperature dependent solubility is less pronounced, despite the generally larger differences in solubility and crystal size. While this can be attributed to the significantly lower amount of fines for all samples, it can similarly be due to limitations of the experimental setup for vacuum filtration. Thus, for the applied system parameters (pressure, airflow, solids content, suspension volume) the maximum filtration speed is already reached and the filter cake does not significantly contribute to the filter cake resistance. With regard to residual moisture in the filter cake as a measure for the necessary drying effort, significant PA differences appear in Figure 5-4. While sulfuric acid TA remains at ~70 % moisture regardless of temperature, acetic acid TA moisture is reduced from 60 % to ~30 % with increasing temperature. This is the clear result of the reduced specific surface of acetic acid TA as displayed in Figure 5-3 in comparison to sulfuric acid TA. However, this parameter appears not as sensitive as filtration times for evaluating processability.

In conclusion, the two investigated parameters (PA and temperature) display promising results. In contrast to approaches applying solvent mixtures or recrystallization leading to improved processability, the displayed method does without additional organic solvents. <sup>18,19</sup> Instead, the system inherent temperature dependence on solubility and a solubility enhancing PA are advantageously exploited. Additionally, the usage of a stirred tank naturally reduces supersaturation as the reactants are diluted and direct contact is avoided. <sup>129</sup>

## 5.1.2 Reactant Dispersion

As introduced in chapter 2.4, dispersion of reactants displays a key parameter for controlling precipitation processes. This is due to its potential in providing even reactant distribution and thus, avoidance of local concentration and supersaturation peaks that induce strong nucleation events in precipitation. Additionally, it can support mass transport of otherwise diffusion limited reactions. On the other hand, increased energy input can lead to crystal abrasion and breakage increasing fines and possibly induce additional secondary nucleation. In this chapter, dispersion is targeted through variation of different parameters, namely stirring rate, dosing velocity and PA concentration.

At first, the effect of an increased stirring rate on precipitation of TA is displayed in Figure 5-5.

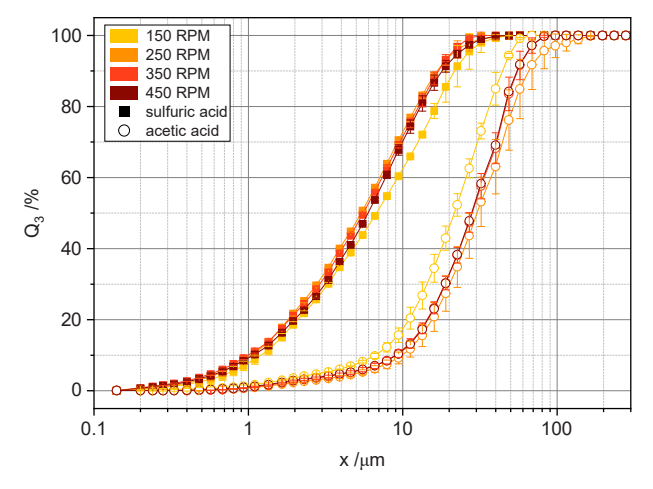


Figure 5-5 Volume-related cumulative PSD of TA after precipitation with sulfuric (45 °C) and acetic acid (65 °C) at different stirring rates, lines are shown to guide the eye.

The volume-related cumulative PSDs are displayed for TA precipitated with sulfuric acid at 45 °C and acetic acid at 65 °C. The distributions for sulfuric acid are almost identical for stirring rates (circumferential velocity  $u_{tip}$ ) of 250 rpm ( $u_{tip}$ = 0.85 m/s) upwards with about 70 % of fines.

The 150 rpm curve instead, shows a slight reduction to 60 % of fines and higher deviations for values exceeding 10  $\mu m$ . Additionally, these distribution values are slightly shifted towards larger particle diameter equivalents. Since, no increase in fines occurs at higher stirring rates it can be deduced that under the given low

supersaturations no significant secondary nucleation could be induced. Nevertheless, the lowest stirring rate promoted growth of longer needles despite a potentially uneven reactant concentrations and higher local supersaturation peaks.

For acetic acid, the contrary effect can be observed as the lowest stirring rate leads to a slightly shifted distribution towards smaller sized crystals. Thus, the amount of fines increases from 10 % to around 15 % for 150 rpm. Similar to sulfuric acid, the respective deviations between repetitive experiments are also higher for these experiments. However, the deviations for precipitation with acetic acid are increased for all distributions, which can be traced back to the irregular dendritical structure presented before. Nevertheless, within the varied parameter range an increased energy input leads to more homogeneous distributions, regardless of the PA. Additionally, higher stirring rates do not induce significant particle breakage, neither for larger acetic acid crystals nor for smaller sulfuric acid TA. Generally, the results lead to the conclusion that mixing in the chosen stirred tank reactor setup displays a low impact in increasing particle size within the experimented parameter range. This is in congruence with the results on TA precipitation by Marlena et al.. They found that mean crystal size slightly decreased when increasing paddle impeller revolutions from 120 rpm to 420 rpm in their semibatch setup. 90 In extensive studies on the semi-batch precipitation of chemically similar benzoic acid by Åslund and Rasmuson as well as Torbacke and Rasmuson covered a wide range of mixing related conditions. 42,45 As they applied strong hydrochloric acid on sodium benzoate, their results can rather be compared to sulfuric acid within this work. Thus, with increasing stirring rate, mean crystal size increases at first while a further increase induces a reduction which they correlated to secondary nucleation, attrition and crystal breakage. They state, that especially an increased mixing intensity at the feed point and macroscale circulation promote a large mean crystal size. The small differences observed in the experiments of this work, lead to the conclusion that the varied mixing intensities did not suffice to significantly disturb the crystallization behaviour.

However, next to a desirable process robustness regarding mixing conditions, an additional explanation can be limitations due to the chosen range of further mixing related parameters. Therefore, additional experiments were conducted to stress the impact of mixing by changing the standard dosing rate of 30 mL/min. The respective volume-related cumulative PSDs are displayed in Figure 5-6.

For precipitation with sulfuric acid, a change in PA dosing speed does not significantly affect PSD. Within the investigated parameter range, supersaturation peaks cannot be avoided, leading to a PSD being unaffected by slow dosing or

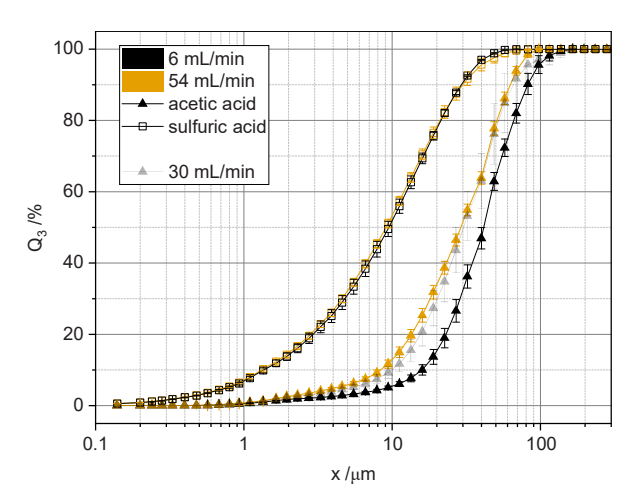


Figure 5-6 Volume-related cumulative PSDs of TA after varying dosing rate for precipitation with sulfuric and acetic acid at 65 °C.

increased mixing. A stronger influence on particle size by dosing variation is revealed for acetic acid precipitation. The curves for 6 mL/min dosing are shifted significantly towards larger sizes compared to faster dosing. Thus, for 54 mL/min the amount of fines with  $x \leq 10~\mu m$  doubles to more than 10 % compared to 6 mL/min. However, for 30 mL/min and 54 mL/min observed differences are minor. Consequently, a mixing limitation can occur and increase nucleation as a result of local supersaturation peaks.

The reason for this pronounced effect for acetic acid in contrast to sulfuric acid can be the instant and complete dissociation of sulfuric acid leading to available hydronium ions and thus protonation of TA. On the other hand, the provision of hydronium ions from acetic acid relies on the shift of the dissociation equilibrium of weak acetic acid by product removal representing a supply limitation. In case of applying a dosing strategy that promotes inhomogeneous reactant dispersion, dissociation is retarded. Instead local supersaturations occur and lead to a reduced mean particle size. The general effect of a slower feed rate is in congruence with the studies on precipitation of benzoic acid by Åslund and Rasmuson as well as Torbacke and Rasmuson. <sup>42,45</sup> However, the fact these observations using hydrochloric acid do not apply for sulfuric acid here, can be correlated with their investigated parameter range. They applied the acid with ~5 wt.-% instead of 25 %wt.-% here, and varied the feed rate between 0.3 mL/min and 12 mL/min. Coupled with the fact that benzoic acid displays a low-soluble but not sparingly

soluble product, supersaturation can be considered substantially lower compared to this work.

High supersaturations are also more likely to occur when increasing the mass fraction of the PA. <sup>42,130,131</sup> This effect is displayed in Figure 5-7 for three different acetic acid concentrations.

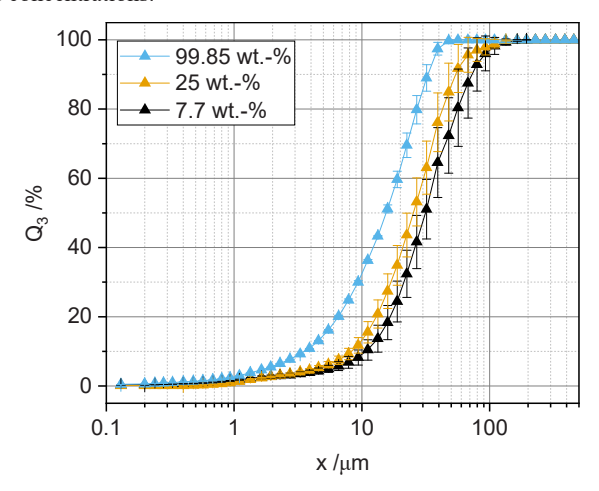


Figure 5-7 Volume related cumulative PSD of TA after precipitation with acetic acid of different concentrations (mass fractions) at 65  $^{\circ}$ C.  $^{17}$ 

While only small differences between the PSDs of the two curves for lower concentrated acetic acid occurs, its pure addition results in a significant drop in size together with a strong generation of fines. Thus, from around 10 % of the crystal population being smaller than 10  $\mu$ m, the amount increases to more than 30 %. These results are the consequence of increased supersaturation due to the increased provision of hydronium ions promoting nucleation. It also shows the limitations of increasing TA solubility on crystal size (see 3.2.4) considering a higher acetic acid concentration in the solvent. Nevertheless, this undesired nucleation effect can be reduced by reducing dosing speed as shown for acetic acid in Figure 5-6. This was already shown for other precipitation systems like salicylic acid and benzoic acid.  $^{42,130,132,133}$ 

The incentive to use concentrated reactants targets the volume reduction of the process streams which is especially useful, as real PET reactants still contain the second monomer EG which has to be separated from low boiling water. Thus, water input should be limited to an extent at which it does not negatively affect the processability behaviour of TA. Thus, alternatively stirring rate could be

increased in order to reduce local concentration peaks of acetic acid. These results could not be conducted for sulfuric acid in batch operation as dosing of concentrated sulfuric acid leads to significant generation of heat. However, the observed fundamental effects are expected to be equally applicable.

In conclusion, the screening experiments revealed that process parameters that directly affect TA solubility exhibit the most pronounced influence on TA crystal size and in consequence, on its processability. While the general effect is in perfect congruence with crystallization fundamentals, the extent to which acetic acid improves precipitation appears exaggerated. With regard to the available TA solubility data for 65 °C, an acetic acid content of ~0.42 g/kg leads to an increase in solubility by factor ~2.5 (Figure 3-9). The reference precipitation with acetic acid of 0.25 g/g, at equimolar addition to 0.021 g/L DST solution, induces an average acetic acid content of ~0.014 g/kg. Consequently, either already low concentrations of acetic acid significantly enhance solubility or locally higher concentrations due to imperfect mixing of 0.25 g/g acetic acid occur. As indicated by the lower 0.077 g/g acetic acid concentration curve in Figure 5-7, only minor differences are visible in comparison with reference 0.25 g/g acetic acid. This confirms that a low acetic acid content in the solvent is already sufficient in significantly promoting solubility.

# 5.1.3 Extended Screening of Alternative Precipitation Acids

As shown for acetic acid, the PA affects the composition of the solvent, having an enhancing effect on solubility and consequently increases crystal size. Thus, for the case of acetic acid a carefully chosen PA can additionally act as solubility enhancer. However, added substances can also have the opposite effect, reduce solubility and thus, increase supersaturation. This perspective extends the single application of a PA as provider of hydronium ions to a co-solvent or additive to tailor the product properties. On the other hand, neutrally acting PAs can be economically interesting e.g. as low-cost by-products of neighbouring processes in a chem-park environment. As seen for acetic acid, this does not exclude weaker acids as TA precipitation can shift the dissociation equilibrium towards the product side. In order to identify the effect of alternative PAs on the final precipitate, experiments were extended to further potentially suitable organic and inorganic acids. Table 5-1 shows the different PAs applied within this work and their respective acid strength together with the individual molality. All PAs were used at 25 wt.-\% mass fractions, except for oxalic acid with 7.7 wt.-\% because of aqueous solubility limitations.

Table 5-1. Acid dissociation constant  $pK_a$  of the PAs, TA and IA. 119

Acid	mol <sub>H+</sub> /kg <sub>PA</sub>	pKa (I)	pKa (II)	pK <sub>a</sub> (III)
Terephthalic	-	3.51	4.82	
(isophthalic)		(3.46)	(4.46)	
Phosphoric	7.65	2.12	7.21	12.32
Citric	3.9	3.09	4.75	5.41
Sulfuric	5.1	-3	1.99	
Oxalic	1.71	1.23	4.19	
Hydrochloric	6.85	-8		
Acetic	4.16	4.76		

With regard to the theoretical availability of protons, shown in the second column, the applied PAs possess clear differences, as well as the individual values for acid strength. Considering phosphoric acid, it has the highest molality but represents the weakest average acid strength. Citric acid appears similar to acetic acid while offering two more protons. From its molecular appearance the similarity between oxalic and acetic acid is even more pronounced with oxalic acid offering two protons. Hydrochloric acid was chosen as an alternative strong precipitation agent which has been applied for TA precipitation by other groups (3.2.3).

#### 5.1.3.1 Yield

Since the respective PAs possess an individual dissociation behaviour they differ substantially in their provision of hydronium ions for the reaction with DST to TA. At the same time the precipitation of TA represents a quasi-irreversible chemical reaction with product removal, affecting the dissociation equilibrium. In order to deliver an insight on the interplay between dissociation of PA and TA precipitation, the pH and yield of different PAs over the standardized addition of hydronium ions is displayed in Figure 5-8.

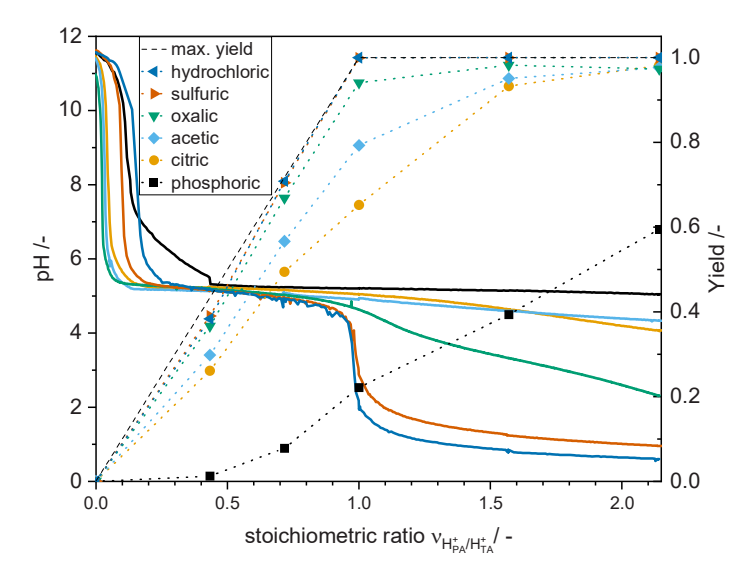


Figure 5-8 pH and yield over stoichiometric ratio of H<sup>+</sup> provision from different PAs and TA demand, results are from single dynamic measurements at 36.5 °C (adapted from Müller et al.).<sup>17</sup>

The addition is standardized to the respective molar availability of hydronium ions of the PAs with respect to the TA demand, as explained in the experimental procedure ("number of functional acid groups per mole"). Thus, at a standardized H<sup>+</sup> addition ratio of 0.7 for example, the respective PA theoretically provides sufficient hydronium ions to reach a maximum TA yield of 0.7. Considering one mole of acetic acid (one hydronium ion per mole), it could theoretically precipitate only 0.5 moles of two-protonic TA. Consequently, at the same standardized H<sup>+</sup> addition ratio of 0.5, one mole of acetic acid is added and only 0.5 mole of twoprotonic sulfuric acid. Full lines represent continuous pH measurement during dosing of the respective PA (left Y-axis). Symbols with dotted lines show the yield of TA at specific stoichiometric ratios with the pure dashed line representing the maximum possible yield in dependence of PA assuming a complete PA dissociation. Initially, the pH drops steeply at low stoichiometric ratios which emphasizes the sensitivity of the system during acid addition. Together with the dynamic measurement, this sensitivity leads to the apparent initial differences in the slope of the various PAs. After the first transition point at pH~8 the pH remains almost constant at ~5 for all applied PAs. Explanation is provided through theory of the buffer equation by Henderson and Hasselbalch for weak acids and their salts. Thus, regarding TA buffering can be observed around the pK<sub>a</sub>(II) value

(Table 5-1). 134 For strong hydrochloric and sulfuric acid also a clear second transition point can be observed. The influence of the PAs on lowering the pH and the maximum observable pH reduction is in accordance with their respective average dissociation constant. However, although the pH is defined as hydronium ion concentration, which equals yield in pH shift reactions, it differs for different PAs. Taking the buffer region at a stoichiometric ratio from 0.3 to 0.7, all applied PAs lower the pH to ~5. In this region, the strongly dissociating PAs provide sufficient hydronium ions leading to the theoretical maximum yield being reached. Instead, the weaker acids do not reach the maximum yield but show an increase in yield when adding more PA despite a constant pH. The similar p $K_a$ value of citric and acetic acid leads to almost identical pH curves over the whole course of the measurement. Regarding yield, pronounced differences at equimolar addition equilibrate at hyper stoichiometric dosing. This effect can be associated with the third hydronium ion of citric acid with the weakest dissociation constant being ineffective for TA protonation but considered in the stoichiometric ratio. The yield of phosphoric acid, which was excluded from particle size measurement as unreproducible, also proves its apparent unsuitability for TA precipitation. It contributes only one proton, thus demanding an approximate threefold excess for full yield. However, as the samples were not taken at equilibrium, changes of yield, especially for the weaker acids cannot be ruled out. However, in consecutive experiments with acetic acid, the yield at equimolar addition remained constant after stirring for 5 hours. Nevertheless, TA yield is generally in accordance with the average dissociation constants. Additionally, weaker acids asymptotically approach full TA yield at hyper stoichiometric ratios, which is comprehensible despite the almost constant pH. Thus, the beforementioned theory on product removal affecting the dissociation equilibrium provides a valid explanation for the high yield of the weak Pas (see 3.2.6). Regarding parameters for process control in a batch or continuous setup the pH has to be considered in its acid-individual behavior with respect to the used PA.

# 5.1.3.2 Alternative Precipitation Acids

In the second part of this evaluation the respective acids were compared in their effect on TA crystal size distribution. Experiments with phosphoric acid have been conducted as well. However, with regard PSD measurements, these were not reproducible and are therefore not considered here. Figure 5-9 shows the PSDs of TA from the respective PA, precipitated at 65 °C.

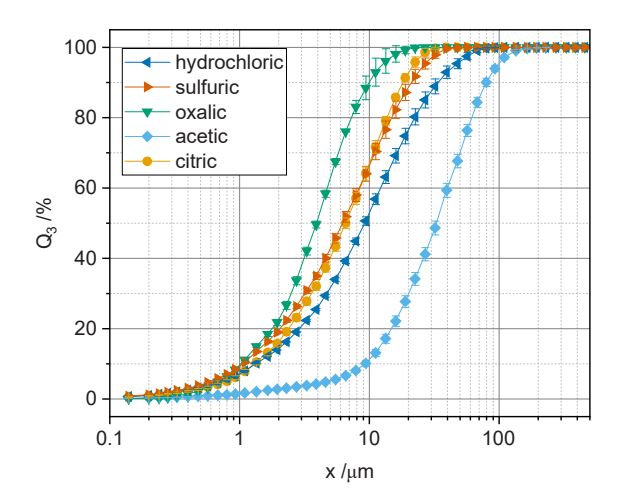


Figure 5-9 Volume-related cumulative PSDs of TA precipitated by different acids, double measurements at 65 °C, lines are shown to guide the eye (adapted from Müller et al.).<sup>17</sup>

Generally, the displayed distributions are in a similar range of size, with the exception of acetic and oxalic acid. On one hand, acetic acid precipitates crystals that are larger by factor 10 on average with around 10 % of fines. Oxalic acid on the other hand, produces the smallest TA crystals with 90 % of the population being smaller than 10  $\mu m$ , although it has been applied diluted at 1/3 of the concentration of the other PAs. The citric acid PSD is almost identical to sulfuric acid while hydrochloric acid is shifted towards larger values as well. Nevertheless, all PAs show an individual impact on the final TA precipitate size. Considering the strong dissociation tendency and molality and thus high theoretical supersaturation induced by hydrochloric acid, the resulting larger TA crystals are unexpected.

However, in comparison to acetic acid the increase is minor and does not positively impact filtration time as shown in Figure 5-10. The normalized filtration time (Equation 4-5) allows for a second perspective on the previously displayed PSDs. In congruence with the distribution and while having an average filter cake height, acetic acid TA filters at least twice fast as any other PA, despite considering that lower yield of weak acids results in smaller filter cake reducing filtration resistance (5.1.3.1).

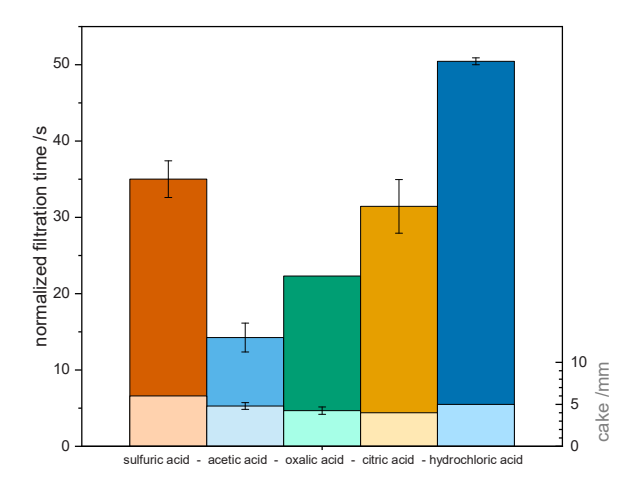


Figure 5-10 Normalized filtration time (upper bars) and respective filter cake height (lower bars) of TA precipitated by different acids at 65 °C (adapted from Müller et al.).<sup>17</sup>

The comparison between strong sulfuric and hydrochloric acid reveals that the resulting apparently larger crystals of do not lead to a faster filtration. However, the apparent faster filtration for strong oxalic acid is compromised due to the large number of fines passing the filter cloth during filtration. While the same leakage was partially witnessed for citric acid, the normalized filtration time is close to the normalized filtration time by sulfuric acid. This is in congruence with the similar PSDs shown before. With regard to an industrial implementation of PAs in a product-recovery-focussed precipitation step, primarily sulfuric and acetic acid can be considered. These positively affect crystal size which transfers to short filtration times.

Nevertheless, the yield of acetic acid of ~78 % when added at equimolar ratio with regard to the proton demand of TA is a significant disadvantage and must be assessed to its promising crystallization behaviour. This includes the economical perspective with the cost of the PAs as well as the cost for process operation. Thus, while more acetic acid is needed for full yield, higher temperatures and thus energy cost are necessary for a similar processability with sulfuric acid. Furthermore, the process costs for recovery of the complementary sodium acid salts and the revenue cannot be neglected. Taking a holistic perspective on a recycling process that should offer a sustainable solution, everything should be incorporated in a lifecycle assessment to evaluate the benefit of each process.<sup>113</sup>

## 5.2 Application to PET Reactants

The presented screening experiments revealed an elevated precipitation temperature and the PA as key parameters to improve crystal size and processability of precipitated TA. Particularly, acetic and sulfuric acid at temperatures above 65 °C show promising effects for precipitation of TA.

In the following these parameters are applied in precipitation of TA from depolymerized PET reactants of different sources. These depolymerized PET fractions have not been purified apart from solids separation up to  $0.05~\mu m$ . This allows for additional evaluation of the precipitation step in its purification potential and validation of the process parameter effects on crystal size and filterability.

A significant part of the data presented in the following originates from the experimental work of the bachelor thesis by Dirk Wilhelm Franke-Hameke and were published in the De Gruyter journal of Green Processing and Synthesis. 102,135

#### 5.2.1 Purification Potential

As introduced in 3.2.5, all PET recycling processes are challenged by a numerous variety of impurities from different origins. While mechanical recycling must only cope with surface and surface migrated impurities, BMR is confronted with impurities that were added during manufacturing and are released (and degraded) during depolymerization. Unlike the model system, the validation of the precipitation parameters found in 5.1 is potentially challenged by its purification performance. As the individual identification of the impurities surpasses the scope of this work, in particular two properties are evaluated, the Hazen colour index and the isophthalic acid (IA) content. The Hazen colour index or colour index (4.3.5) is a measure for the yellowness of TA due to contained impurities (3.2.5). 14,79,125 As highlighted in section 4.3.5, the assessment of purity can be efficiently and reliably conducted using the Hazen colour index. Lower values within this index signify reduced traces of impurities, while higher values indicate the opposite. Thus, it is necessary that fossil-based PTA does not exceed colour index values above 10. Additionally, it must be considered that the Hazen colour index represents only one quality parameter of several in the PTA industry as it cannot assess colourless impurities. 125

#### Hazen Colour Index

In Figure 5-11 the effect of temperature on precipitation with acetic and sulfuric acid on the Hazen colour index of TA is displayed.

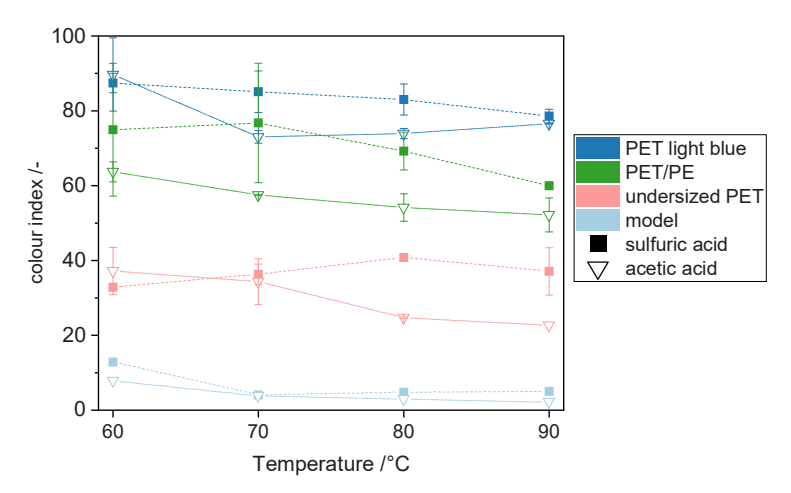


Figure 5-11 Hazen colour index of TA precipitated with sulfuric and acetic acid at various temperatures, single measurements for model reactant only, lines are shown to guide the eye. 102

With regard to temperature, a tendency of increasing precipitation temperature leading to a reduction of the colour index can be observed. A possible explanation can be an increased mass transfer of colouring impurities into the bulk. Thus, impurities do not accumulate in the boundary layer after rejection from crystal incorporation and remain in solution at higher temperatures.<sup>23</sup> Additionally, the reduced supersaturation ( $S_{c,60\rightarrow90} \sim 1600 \rightarrow 650$ ) promotes a slower growth of TA reducing the incorporation of impurities.<sup>23</sup> The purifying effect of an increasing crystal size due to the reduced surface volume ratio can only be considered assuming a pronounced surface integration of colourants. Otherwise, smaller crystals are reported to reduce the tendency to form inclusions.<sup>23</sup> These effects and their possible mechanisms can be observed for both PAs. Nevertheless, acetic acid reduces the colour index in direct comparison to sulfuric acid to a larger extent. While this could be due to the significantly larger TA crystals (reduced surface) after precipitation with acetic acid, solubility and supersaturation are probably more dominant. On the one hand, precipitation of TA with acetic acid is a slow and gradually increasing solids formation process, whereas sulfuric acid acts fast. A slowed down growth reduces the probability of inclusion

incorporation.<sup>23</sup> Additionally, it is possible that acetic acid also promotes solubility of impurities that are chemically similar to TA as seen for its isomer IA (3.2.4). A higher temperature and also the application of acetic acid as PA also show a purifying effect for the model reactant prepared from PTA (single measurement). However, in the investigated temperature region the absolute reduction of the colour index is low and shows strong deviations for repetitive measurements. Additionally, the colour index values differ significantly between the respective depolymerized PET reactants as consequence of individual levels of impurities. Thus, PET light blue and PET/PE reactant show higher levels of yellow coloured impurities being incorporated than in TA precipitated from undersized PET. This is the result of the conditions during alkaline hydrolysis, favouring discolouration of TA which is for example sensitive to torque and process temperature. 13,14,110 A similar undesired colouration is caused by oxidative and hydrolysing conditions during thermomechanical PET recycling as described in 3.1.2. 8 In the revolPET® approach, the highly alkaline solid-solid reaction and elevated temperatures additionally favour EG degradation, partially decomposing into yellow coloured fragments. Nevertheless, the general TA colour index from colourless packaging depolymerized in the revolPET® process is between 100 -140 at depolymerization temperatures from 100 °C - 160 °C as reported by Biermann et al.. Their results represent an approximate base value for the colour index of TA from PET light blue reactant, as they precipitated TA for purity analysis at room temperature. 110 Thus, it can be concluded, that discolouration is significantly reduced for precipitation at more than 60 °C instead of room temperature. Furthermore, TA colour primarily depends on the initial reactant colour whereas an increase in temperature displays a secondary influence only. Additionally, it was found that discolouration of PET reactants decreases with storage time, which complicates comparison of single parameter effects for different reactants. Nevertheless, the results reveal a general potential of the precipitation step for TA purification on one hand. On the other hand, its limits are shown as precipitation cannot replace additional decolouration measures. A suitable approach applied for dyed polyester is reported to be adsorptive pretreatment with active carbon. 106,107,136 Alternatively, originating from the purification step during synthesis of TA from p-xylene, also selective hydrogenation can be used to reduce the amount of colouring impurities.

## Isophthalic acid content

In addition to coloured impurities also present in crude TA, for which alternative purification measures exist, rTA especially of packaging origin is commonly contaminated with IA, making it a recycling specific impurity. This is because TA

precursor p-xylene is practically free of m-xylene, the reactant for IA production, as it is separated from its isomeric mixture by the highly selective chromatographic Parex<sup>TM</sup> process (3.2.1).<sup>137</sup> However, PET manufacturers adjust IA content to the respective demand with regard to the final PET application. With regard to BMR control of IA content can be accomplished by mixing feedstocks with different IA amounts until reaching a mixture with the desired content as patented by RITTEC Umwelttechnik GmbH.<sup>138</sup> This approach comes with the downside of mixing low ( or no) IA containing feedstocks like polyester textiles with high IA content PET of food packaging origin, which might limit the monomer reapplication regarding legislation.<sup>100</sup> Consequently, it is of importance for BMR to provide measures for controlling IA content in rTA. In the following, the potential of the precipitation step on IA reduction is analysed.

Therefore, Figure 5-12 displays the influence of PA in dependence of the precipitation temperature on the IA content in the TA precipitate for different PET reactants.

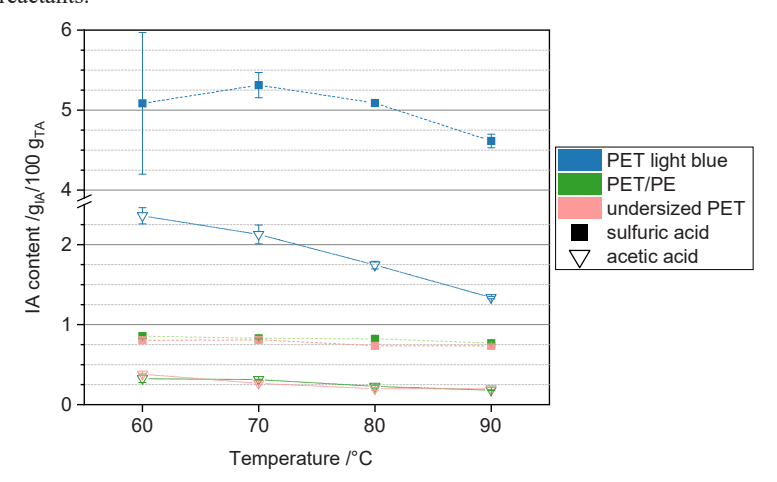


Figure 5-12 IA content in TA precipitated with sulfuric and acetic acid at various temperatures, lines are shown to guide the eye. 102

As the amount of IA added during PET manufacturing is chosen to meet the desired properties (e.g. crystallinity, transparency<sup>53</sup>) of the respective application, the initial isophthalate content varies between the PET reactants. Thus, TA from PET light blue reactant, originating from bottle-to-bottle recycling, contains the highest amount of IA. TA from undersized PET and PET/PE contain a significantly lower and almost identical amount of IA. In contrast to the colour index values shown previously, the trends of IA content show an unambiguous

dependence of temperature and PA. Thus, at higher temperatures a significant reduction of IA content can be observed regardless of the IA content of the applied PET reactant. Additionally, the relative degree of IA reduction appears to be constant for each PA respectively regardless of the PET reactant and its initial IA content. Thus, IA in TA precipitated with sulfuric acid is reduced by approximately 9.5 % and by around 45 % for TA precipitated with acetic acid between 60 °C and 90 °C. This effect can be clearly connected to the steeper inclination of IA solubility with temperature next to its generally higher solubility in comparison to TA (3.2.4). While IA solubility more than triples from 0.45 to 1.52 g/kg C, TA solubility only doubles from 0.08 to 0.176 g/kg between 55 °C and 85°. Consequently, a larger amount of IA remains in solution without coprecipitating with TA. As the samples are cooled to room temperature in the mother liquor prior to analysis, they will become supersaturated for IA during cooling. However, under the applied conditions, it could be influencing for more concentrated PET reactants near the DST solubility limit and higher IA content. Additionally, performing solid/liquid separation at higher temperatures under such conditions could increase the amount of IA remaining in solution. This IA could subsequently be recovered by cooling crystallization even though at high dilution.

In addition to the impact of temperature, acetic acid as precipitation agent reduces IA to an even larger extent. In comparison to sulfuric acid, acetic acid TA incorporates up to 80 % less IA under otherwise identical conditions. This effect also persisted upon addition of hyper stoichiometric amounts of acetic acid. Therefore, the reduced yield is not responsible for this effect. Instead, it can be related to the promoted solubility of IA in aqueous acetic acid as shown in 3.2.4. Even though, acetic acid enhances TA solubility as well, its effect on IA solubility is significantly higher. However, in screening experiments with alternative PAs it was found that citric and phosphoric acid reduced the IA content in TA at equimolar addition to an identical extent as acetic acid. 139 As this cannot be explained by solubility enhancement (Figure 3-9) it can theoretically be the result of the interplay between proton provision by weak acids and proton acceptance between TA and IA. As shown in 5.1.3, acid dissociation constants for IA are lower compared to TA, making IA the stronger acid isomer. However, protonation without solubility induced product removal would demand for a stronger acid in order to substantially protonate a weaker one. Thus, considering a competition for protons provided by a weak acid, the protonation barrier for weaker TA is lower than for protonation of stronger IA. Simulation of species distribution with software CurTiPot© revealed 50 % more TA than IA being protonated at pH 4. Instead at pH 2 as for sulfuric acid, the degree of IA/TA protonation is almost

identical.<sup>140</sup> Considering acetic acid as the weak PA of interest, hyper stoichiometric addition did only increase overall yield but did not affect the IA content in the final precipitate while the pH dropped only slightly. Thus, the mild pH of acetic acid at hyper stoichiometric ratios promotes a selective TA precipitation. However, higher concentrations of acetic acid also lead to a higher IA solubility for which reason the different IA/TA protonation acceptance cannot be considered separately from solubility differences.

On the opposite, sub stoichiometric amounts of sulfuric acid could not induce an IA reducing effect in batch operation.<sup>141</sup> It can be assumed that the local pH at the dosing nozzle is too low and direct precipitation of IA and TA takes place. This direct precipitation could only be reduced by measures that avoid high local supersaturations e.g. a high PA dilution.

Concluding the displayed results, the final IA content in precipitated TA highly depends on the respective depolymerized reactant. Thus, even PET of similar applications, e.g. PET light blue and undersized PET of bottle recycling origin, possess completely different IA levels. Therefore, when assuming precipitation as the last crystallization step, r-TA should be reapplied in products demanding for similar IA levels, under the terms of successful certification (e.g. REACH). <sup>103</sup> Nevertheless, acid strength induced pH and TA solubility impact of acetic acid result in an apparent selectivity for precipitation of TA. Thus, acetic acid significantly reduces IA content in the final TA. Additionally, as hyper stoichiometric dosing hardly affects pH, high TA yield is possible without compromising IA content.

# 5.2.2 Validation of Temperature and Precipitation Acid Influence

Apart from r-TA purity, its processability and particle size are main qualitative parameters considering recovery and reapplication as already mentioned. As shown for the model reactant, larger TA crystals lead to faster filtration and also improve rheological behaviour.<sup>17</sup> The latter gains importance during TA polycondensation as mixtures with equimolar amounts of EG must be capable of flowing (see also 3.1.1 and 3.2.2).<sup>17,20</sup> As stated before purity can be affected by particle size, but reversely impurities can also affect particle size e.g. if reducing target solubility (2.5.1). Since critical impurities must not necessarily be detectable by the applied analytical measures, validation of the previous results (5.1.1) was conducted. For comparison and improved visualisation of the broad distributions the volume-related logarithmic density distribution  $q_3^*$  over the equivalent mean particle diameter x is used. It expects the logarithm of the particle size being normally distributed instead of the particle size itself. Conversion can

of a normal mean distribution into a log-mean distribution can be conducted by substituting the abscissa (see also Müller et. al.<sup>17</sup> Figure 5-13 displays the logarithmic volume-related density PSDs of TA of different reactants precipitated with sulfuric and acetic acid at 60 °C and 90 °C. In order to simplify qualitative comparison and visualization, the distributions are stacked along the y-axis and displayed as continuous and dashed lines instead of single points.

In accordance with the model reactant, the effect of a higher precipitation temperature causing larger TA crystals is confirmed for PET reactants as well. <sup>17</sup> Furthermore, the distribution of depolymerized reactants and model reactants without EG show a good comparability. Thus, the sulfuric acid precipitated TA distributions represent an almost congruent curvature with only the PET light blue

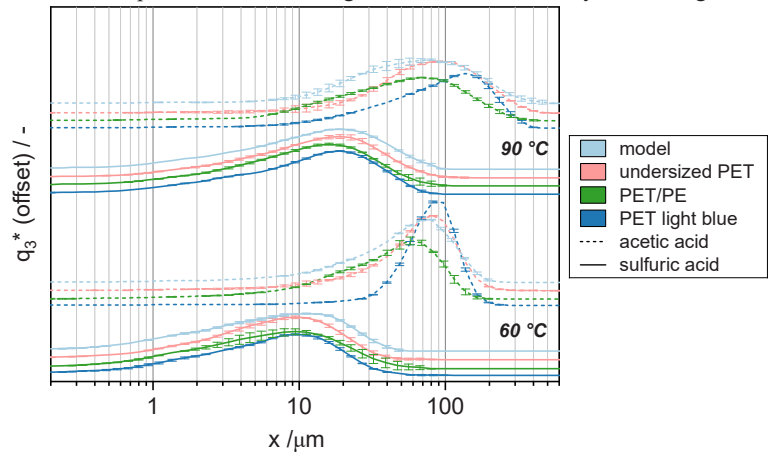


Figure 5-13 Logarithmic volume-related density PSDs of TA precipitated by sulfuric and acetic acid from different PET reactants at 60 °C and 90 °C, lines are shown to guide the eye. 17,102

reactant at 90 °C clearly deviating towards larger crystals. A similar shift is especially pronounced for the results of PET light blue with acetic acid. However, a significant impact on the distribution measurements of acetic acid TA can be observed for the remaining reactants as well. Opposed to the similar distributions of sulfuric acid, all acetic acid distributions differ substantially. Regardless of the applied temperature, PET light blue and subsequently undersized PET show their distribution peak at a larger crystal size than PET/PE. The model reactant appears to crystallize in a similar size like PET/PE.

A reason for the behavioural differences between PET and model reactants could be EG known to reduce DST solubility.<sup>74</sup> On the other hand, EG represents a less

polar solvent compared to water which could positively affect solubility off nonpolar TA which could contribute an explanation for the smaller model reactant crystals. However, this does not explain the differences between model reactants nor why these differences appear for precipitation with acetic acid only. While the PET reactants did apparently not contain critical amounts of contaminants negatively affecting the crystallization of TA, they differed substantially with regard to the IA content. Additionally, only precipitation with acetic acid had an IA reducing effect as IA is generally more soluble in water than TA and even more in acetic acid. With the PET light blue reactant containing five times more IA in comparison to the other reactants, the mean benzene carboxylic acid solubility is higher. Consequently, the solubility of the final crystalline product being a TA/IA mixture is higher for PET light blue as well. As shown in 3.2.4, IA solubility temperature dependence is substantially more pronounced than for TA which leads to increasing solubility differences between IA and TA as temperature increases. This could deliver a possible explanation for the larger PET light blue distribution peak at 90 °C for acetic acid. In order to examine the described differences of both PAs in their effect on processability, Figure 5-14 visualises the normalized filtration times for the respective PET reactants.

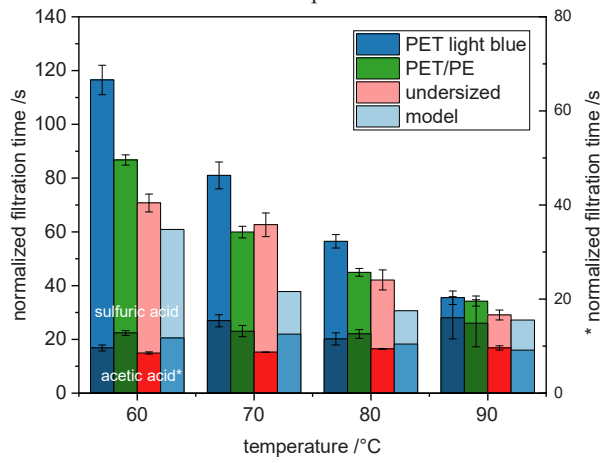


Figure 5-14 Normalized filtration times of TA precipitated by sulfuric acid (left y-axis) and acetic acid\* (right y-axis), acetic acid is displayed by dark coloured bars.

The results from acetic acid are represented by the lower dark coloured bars and refer to the right y-axis, while the results for light sulfuric acid are displayed by the light-coloured bars on the left y-axis. The general faster filtration for

#### Batch Precipitation of Terephthalic Acid

increasing precipitation temperature can be validated for PET reactants precipitated with sulfuric acid. Nevertheless, in contrast to the almost identical crystal size distributions, the

filtration times between reactants vary substantially. Especially for 60 °C the PET light blue reactant appears to filter almost twice as slow as the model reactant, which displayed the largest crystals in the distribution in Figure 5-13. These differences equilibrate at higher temperatures and almost vanish at 90 °C. For PET/PE and undersized PET differences are minor and lie within the experimental deviations. For acetic acid, no significant tendency can be deduced, as filtration times for PET light blue and PET/PE appear to increase with temperature while Undersized PET and the model reactant remain almost constant. However, this is in accordance with the ambiguous results on the parameter screening in 5.1.1, in which a temperature increase from 65 °C to 90 °C did not reduce filtration time further. Consequently, the displayed fluctuations and inconsistencies for acetic acid precipitated TA can be attributed to the limitations of the filtration setup.

Nevertheless, these results on real depolymerized PET reactants reveal that a higher precipitation temperature balances influences on crystallization behaviour of possible contaminants. The use of acetic acid shows great potential as it leads to significantly larger crystals and reduces IA content and probably discolouration as well. Industrially common amounts of IA do not critically affect crystal size and subsequent processability. Instead, it can be deduced that PET reactants crystallize similarly to the model reactant (see Appendix, Figure 8-6). However, within the variety of PET applications, the investigated reactants represent only a small sample group. Therefore, it can cannot be excluded that some additives possibly complicate TA crystallization. On the other hand, these might be removed beforehand by adsorptive treatment or in a subsequent recrystallization step.

The second part of this work focusses on analysis and establishment of a continuous operation of the precipitation step. Next to the general advantages of continuously operated processes (e.g. constant quality, reduced start-up/shut-down time, higher capacities<sup>142</sup>) over batch operation, the continuous crystallization in a stirred tank reactor also has additional benefits. Thus, its setup inherently induces an additional dilution of reactants which reduces effective supersaturation. Furthermore, residence time distribution leads to the constant presence of crystal seeds in the reactor which potentially provide surface for secondary nucleation. Furthermore, continuous precipitation displays the consequential operational mode regarding a continuous depolymerization as conducted within revolPET® technology (3.1.3.2). Therefore, the following chapters present the results of the parameter studies in a continuous setup, conducted in continuation of the previously shown batch investigations.

The experimental procedure follows the method described in 4.1.3., introducing the dimensionless residence time which is applied throughout the following results, in order to compare results for experiments with different residence times. A significant part of the experimental work has been conducted during the master thesis of Michelle Biermann, the student research project of Saskia Gottwald and the bachelor thesis by Henrik Schneemann and Yunis Jansen. 111,143–145

# 6.1 Precipitation Acids Comparison

Following the most influencing parameters of the initial parameter screening in model reactants and their transfer to real PET reactants, an elevated precipitation temperature of 80 °C was chosen as starting point. The experimental duration (70 min) and reactant volumes were adjusted to allow for approximately ninefold reactor volume exchange and the possible establishment of a steady state (see also 4.1.3). The parameters of the standard procedure are displayed in Table 6-1. This standard procedure starts with a batch precipitation up to the target pH at equimolar addition of the respective PA (see 5.1.3.1) after which the first sample at t<sub>0</sub> is taken. By simultaneously starting product and feed pumps the continuous process is initiated.

Table 6-1. Standard parameters for reference experiment during continuous operation.

Parameter	Value		
Temperature	80 °C		
Precipitation acid   conc.   volume	Sulfuric acid   25 g <sub>acid</sub> /g <sub>total</sub>		
flow	6.2 mL/min		
PET reactant   conc.   volume flow	PET/PE   25.6 g <sub>DST</sub> /L   121 mL/min		
Residence time	7.9 min		
Reactor hold up	1 L		
рН	2		

Figure 6-1 shows the logarithmic volume-related density PSD of TA after the reference precipitation at 80 °C for acetic and sulfuric acid at three different moments.

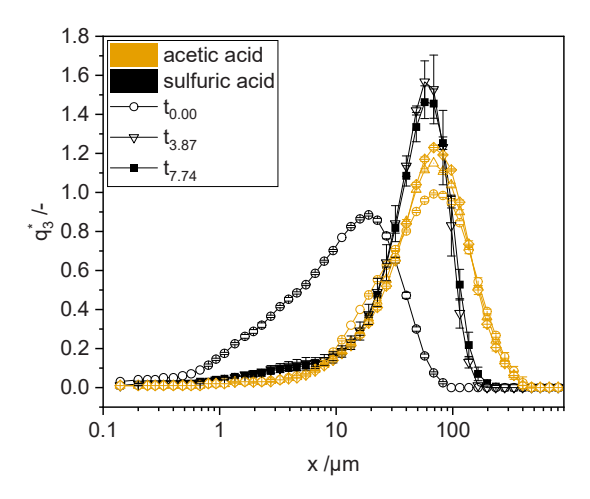


Figure 6-1 Logarithmic volume-related density PSDs of TA from PET/PE reactant after precipitation with acetic and sulfuric acid at 80 °C, samples taken at the beginning  $t_0$ , middle  $t_{3.87}$  and end  $t_{7.74}$  of the experiment.

The initial distributions of acetic and sulfuric acid precipitated TA are comparable to the already presented distributions after batch precipitation. While the acetic acid remains almost constant over the course of the experiment, the distribution of sulfuric acid changes substantially. Thus, the number of fines is reduced and the overall shape approximates the acetic acid distribution. Additionally, the entire distribution is shifted towards larger values leaving the final distribution of

sulfuric acid similar to acetic acid. This behaviour for sulfuric acid can be traced back to two conditions induced by the continuous operation. First the precipitation is conducted in a media already containing TA crystals.

These crystals represent surface for growth of dendritic crystal structures, shown in Figure 8-7. Second, the PA and reactant concentration is continuously diluted as precipitation is performed in desaturated media, assuming instant and complete precipitation. As this dilution drastically reduces supersaturation, secondary instead of homogeneous nucleation and crystal growth can occur which eventually supports formation of larger crystals. These effects have already been stated by O'Hern and Rush for continuous precipitation of barium sulfate. <sup>147</sup> Thus, even for concentrated barium hydroxide and sulfuric acid reactants no decrease in crystal size was observed in contrast to batch and T-mixer produced crystals.

Another sign of crystal growth is also visible in Figure 8-7, where the central stem of the dendrites appears significantly thicker at the end of the experiment. In accordance with the distributions, this effect is especially pronounced for sulfuric acid whereas acetic acid partially induces dendrite formation in batch operation already. As stated before, this is the result of the retarded and reduced provision of hydronium ions for protonation of DST to form TA and solubility enhancement, reducing supersaturation. However, these effects could not be witnessed in batch experiments by addition of crystal seeds nor by mere application of diluted reactants. It can be concluded that the combination of dilution and seeding, inherent for MSMPR operation is the prerequisite condition for this change in TA crystallization behaviour. Moreover, the distributions for t<sub>3.87</sub> and t<sub>7.74</sub> for sulfuric acid appear almost congruent, indicating a stationary state after t<sub>3.87</sub> while distributions for acetic acid appear almost unchanged throughout the experimental duration.

In order to improve temporal resolution of the continuous process and crystal growth while maintaining a clear and comprehensive presentation, the  $x_{3,10}$ ,  $x_{3,50}$  and  $x_{3,90}$  quantile values of the cumulative Q<sub>3</sub> distributions were chosen for subsequent presentation. Figure 6-2 shows these quantile values at five different moments for the respective precipitation experiments. It also includes comparative results with model reactant.

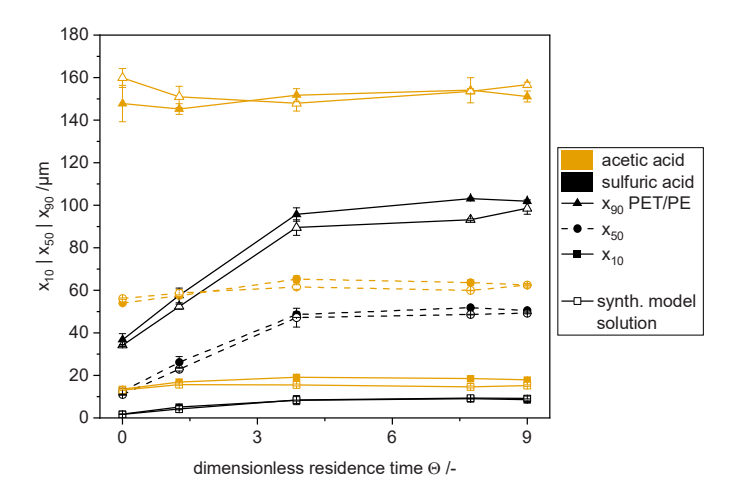


Figure 6-2  $x_{3,10}, x_{3,50}$  and  $x_{3,90}$  quantiles of TA from PET/PE reactant after precipitation with acetic and sulfuric acid at 80 °C, empty symbols represent synthetic model reactant, lines are shown to guide the eye.

As indicated by the distributions of the previous diagram, acetic acid quantiles remain almost constant during the experimental duration. Next to fluctuations for the 90 % quantiles, a slight inclination can be initially seen for x<sub>3,10</sub> and x<sub>3,50</sub> until reaching t<sub>3,87</sub>. Within the same time span, all quantiles for sulfuric acid increase substantially. Especially the x<sub>3,10</sub> and x<sub>3,50</sub> almost grow by factor ~5 whereas x<sub>3,90</sub> almost triples. Thus, initially 50 % of the population (x<sub>3,50</sub>) consists of fines while at the end of the experiment, it drops to 10 % of the population (x<sub>3,10</sub>). However, the inclination changes after t<sub>3,87</sub> with approximately four times reactor volume exchange and the values stay almost constant, which consequently leads to assuming a constant supersaturation. The comparison between PET/PE and model reactant additionally reveals a slightly reduced size for the model reactant. However, these small differences do not appear significant in the respective SEM images (Figure 8-7). Instead SEM images show that the continuous operation leads to a morphological and size convergence between acetic and sulfuric acid precipitated TA.

This is also represented by the processability of TA, measured as normalized filtration time and displayed in Figure 6-3.

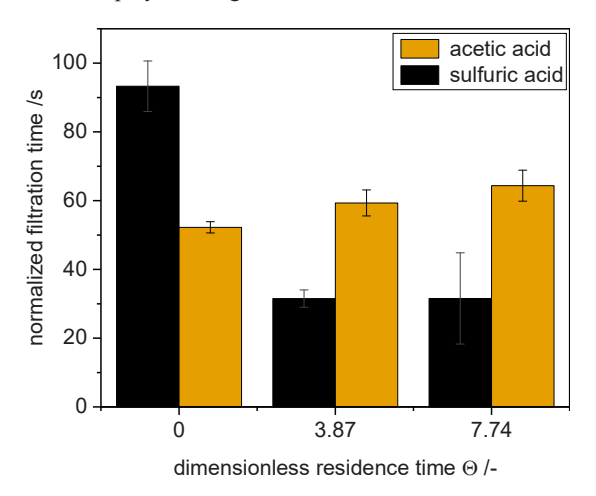


Figure 6-3 Normalized filtration time of TA from PET/PE reactant after precipitation with acetic and sulfuric acid at 80 °C.

Thus, after batch precipitation at to filtration time for sulfuric acid is about double in comparison to sulfuric acid, which agrees with the previously presented batch results. Nevertheless, sulfuric acid filtration times significantly drop after t<sub>3.87</sub> and stay almost constant, confirming the stationary state. On the contrary, acetic acid filtration times are low initially but appear to increase over the course of the experiment. Due to its lower filter cake mass and yield the normalized filtration time after the stationary state is about double the filtration time of sulfuric acid, despite generally larger crystals. As the possibility of clogging of the filter cloth cannot be excluded, the differences should be regarded with reservation.

However, precipitation process with acetic acid was additionally complicated as the large dendritic crystals showed a tendency of blocking the tubes of the peristaltic product and acid pump. While this could only be a problem of the small-scale laboratory setup, it could instead indicate a pronounced fouling issue for acetic acid too.

Next to crystal size and processability, TA purity is of major concern regarding its later reapplication. As introduced in 5.2, yellow colouring and recycling specific IA content are used as markers representing the purification potential of the precipitation. In order to evaluate the risk of impurity incorporation Figure 6-4 presents the results of purity analysis for both acids.

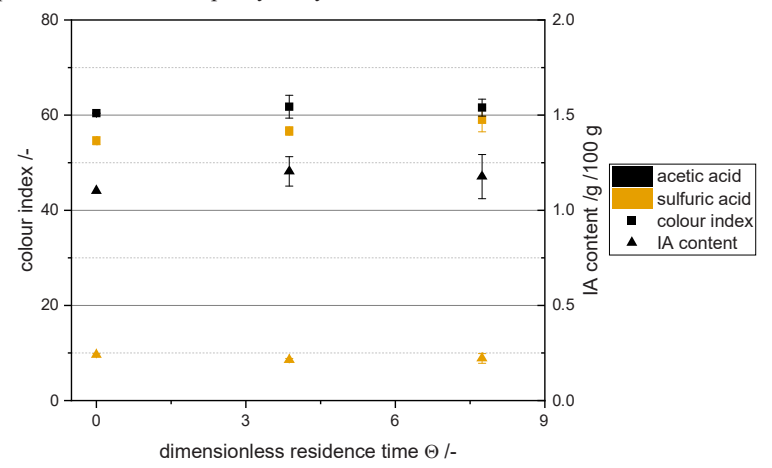


Figure 6-4 Colour index and IA content of TA from PET/PE reactant after precipitation with acetic and sulfuric acid at 80 °C.

With regard to the colour index, no significant differences occur between the different PAs, although acetic acid appears to reach lower values as indicated by the batch results before. However, these values approach each other over the course of the experiment and consequently indicate a slight increase in discolouration. A similar, yet stronger fluctuating effect can be seen for IA content in TA precipitated with sulfuric acid. Acetic acid instead shows a constant but significant IA reduction of up to 70 % compared to sulfuric acid, which is in a comparable order of magnitude with the batch experiments (Figure 5-12). Likewise, the IA content does not appear to change with time. In contrast, after batch precipitation at t<sub>0</sub>, sulfuric acid leads to a lower IA content, compared to its stationary state after 3-4 dimensionless residence times.

As crystal size for acetic acid TA does only slightly increase with time as well, constant TA purity might be connected to TA crystallization behaviour, while sulfuric acid changes morphology from thin needles to thicker needles with branching dendrites. As stated in 2.5.2, larger crystals possess a higher tendency for incorporation of inclusions and impurities. Therefore, as crystal size remains constant, purity reaches a steady state too. Together with a good repeatability of

the experiments, the stationary state represents the fundamental requirement for a successful transfer of the precipitation step towards continuous operation. This steady state for crystal size and purity was also confirmed in long-time experiments shown in for sulfuric acid (shorter residence time of 3.5 min vs. 7.9 min).

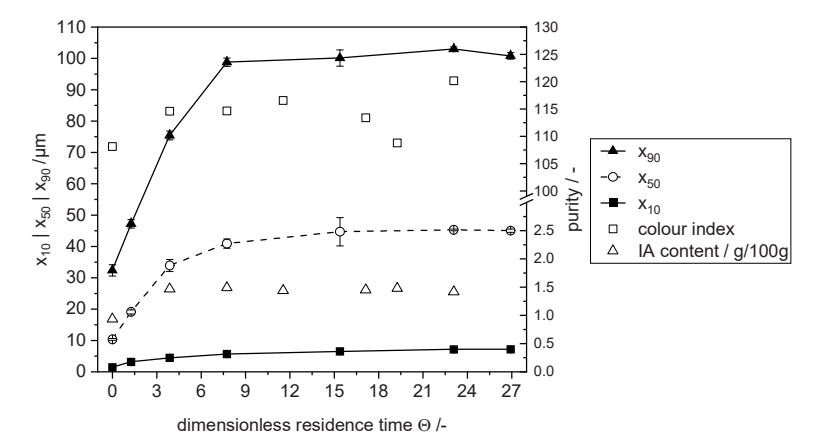


Figure 6-5 Quantile values and purity of long-time experiment with sulfuric acid at 80°, for PET/PE reactant and a residence time of 3.5 min, purity values were measured once only.

While the colour index fluctuates significantly, IA content displays a clear course of an initial inclination ending up in a steady state concentration below 1.5 g<sub>IA</sub>/100g<sub>total</sub> after threefold residence time. The quantile values show a similar development with the x<sub>3,10</sub> and x<sub>3,50</sub> quantiles flattening after about 3 times reactor volume exchange. This confirms reaching of the steady state which is in agreement with literature. 146 While the colour index initially displays a comparable course, it significantly fluctuates towards the end of this experiment. As the purity analysis was conducted for a single experiment only, handling errors cannot be excluded. Nevertheless, it can be confirmed that during initial batch precipitation, less impurities are incorporated into the crystal in comparison to continuous operation. These long-time results could not be confirmed for acetic acid as clogging and fouling of tubes already occurred during short-time experiments due to the larger crystals and a pronounced fouling effect. All in all, impurities remain constant over the course of the experiment and are only affected by the choice of PA, since an elevated process temperature is already applied. This reduced impact emphasizes again the necessity of prior purification measures

like adsorptive activated carbon treatment of the raw PET reactant in order to meet TA colour specification. However, these measures do not affect IA content which instead could demand for an additionally recrystallization step as during PTA purification (3.2.1). While acetic acid exerts a promising purification effect it also led to significant issues regarding crystal fouling as well as blockage of tubes and pumps of the experimental setup. It can be assumed that these effects especially represent small-scale issues only. Nevertheless, for consecutive experiments, the main focus was set to sulfuric acid which showed beneficial growth after continuous operation.

## 6.2 Variation of Throughput

Considering the initially presented results, continuous TA crystallization induces crystal growth resulting from a lowered supersaturation as reactants are diluted by the reactor content and from seed crystal presence. However, this diluting effect is directly connected to the dispersion of the reactants to avoid local supersaturation. Thus, higher reactant mass flows stress possible mixing limitations. Additionally, despite the fast reaction kinetics, TA crystals require time to grow. A generally higher throughput reduces the time for crystals to grow on existing crystals which could reduce crystal size and deteriorate processability. Therefore, throughput and thus residence time for continuous precipitation with sulfuric acid at 80 °C was varied aiming for identification of residence time limitations and the determination of its optimum. In order to facilitate the comparison between different residence times, samples were taken at normalized sampling times as introduced in 4.1.3. Consequently, samples for analysis were taken at moments of identical multiples of the dimensionless residence time but different absolute time. Considering experimental duration, the 3.5 minutes experiment lasted 31 minutes whereas the 15.7 minutes precipitation lasted more than 120 minutes. During each of these experiments, a constant reactor volume of 1 L was exchanged 9 times.

Figure 6-6 displays the 10 %, 50 % and 90 % quantile values of the cumulative  $Q_3$  distribution over the normalized time. Generally, the development of the quantile values is similar for the different residence times. Thus, the initial inclination of the  $x_{3,50}$  and especially  $x_{3,90}$  quantiles appear almost identical for all residence times. Nevertheless, some differences occur which could be a result of the changed residence time. Thus, at  $t_{3,87}$ , the  $x_{3,10}$  and  $x_{3,50}$  quantiles arrange in order with the samples for the longest residence time being significantly larger. These values of the 16 minutes residence time experiments fall subsequently for

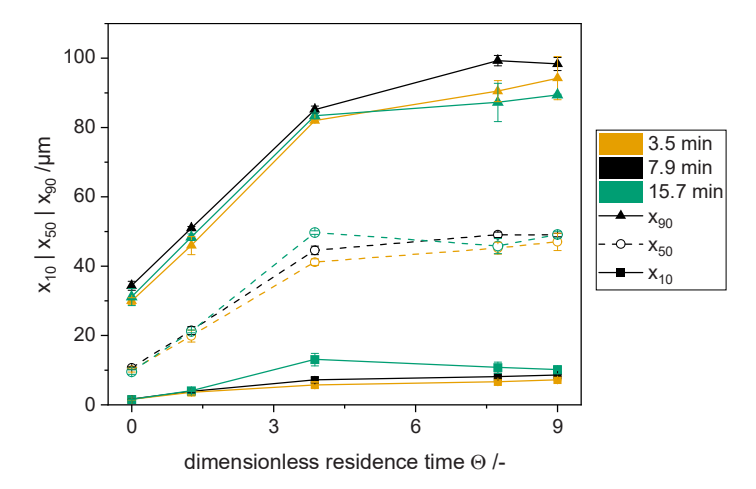


Figure 6-6  $x_{3,10} x_{3,50}$  and  $x_{3,90}$  quantiles of TA from PET/PE reactant after precipitation with sulfuric acid at 80 °C for different residence times, connecting lines are shown to guide the eye.

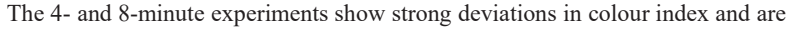
both quantiles leading to an average  $x_{3,50}$  value but the  $x_{3,10}$  remaining slightly larger. Such effects cannot be seen for the 90 % quantile, which instead appears more constant after  $t_{3.87}$ . Instead the shorter residence time quantiles apparently grow over the entire course of the experiment, although their inclination drops after  $t_{3.87}$  as stated before.

A positive effect of longer residence times on crystal size has also been reported for barium sulfate and salicylic acid. 130,148 Pohorecki and Baldyga pointed out that this is due to a lowered mean reactant concentration and thus supersaturation during continuous operation. 148 This was also shown by Franke and Mersmann in an extensive study on the effect of operational conditions on precipitation.<sup>41</sup> They additionally determined nucleation and growth rates for calcium carbonate and sulfate dihydrate. Thus, by prolonging residence time from ~10 min to ~80 min, the nucleation and growth rate were substantially reduced. For calcium sulfate dihydrate at low mean specific power input of 0.1 W/kg, this induced a steep increase in median particle size from ~90 µm to ~150 µm after ~30 minutes residence time. Longer residence times induced a slight decrease. They explain this maximum by different phenomena like a higher probability of crystal breakage and attrition for longer residence times in addition to the previously stated reduction in growth rate due to the lowered mean concentration and thus supersaturation. Moreover, local supersaturations cannot be avoided completely in real crystallizers, for this reason nucleation rates remain higher than under ideal conditions, even for significantly longer residence times.<sup>41</sup>

It can be concluded that also for TA precipitation longer residence times promote the formation of larger crystals, as indicated by the larger  $x_{3,10}$  and  $x_{3,50}$  quantiles at  $t_{3.87}$ . On the other side these values almost equilibrate until the end of the experiment. Considering the expectations from literature, longer residence times should be evaluated to confirm the negligible influence.

Additionally, the starting point of the steady state regarding crystal size is not altered within the investigated residence time range. Consequently, a shorter residence time can accelerate reaching a steady state regarding crystal size. However, a longer residence time demands for less volume exchange to reach steady state, which eventually produces less off-spec precipitate. Considering integration in an overall continuous process, the start-up phase represents only a relatively short period. Instead a faster production through shorter residence time leads to smaller reactors that ease scale up effects like heat transfer and reactant dispersion. Nevertheless, in order to determine advantages of a larger or smaller reactor, further experiments with constant throughput but varying reactor volume could be conducted.

Next to crystal size, residence time can also affect crystal purity considering a more controlled and slower growth next to possible ripening effects as introduced in 2.5.2. Therefore, Figure 6-7 shows the colour index and IA content for three different residence time experiments for the respective normalized sample times.



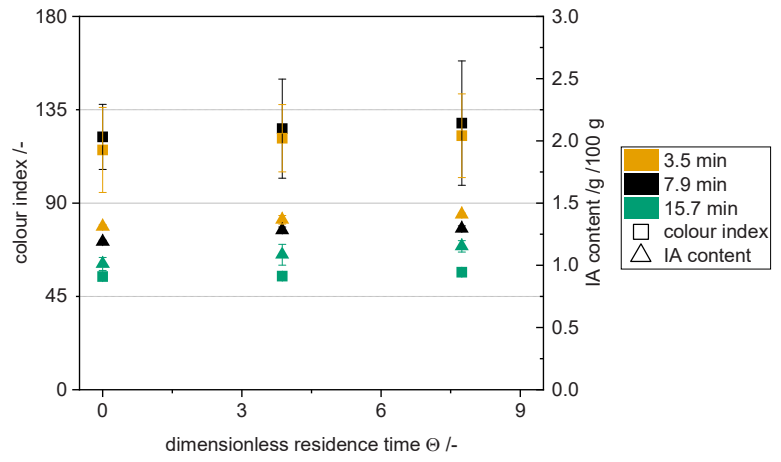


Figure 6-7 Colour index and IA content of TA after precipitation with sulfuric acid at 80 °C for different residence times

additionally more than double in comparison to the 16-minute experiments. However, the PET product for the latter experiment originated of a different depolymerization batch with the same PET/PE material. As these colour differences significantly exceed expectations, the stronger impact of the overall level of discolouration of PET reactant probably represents the major contributor (5.2.1). Despite these ambiguous results, one effect can be drawn regarding discolouration since the colour index values do not appear to increase over the course of the 16-minute experiments. Thus, the longer residence time and reduced mean concentration, applying to the impurities as well, and slower growth might reduce accumulation of impurities in the crystal. Nevertheless, as colour index values are commonly higher, a contribution of the low impurity level cannot be excluded as an explanation.

This is also applicable for IA, which clearly increases with time but also differs for the different experiments. Thus, the amount of IA incorporated in TA decreases as the residence time increases, which can be correlated with a reduced mean IA concentration for longer residence times, as for the main component TA/DST too.  $^{41}$  The shortest applied residence time of 3.7 min leads to almost  $1.5~\rm g_{IA}/100g_{total}$  and consequently almost no reduction regarding the original reactant ratio. On the other side, for the 16 min residence time, IA content is reduced substantially, to almost 80 % of the original content.

Due to limitations of the setup and the manual control of the process, longer or shorter residence times could not be tested. Instead, a linear extrapolation of IA content over residence time was applied to estimate the theoretical residence time for a complete IA removal (Appendix, Figure 8-8). This results in a possible optimal residence time range between 60 and 75 min for complete removal. However, it has to be considered that the IA purifying effect of longer residence times does probably not follow a linear trend and cannot be exploited indefinitely. This is especially relevant with regard to application of higher concentrated PET reactants and higher IA contents. For these conditions, an increase in residence time ( $\rightarrow$  larger vessel size/-number/ hold-up) might not be economically feasible, yet it could promote TA crystal size next to purity. Therefore, the effect of a longer residence time of at least 30 and 60 min should be tested and confirmed for higher PET reactant concentrations.

## 6.3 Reactant Concentration and Dispersion

While the reduction of reactant water content displays a promising approach generally, it also leads to disadvantages regarding TA crystallization. Thus, supersaturation increases for higher reactant concentrations and additionally, the overall concentration of impurities grows which can lead to more accumulation in the TA crystal. Moreover, a higher solid crystal content can complicate a homogeneous distribution while demanding a higher energy for agitation. On the other side, the targeted reduction of process streams can lead to reduced investment and operational costs (smaller pumps/ vessel size).

Next to these generally crystallization applicable facts, the mother liquor after TA precipitation still contains the second target monomer EG. As a high boiler, the remaining water must be separated first before allowing for EG recovery (max.  $\sim\!0.035~g_{EG}/g_{water}$ ) and purification by rectification. Furthermore, this stream displays an even more complex mixture as it contains sodium sulfate (or acetate) with high aqueous solubility, demanding for cooling or evaporative crystallization for recovery. This additionally emphasizes the general motivation to reduce process water input.

In contrast to the stated disadvantages regarding crystal size, Marlena et al. found that a higher PET reactant concentration of 105 g<sub>DST</sub>/L leads to significant increase in mean crystal size in their double feed semi-batch experiments (with 5 wt.-% sulfuric acid). On the other hand, their results for 21 g<sub>DST</sub>/L and 83 g<sub>DST</sub>/L revealed no differences. Regarding stirring rate, no significant impact was found between 120 rpm and 420 rpm, as stated before. In order to identify the interplay between reactant concentration and energy input during continuous TA precipitation and evaluate its impact on the crystalline properties, experiments with increased stirring rate and reactant concentration were conducted. Since 300 rpm did not sufficiently mix in 75.9 g<sub>DST</sub>/L experiments, deduced from optically visible segregated zones at the reactor wall, stirring rate was doubled to achieve homogeneous dispersion.

Figure 6-8 shows the respective quantile values for the 75.9  $g_{DST}/L$  experiments with 300 rpm ( $u_{tip} = 1.02$  m/s;  $Re_i = 5.80 \cdot 10^4$ ) and 600 rpm ( $u_{tip} = 2.04$  m/s;  $Re_i = 1.16 \cdot 10^5$ ) together with the equivalent values for standard PET reactant concentration within this work of 26.6  $g_{DST}/L$ . The initial quantile values at to are almost identical for all experiments and only show slightly larger 90 % quantile for the 300 rpm samples. These results represent the crystal after semi-batch precipitation and confirm the findings by Marlena et al. on the model reactant (5.1.2). However, over the course of the continuous operation, the TA crystals develop differently.

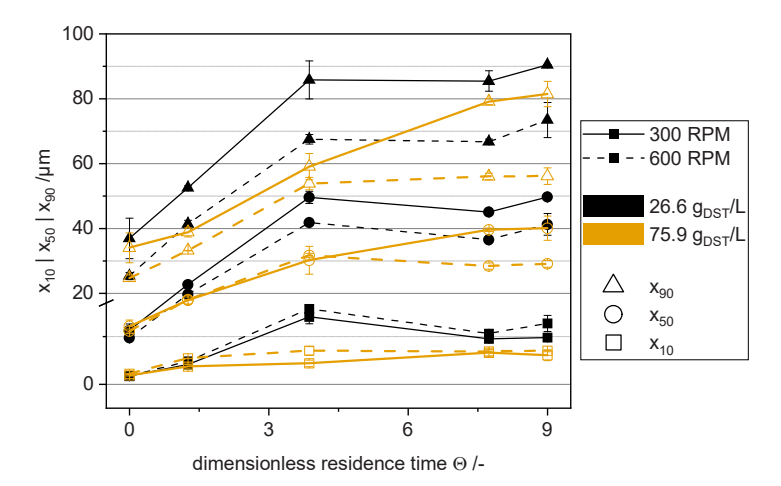


Figure 6-8  $x_{3,10}, x_{3,50}$  and  $x_{3,90}$  quantiles of TA from PET/PE reactant after precipitation with sulfuric acid at 80 °C with different concentrations and stirring rates, lines are shown to guide the eye.

Generally, for the 50 % and 90 % quantile, the increased stirring rate leads to

crystal breakage, probably due to pronounced secondary nucleation. However, this effect does not appear for the 10 % quantiles which do not show an impact for the different stirring rates, regardless of the respective concentration or time. Thus, smaller crystals do not develop due to mechanical abrasion but because of increased supersaturation indicated by the course of the high concentration  $x_{3,10}$  values lying below the standard concentration or both stirring rates. The fact that higher concentrated reactants generally lead to smaller crystals due to the increase in supersaturation is also widely reported in literature.  $^{41,43,131}$  This effect can be

partially compensated through increased mixing as shown by Caro et al. for

salicylic acid and Åslund and Rasmuson for benzoic acid. 42,43 Another effect can be seen by comparing the 300 rpm results at 75.9 g<sub>DST</sub>/L in comparison to all other test series. While the quantiles of the remaining experiments indicate an apparent steady state after t<sub>3.87</sub>, as the inclination bends down and flattens, the 300 rpm at 75.9 g<sub>DST</sub>/L quantiles continue to grow. They surpass the x<sub>3,50</sub> and x<sub>3,90</sub> quantiles of almost all distributions and maintain a linear slope, until reaching t<sub>7.74</sub> after which the slope kinks. Thus, for this experimental run a steady state was probably not reached and a further increase in crystal size possible.

The comparison of the SEM images displayed in Figure 6-9 reveals the effect of reactant concentration and dispersion on the morphological appearance of the TA.

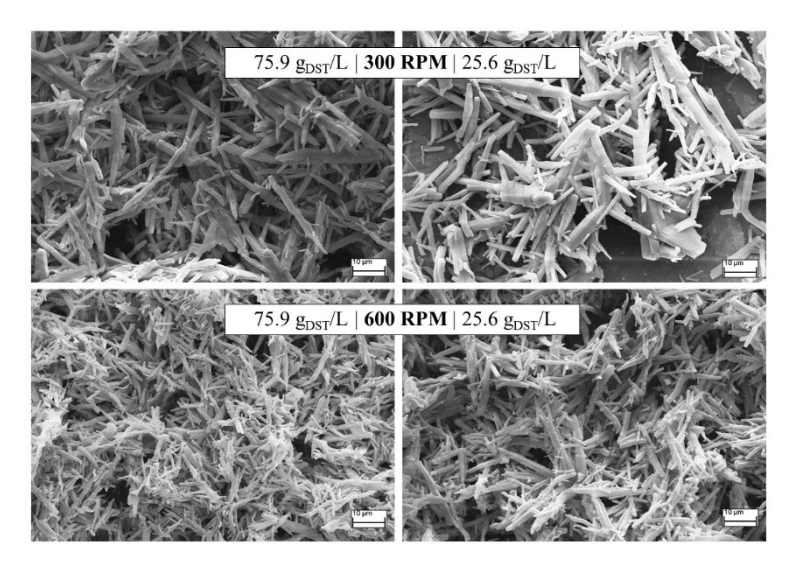


Figure 6-9 SEM images of TA samples (19) precipitated with sulfuric acid at 80 °C for different reactant concentrations and stirrer speed.

In congruence with the quantile development, especially the crystals precipitated at high concentration and 300 rpm possess a significant resemblance with the low concentration 600 rpm samples. The central "trunk" needle and the "branches" show a similar thickness while the low concentration and low speed sample is even thicker. Additionally, the dendritical structure appears to be more pronounced as a higher number of "branches" is visible. On one hand, this can be attributed to the reduced probability of collision under these conditions in comparison to higher stirring speed and crystal mass inducing abrasion.

On the other hand, it could be an indicator for a pronounced nucleation as a result of shear or mere supersaturation due to reactant concentration. Additional evidence for this interpretation is also given by the needle tips being flat and the smoother crystal surface only visible for the low concentration and low speed sample.

The remaining samples show dendrites with pointed tips and rough surface, which also promotes nucleation over a smooth surface. While this appearance can be the result of faster growth, it also leads to higher nucleation rate. In addition, the more intense mixing and higher reactant concentration reduce the diffusion limitation

of the precipitation. Together with a micro-mixing controlled reaction this can lead to a reduction in mean crystal size, as stated in 2.5.1.<sup>41</sup> These results indicate that a moderate mixing intensity promoting macro-mixing is advantageous for TA crystal size.<sup>24</sup>

In order to evaluate its impact on crystal purity, Figure 6-10 displays the colour index values and IA content for the respective reactant concentrations and stirring rates.

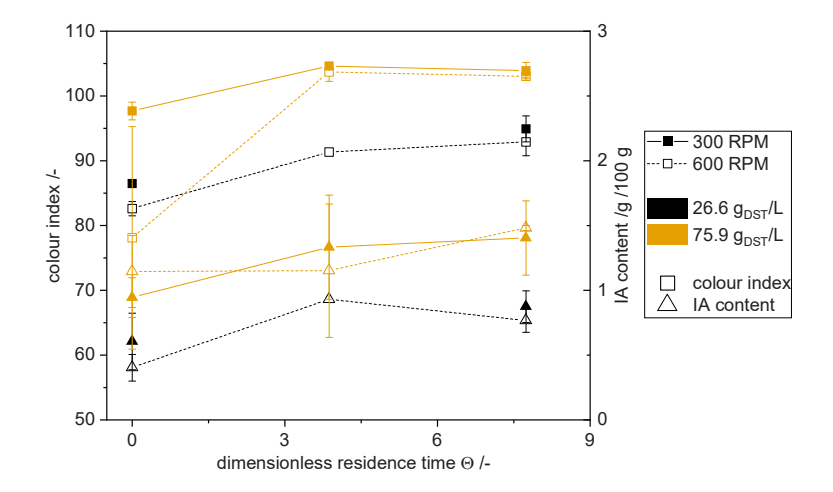


Figure 6-10 IA content and colour index of TA from PET/PE reactant after precipitation with sulfuric acid at 80 °C with different concentrations and stirring rates, lines are shown to guide the eye.

In contrast to the crystal size, purity primarily depends on reactant concentration. Thus, the results for IA content and colour index do not show significant differences, regardless of the stirring speed. This is in contrast to the expectation that diffusion of impurities from the crystal into the bulk would be promoted by increased stirring rate and a thinner diffusion boundary layer. On the other hand, IA content and colour index increase with increasing reactant concentration and also over the course of the experiment as before. Regarding colour index, tripling of the reactant concentration leads to a 10 % increase which is the result of a higher concentration of impurities and thus a higher probability of incorporation. The reduced correlation between colour index and reactant concentration is evidence for the purification effect of the precipitation.

However, IA content is ~50 % higher for the high DST concentration despite

constant TA/IA ratio in the PET reactant. Similar to results with 4.1 min residence time, the IA content in the 75.9  $g_{DST}/L$  solution of  $\sim 1.5$   $g_{IA}/g_{total}$  represents the original TA/IA ratio of the PET reactant. This can be interpreted as the consequence of multiple factors. Although IA solubility is generally higher, it can be assumed that IA solubility in mixtures with TA is reduced. Coupled with the higher reactant concentration, both effects induce a higher supersaturation for IA and therefore an increased probability of its incorporation in the crystal.

In a subsequent analysis the purification effect has been stressed even more through application of concentrated (96 %) sulfuric acid and a PET light blue reactant with a higher original IA content of  $\sim$ 3.5 %. The purification results are shown in Table 6-2.

Table 6-2. IA content and colour index of reactant/ PA concentration combinations.

PA Reactant	25 %sulf. acid	96 %sulf. acid		
$26.6~\mathrm{gdst/L}$	$2.95 \pm 0.07$	$3.01 \pm 0.13$	IA content /	
75. 9 gdst/L	$3.52\pm0.01$	$3.62\pm0.08$	$g_{IA}/100$ $g_{total}$	
26.6 g <sub>DST</sub> /L	114.1 ± 5.1	$130.4 \pm 1.8$	Colour index	
75. 9 g <sub>DST</sub> /L	$133.4\pm0.1$	$137.9 \pm 2.6$	Colour mucx	

With regard to decolouration potential, the results confirm that diluted PET reactants lead to a lower TA colour index, which also applies to the diluted PA. Consequently, the use of concentrated sulfuric acid provokes a similar TA discolouration in diluted PET reactant and vice versa. Regarding IA, the limits of the purification effect described before are even clearer. While IA content does not correlate with PA concentration, it is significantly lower for the diluted PET reactant. The absolute reduction of  $\sim 0.5~\rm g_{IA}/100~\rm g_{total}$  is almost identical to the results stated before. Considering absolute IA solubility of almost 1  $\rm g_{IA}/kg_{solvent}$  at 80 °C (3.2.4) and the IA content for the concentrated reactant of 2.1  $\rm g_{IA}/kg_{solvent}$ , a higher reduction could be possible. However, it can be assumed that the applied sampling method contributes to the accumulation effect. As the samples are taken

hot and left to cool prior to analysis, the samples become supersaturated for IA due to the higher absolute IA concentration. This could induce subsequent crystallization and thus a higher IA content. In an industrial process this issue is likely to be overcome by hot separation of the IA containing mother liquor. However, as the effect on IA reduction probably remains low, its advantage must be carefully balanced of the technical effort.

For sake of completeness, the respective PSDs are displayed in the Appendix in Figure 8-9. They show, that the tripled DST concentration with 25 % sulfuric acid leads to smaller crystals in comparison to the higher acid concentration dosed in diluted reactant. In extended investigations the PET reactant concentration (PET/PE) was increased to 127 g<sub>DST</sub>/L near DST solubility limit. While the colour index shows a comparable behaviour as before, IA content does not differ in comparison to 75.9 g<sub>DST</sub>/L. The development of the quantile values shows only a slight decrease of the x<sub>90</sub> value in the apparent steady state (Figure 8-10 and Figure 8-11).

In conclusion, these results show that TA quality benefits from higher dilution, which is in agreement with its fundamental effect on supersaturation. Thus, crystal size is larger and impurities like IA and discolouration are reduced. Nevertheless, the magnitude of quality improvement through dilution appears negligible when considering the potential of adsorptive purification and the possible reduction of process streams. Additionally, as stated before, a lower DST equally represents a lower EG concentration which has to be recovered subsequently from the mother liquor. Thus, from a holistic process perspective the benefit on TA quality from the use of low concentrated reactants does not compensate the consecutive downstream effort (e.g. water recycling, EG recovery).

Nevertheless, the industrial applicability must also be confirmed with regard to neighbouring unit operations (dissolution time, neutralization, adsorption, filtration, washing) that can be critically affected.

# 6.4 Start-up and pH Effect

The results presented in the previous chapters on the transfer towards a continuous operation are based on an initial batch precipitation and the same base parameters of 80 °C process temperature at a target pH of 2. Regarding precipitation temperature, further experiments between 87 °C (max.) and 40 °C have been conducted as well and show a similar behaviour as reported for batch operation (5.2). Thus, higher temperatures lead to larger crystals with higher purity (Figure 8-12 and Figure 8-13).

However, a closer determination of the optimal precipitation temperature will not

be focused further in this work. Instead the influence of the start-up procedure and target pH on the steady state and crystal properties are focussed.

# 6.4.1 Variation of Start-up

As the initial batch precipitation start-up procedure can be regarded as a crystal seeding step providing crystals for subsequent growth, a variation of these seeds was investigated. Therefore, temperatures were changed from 40 °C during initial batch precipitation to 80 °C during continuous operation while maintaining pH 2. However, the intention to provide a larger number of smaller seed crystals with consequently more crystal surface did not significantly affect TA crystal size. Instead the necessary time to reach steady state was prolonged in comparison to the standard procedure at constant temperature (Appendix Figure 8-14). In extensive studies regarding the application of seed crystals of different origin (e.g. PTA, ground PTA, ground needles), no effect on TA crystal size nor morphology could be induced. 149

During these experiments the initial reactor content was replaced by distilled water at 80 °C in order to avoid dissolution of seed crystals in the alkaline PET reactant during start-up (Case B; 4.1.3). Afterwards, feed and product pumps were initiated simultaneously and the continuous process started directly as reactants contacted in the distilled water. While seeding itself did not affect crystallization, the high initial dilution of the reactants with water reduced supersaturation substantially. This led to longer crystals (>> x90; see also Figure 8-5) initially. However, over the course of the experiment these trends equilibrate and reach a comparable scale to the standard batch procedure (Figure 8-15). An application of this start up procedure can be useful to avoid crystallization fouling and encrustation due to high initial supersaturations which can dramatically affect process runtime.<sup>24,150</sup> Furthermore, a short start-up time of the continuous process in addition to avoidance of supersaturation peaks is desired, which can equally be accomplished by using the product suspension itself.<sup>150</sup>

This short description of the different applied start-up procedures demonstrates that the final TA crystal size apparently only depends on process parameters during continuous operation. Thus, the provision of different seed crystals or the initial reduction in supersaturation did not change the properties of TA crystals.

## 6.4.2 pH Variation

Next to these approaches that partly facilitate a temporary reduction of supersaturation during start-up, a permanently lowered supersaturation can be induced through changing the pH through the PA dosing amount. By decreasing the provision of hydronium ions, supersaturation and thus nucleation is mitigated. While this induces a lower yield on one side, a higher pH has already demonstrated an IA reducing effect on the other side, shown in 5.2.1.

In consequence, next to acetic acid, also phosphoric and citric acid significantly lowered IA content in TA. This influence of pH was not seen for sulfuric acid so far as high local supersaturations at the dosing nozzle and thus, a temporary low local pH cannot be avoided during batch precipitation. However, the diluting effect of the continuous crystallizer operation facilitates analysis of this effect during application of sulfuric acid.

Therefore, Figure 6-11 shows the IA content and colour index of TA together with the respective pH courses that were increased or decreased stepwise during continuous operation.

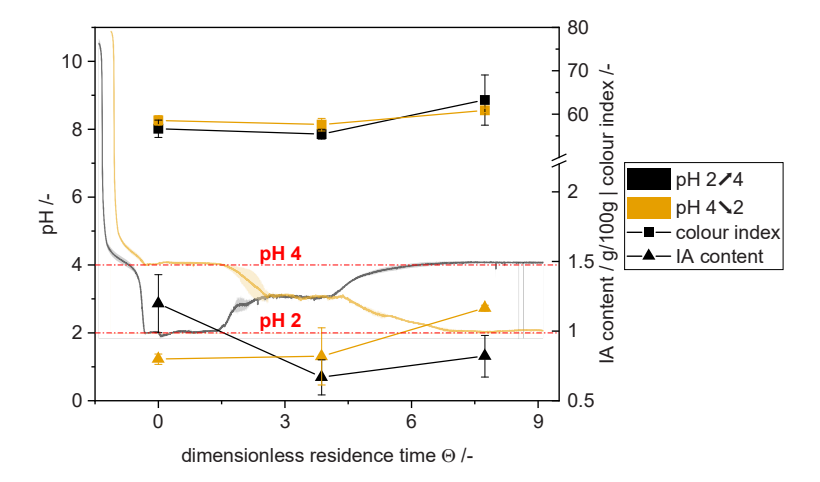


Figure 6-11 IA content and colour index of TA from PET/PE reactant after precipitation with sulfuric acid at 80 °C with variation of pH, lines are shown to guide the eye.

Both variations start with a batch precipitation, differing with regard to the respective target pH. At pH 2, the highest IA content is observed regardless of the previous procedure. On the other side, at pH 4 the IA content is almost 50 % lower

while IA reduction apparently already starts at pH 3 for both variations. However, due to the short time interval at pH 3 together with a residence time of 7.9 min. the total magnitude of the pH effect cannot be individually derived. In contradiction to the previous results on IA reduction during sub stoichiometric amounts of sulfuric acid, the initial pH 4 reduces IA content for IA directly. Since pH has not been monitored for the respective batch studies (5.2), operational errors cannot be excluded. In contrast to IA the colour index does not show a significant impact upon variation of pH. It remains constant and only shows elevated deviations for the last sample at pH 2.

Nevertheless, these results are in congruence with the previous explanation on the protonation behaviour of weaker PAs favouring precipitation of TA over IA due to the milder pH. It can be assumed that application of sulfuric acid at a similar pH as acetic acid at TA-equimolar addition would similarly reduce IA content in TA. According to Figure 5-8 this would induce a TA yield of  $\sim$ 50 %, assuming no partially protonated TA species.

Next to purity, the influence of pH variation on crystal size of was analysed. The quantile values are displayed in Figure 6-12 together with the respective pH courses as before.

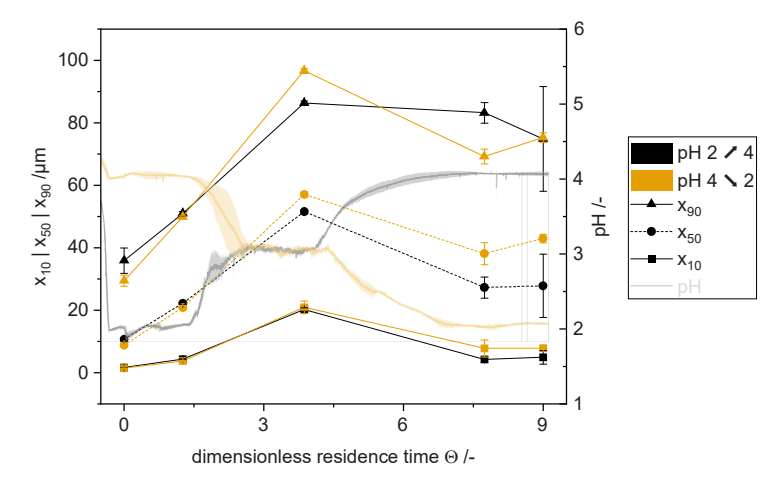


Figure 6-12  $x_{3,10}, x_{3,50}$  and  $x_{3,90}$  quantiles of TA from PET/PE reactant after precipitation with sulfuric acid at 80 °C with variation of pH, lines are shown to guide the eye.

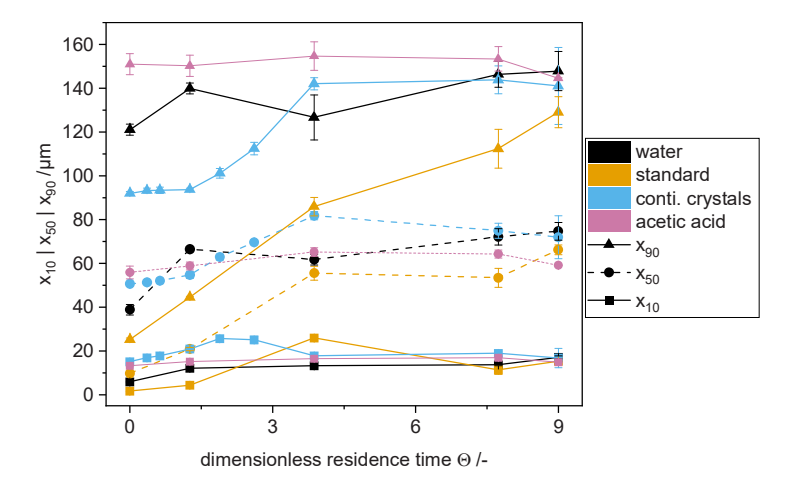
After the batch precipitation the quantile values are all in a comparable range for both pH values which also continues for the next sample at t<sub>1.26</sub>. Afterwards the pH is adjusted to pH 3 by adjusting the PA flow. This leads to a slight positive

kink in the development of the quantiles of the dropping pH curve  $(4\rightarrow 2)$ .

While the  $x_{3,10}$  quantile appears to be almost 20 µm for both, the  $x_{3,50}$  and  $x_{3,90}$ quantiles even surpass the quantiles of the inclining pH  $(2\rightarrow 4)$ . SEM images show a strong aggregation of the needles. This appears to occur also partly along the longitudinal axis (Appendix Figure 8-16). The subsequent second adjustment of the pH to the final target pH of 2 and 4 respectively, leads to a substantial decrease of the quantile values for both courses. While the x<sub>3,90</sub> quantile of the inclining pH course remains constant as before, the quantiles of the declining pH course drop. Especially the x<sub>3,10</sub> quantiles drop below 10 μm, which represents a significant increase of fines. The SEM images of the t<sub>7.74</sub> samples show only a few aggregates or dendrites primarily for the experiment with dropping pH curve. However, the crystals of the inclining pH appear to be thicker with hardly any singe needles occurring (Appendix Figure 8-16). Generally, as for the purity before, the region around pH 3 appears to have a significant impact on the crystal growth as well. Additionally, the stability of the aggregates appears to be sensitive to changes of the pH. Moreover, it can be possible that this disturbance of the continuous operation induces a different stationary state, which is for example reported for reactive distillation (multiple stationary states). 142

However, proving this assumption requires long term experiments, which have not been conducted in the present work for pH variation. Instead, the findings of the previous chapter on start-up procedures have been applied in combination with a pH adjustment. Therefore, Figure 6-13 displays the quantile values for three different initial reactor contents.

"Standard" refers to the initial batch procedure (case A; 4.1.3) and "conti. crystals" refers to TA crystals produced in a previous continuous experimental run with pH 2 for start-up. Acetic acid refers to the results from 6.1 and is displayed for comparison only. The procedure using "water" (Case B; 4.1.3) was conducted without initial seed crystals as introduced in 6.4.1, which is why the first sample was taken 90 seconds after start of the experiment. The application of water as start-up media results in an initially large x<sub>3,90</sub> quantile and generally larger crystals compared to the standard procedure, as already stated before. Starting with the product of a previous continuous precipitation leads to a generally narrower absolute quantile distance between x<sub>3,10</sub> and x<sub>3,50</sub>. However, the higher number of measurements for the conti. crystals reveal an initial growth lag-phase which can be correlated with its initial pH of 2 adjusting to target pH of 3.5. Instead, the water and standard procedure lead to a direct increase in crystal size.



This quantile growth continues for the standard procedure  $(x_{3,50} \text{ and } x_{3,90})$  almost until the end of the experiment but apparently stops for the water start-up after  $t_{1.26}$ . On the other side, the conti. crystal procedure induces a steep growth after the lag phase, which is especially pronounced for the  $x_{3,50}$  and  $x_{3,90}$  quantiles. However, the  $x_{3,10}$  quantiles reach a maximum above 20  $\mu$ m after 20 % of the experimental duration and slowly drop afterwards.

Nevertheless, at the end of the experiment, all start-up procedures lead to similar quantile sizes, although a stationary state is probably not reached for the standard procedure for this experimental run. This can be connected to individual procedure deviations between different operators. Additionally, regardless of the start-up content at pH 3.5 especially the  $x_{3,50}$  and  $x_{3,90}$  quantiles are substantially larger in comparison to the standard procedure at pH 2. Thus, instead of an  $x_{3,50}$  and  $x_{3,90}$  of  ${\sim}45~\mu m$  and  ${\sim}100~\mu m$ , the quantiles reach  ${\sim}70~\mu m$  and  ${\sim}135~\mu m$  respectively. Due to the pH adjustment, almost identical values compared to acetic acid are reached during continuous operation.

SEM images reveal that the needles and dendrites aggregate to larger structures that align along the needle direction and its "branches" (Appendix Figure 8-17). While these aggregates appear to grow to substantial scales, the attractive forces between needles represent a rather week connection. Thus, application of ultrasonication during particle size measurement, increased the optical density measured by the instrument significantly (10 %  $\Rightarrow$  20 %). This did not occur for

standard precipitation procedure at pH 2 and delivers an alternative explanation for the dropping crystal size. Due to the dynamic behaviour of the continuous precipitation an oscillating behaviour can occur before a steady state is reached. According to Lewis et al., a drop in crystal size reaching a maximum is caused by more large crystals being removed from the crystallizer than are able to grow into the larger size.<sup>151</sup> An alternative explanation can be the increased attrition probability of larger crystals leading to an increase in secondary nucleation. Nevertheless, the amplitudes of the resulting oscillations eventually decrease and end into a steady state.<sup>151</sup> In further similar experiments, pH was varied after an initial batch precipitation (pH 2) to a pH of 3 and 3.5 respectively. This resulted in a rounded aggregates of TA needles, displayed in Figure 6-14.

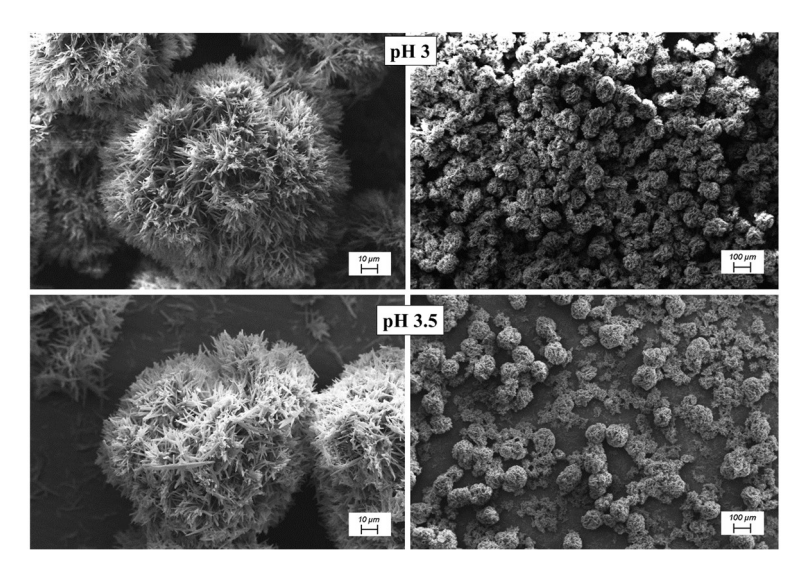


Figure 6-14 SEM images of rounded TA morphology after precipitation with sulfuric acid at 80 °C at constant pH of 3 (75.9  $g_{DST}/L$ ) and 3.5 (26.6  $g_{DST}/L$ ), left images show 500 x and right 50 x magnification.

The majority of these rounded aggregates features an average diameter of  $100~\mu m$  and appear very homogeneous in their morphological appearance. The single needles at the outside of these aggregates appear significantly slimmer in comparison to previously shown dendrites. Examples of larger spherical agglomerates revealed their inside which was again filled with spherical dendrites (Figure 8-20). However, this example also resembles a gas bubble which could be

an experimental artefact or evidence for surface nucleation on gas bubbles. Additionally, the elevated pH favours agglomeration as a consequence of a reduced zeta potential. Thus, Berg et al. reported a strong tendency of nanoparticles to agglomerate and increase size for a zeta potential approaching 0 at their isoelectric point. 152 For dicarboxylic TA this can be estimated to be at a pH of ~4 which provides explanation for the occurrence of these aggregates. Besides this fact, these aggregates could not be reproduced intentionally during every experiment when applying similar conditions by different operators. This again can be attributed to the sensitivity of their formation process. Despite their fragile appearance these aggregates remained stable during filtration and washing. This resulted in a significant improvement of processability with regard to filtration and washing time reduction, displayed in the Appendix Figure 8-19. Thus, a pH 2 batch precipitation reduced filtration and washing time to ~8-10 % of the initial filtration time at t<sub>0</sub>. Instead, the rounded morphology at pH 3.5 induced an even higher reduction to 2-3 % of the initial filtration and wash time. For the sake of completeness, it has to be considered that wash time does only refer to the time for 200 mL of distilled water to pass the compressed filter cake, but does not evaluate its efficiency. This efficiency could by particularly compromised due to the very pronounced dendritical appearance as stated in 2.5.2. It can be concluded, that the choice of pH displays a crucial role for an advantageous TA precipitation, whereas parameters like residence time or reactant concentration appear almost negligible. Considering BMR process implementation, precipitation at elevated pH facilitates a partial removal of IA using sulfuric acid. Additionally, it induces growth of large dendritical crystals that can aggregate to a spherical morphology which significantly reduces the filtration effort. However, an elevated pH precipitates less TA and consequently reduces yield, which must be considered in a precipitation concept.

## 6.5 Precipitation Concept

Apart from the previously presented pH influence, several parameters have been analysed throughout this thesis in their influence on a high TA purity, high yield as well as large crystal size promoting TA processability. A qualitative overview and summary of these parameters is displayed in Table 6-3.

Generally, the most influencing parameters have been found to be precipitation temperature, the applied PA and the pH during application of sulfuric acid. The impact of the remaining parameters was found to be comparably low, while inducing significant operational consequences. Thus, for example a high dilution of reactants increases the overall downstream effort and a high residence time demands for significantly larger reactors. Based on these findings, a precipitation concept for continuous precipitation of TA is derived.

<i>Table 6-3. Q</i>	ualitative e	ffects of	process	parameters o	on TA o	quality	parameters.
---------------------	--------------	-----------	---------	--------------	---------	---------	-------------

Effect Parameter	Large Crystal Size	High Purity	High Yield
Temperature	high	high	(low)
Precipitation Acid	Acetic acid	Acetic acid	Sulfuric acid
Concentration	low	low	-
Agitation	low	-	-
Residence time	high	high	-
pН	high	high	low

However, although the use of acetic acid leads to especially large crystals and a significant reduction of IA content, it is not considered for application in this concept which is instead focused on sulfuric acid. This is justified by several issues that can partially be resolved during scale up.

Thus, a fouling issue occurred in lab scale during continuous operation leading to blockage of tubing and pumps, which could be resolved as the dimensions during scale up increase. Furthermore, in order to overcome the reduced yield, hyper stoichiometric amounts of acetic acid or partial recirculation of mother liquor would have to be applied, questioning the economic advantages of acetic acid application. Moreover, as the residual sodium acetate acts as a buffer, the precipitation potential of additional acetic acid might be reduced even further, indicated by experimental results outside the scope of this thesis. Nevertheless, sodium acetate represents a high value by-product that also can compensate higher

procurement costs for acetic acid if recovered in sufficient purity (see also 3.2.6). These acetic acid specific counter-arguments complicate its industrial implementation at this stage of development.

Additionally, the application of sulfuric acid has been found to benefit substantially from continuous operation as the reduced supersaturation induced dendritical growth of TA crystals with advantageous filterability compared to acetic acid. Moreover, a pH adjustment to values between 3 and 4 leads to a significant reduction of IA content to almost a similar extent like acetic acid. Under these conditions, the TA dendrites partially developed a spherical structure which promoted filterability even more. Thus, as an interim conclusion, continuous precipitation with sulfuric acid at elevated temperature (e.g. 80 °C) and a pH between 3 and 4 can be derived as starting point of a precipitation concept.

Despite of these significant benefits, precipitation at an elevated pH reduces TA yield, caused by the insufficient provision of hydronium ions for protonation of TA. However, this represents a substantial opportunity for the separate recovery of an IA enriched TA which can be separately applied to tailor the final PET properties to individual demand. Thus, considering the reduced IA content in crystalline TA after precipitation between pH 3 to 4, the residual IA must consequently accumulate in the liquid mother liquor. This IA enriched mother liquor can subsequently be isolated and separately precipitated at pH 2 for recovery of an IA enriched TA(2). In this second monomeric product, TA would represent the impurity as a maximum IA content is targeted.

However, the degree of IA enrichment depends on the ratio between residual IA and TA in the mother liquor, which is simultaneously represented by a low IA content in the first TA(1) recovered and its yield, both depending on ph. Therefore, in order to identify a suitable parameter window for the pH cut between both steps, several continuous precipitation experiments with varying target pH values were conducted. As pH in the region of interest is highly sensitive to changes in PA flow, pH fluctuations during steady state occurred due to manual handling (pH curves in Appendix Figure 8-20). The results regarding purity, yield, and processability of these experiments are displayed in Figure 6-15. The respective pH ranges due to the described fluctuations are displayed as error bars in the diagram. They represent the pH range which was averaged over one residence time before the sample was taken ( $t_{2.87} \rightarrow t_{3.87}$ ;  $t_{8} \rightarrow t_{9}$ , Figure 8-20). All experiments started with a batch precipitation to pH 2 and were subsequently adjusted to the respective target pH while samples were taken at times t<sub>3.87</sub> and t<sub>9</sub> assuming a steady state. With regard to Figure 6-15, the displayed quality parameters for IA purity, TA crystal size and filterability were modified to relative

parameters for improved comparability according to the following Equations 6-1 to 6-3.

$$filtration\ time\ reduction\ (t_{3.87}\mid t_9) = \left(\frac{filtration\ time\ (t_{3.87}\mid t_9)}{filtration\ time\ (t_0)}\right)\cdot 100$$
 6-1

$$IA_{residue}(t_{3.87} | t_9) / \% = \left(\frac{IA_{content}(t_{3.87} | t_9)}{IA_{content}(t_0)}\right) \cdot 100$$
 6-2

$$span_{normalized} = (span_{t_{3.87|9}} - 1) \cdot 100 = \left[ \left( \frac{x_{3,90} - x_{3,10}}{x_{3,50}} \right)_{t_{3.87|t_9}} - 1 \right] \cdot 100$$
 6-3

Thus, the filtration time reduction correlates the filtration time at the sampling time ( $t_{3.87}$  and  $t_9$ ) with the filtration time at  $t_0$  after batch precipitation at pH 2. The same comparative approach applies for the IA<sub>residue</sub> at  $t_{3.87}$  and  $t_9$  which is connected to the initial content at pH 2. The span is a common measure for evaluation of the width of a distribution. It combines all three previously used quantile values and serves as a measure for a homogeneous crystal size represented by small span value. In order to visualise it in one diagram it has been normalized and shifted while not altering the shape of the curvature.

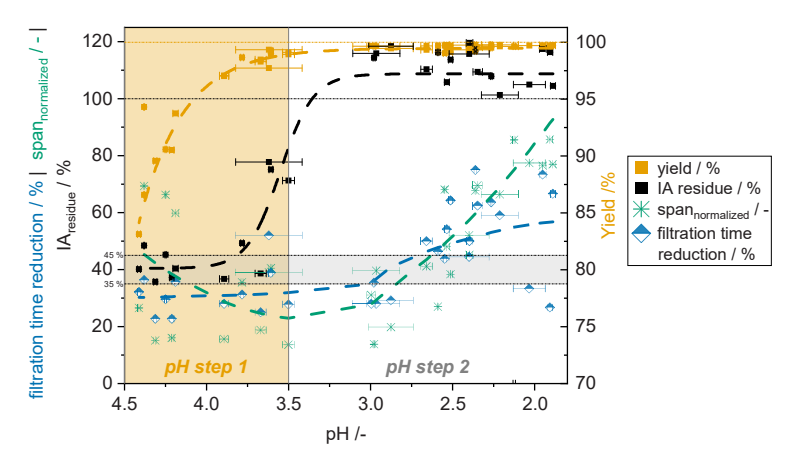


Figure 6-15 Yield, IA residue, normalized span and filtration time reduction of TA after precipitation at 80 °C with sulfuric acid over respective pH, all values refer to pH at t3.87and t9 according to Figure 8-20, lines are shown to guide the eye.

Starting with the normalized span, a steep reduction with increasing pH with a minimum around pH 3.5 can be observed. This span minimum is in congruence with the occurrence of spherical aggregates shown in the previous chapter. Similarly, the filtration time reduction drops steeply until reaching pH 3 and remains almost constant upon further increase of pH whereas span rises again. As this increase does not negatively affect the filtration time reduction, consecutive focus is set on the optimal ratio between yield and IA residue. Despite the scattering of the values, the relation between TA yield and IA residue over pH appears concise. Thus, in congruence with 5.1.3.1, yield decreases drastically between pH 3.5 and 4.5. Likewise, IA residue drops to values between 45 % to 35 % of the original IA content, apparently representing a minimum (grey horizontal marking). On the contrary, IA appears to accumulate at pH values between 2 and 3 where overall yield is at its maximum. For comparison, acetic acid led to an even lower 20 % IA residue without accumulation as shown before (Figure 6-4). Consequently, in order to achieve a maximal reduction of IA in TA(1), a pH between 3.5 to 4.5 must be chosen in a first precipitation step, representing a vield between ~96 % and 83 %. Assuming a constant IA residue between 35 % and 45 % of the initial IA content after batch precipitation IA<sub>0</sub>, it can be derived that IA accumulates in the subsequently precipitated TA(2). This derivative is based on a theoretical mass balance assuming complete yield possible and a sharp separation between mother liquor and crystals without residue. By assuming a constant IA residue percentage, the IA content in TA(1) remains constant over yield in the pH range between 3.5 and 4.5 and can be calculated using Equation 6-4 (derived from mass balance in Appendix Equation 8-1 to 8-4). Together with the directly obtained IA residue in TA(1) the IA partition coefficient K<sub>IA</sub> can be calculated with Equation 6-5 (Appendix Figure 8-21).

$$IA_{TA(2)} = IA_0 \cdot \frac{residue.}{(1 - yield)}$$

IA partition coefficent 
$$\kappa_{IA} = \frac{TA.2.}{IA_{TA.}}$$
 6-5

In order to visualise the interplay between yield and IA content in TA(1) after a first precipitation and TA(2), Figure 6-16 displays an example for 3 different initial IA contents IA<sub>0</sub> of possible PET reactants.

IA content in TA(1) is displayed by dotted lines and for TA(2) with continuous

lines. Different shades of colour refer to two different levels of IA<sub>residue</sub> in TA(1) according to Equation 8-3.

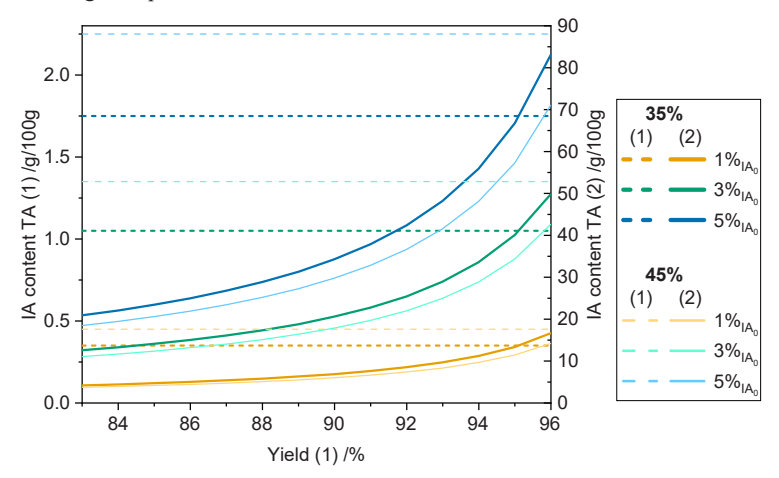


Figure 6-16 Distribution of IA between TA (1) and TA (2) of two consecutive precipitation steps for two different levels of IA residue and 3 different initial IA contents IA<sub>0</sub>, calculated from mass balance

As declared before, this IA<sub>residue</sub> remains constant at a pH between 3.5 and 4.5 indicated by the parallel dotted lines. As a result of this condition, the absolute IA content in TA(1) remains constant over yield. On the other side, the IA content in TA(2) increases with increasing yield of the first precipitation step as residual IA allocates on less TA. It can be deduced that a high yield of the first precipitation step promotes a higher IA content and thus isomeric purity of TA(2). For the Example of a high IA<sub>0</sub> content of 5 %, TA(2) eventually consists of more than 80 % IA, making TA the impurity. For a TA(2) precipitated from a 3 % IA<sub>0</sub> PET reactant at 96 % TA(1) yield, could already contain  $\sim$ 50 % IA.

However, this theoretical balance is based on the results of one PET light blue reactant with a comparably high IA content of  $\sim\!\!3\text{--}3.5$  %. For lower IA contents a different IA residue percentage could apply. On the contrary, the present results are based on a temperature of 80 °C only. As IA solubility significantly increases with temperature ( $\Delta c_{IA}[80\ ^{\circ}\text{C}\text{--}90\ ^{\circ}\text{C}] \sim \!\!0.5\ g_{IA}/kg_{water}),\;$  a higher precipitation temperature would drastically promote IA separation (Appendix Figure 8-13).

Nevertheless, a possible subsequent IA supersaturation caused by cooling should be avoided by performing solid liquid separation for TA(1) preferably at the precipitation temperature. To summarize, a simplified block flow diagram of the proposed precipitation concept is shown in Figure 6-17. Additionally, it contains

the values of a mass and component balance for IA (Appendix Equation 8-1 to 8-4) for a PET reactant with  $3 \square \text{wt.} \%$  IA content. Total masses  $m_{TA(i)}$  refer to the hourly production of rTA from 6.9 kg PET.

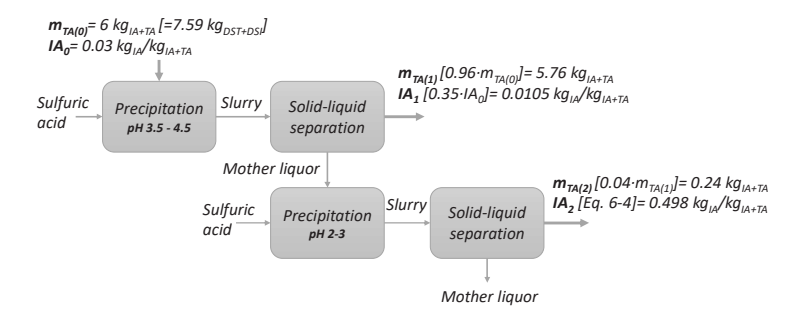


Figure 6-17 Block flow diagram of two-step precipitation concept with mass balance example for a PET reactant with an initial  $IA_0$  of 3 %.

In consequence, of the total IA mass of 180 g of TA(0), about one third is incorporated in TA(1); while the remaining two thirds are incorporated in TA(2). While this concept primarily facilitates substantial reduction of IA in TA(1) and the parallel recovery of a second IA enriched product TA(2), the final products still differ from PTA (and purified IA) in shape and isomeric purity. Consequently, a subsequent recrystallization step similar to flash crystallization after fossil synthesis (3.2.1) must be applied in order to meet industrial specifications. Therefore, the necessity of applying an additional precipitation step is questionable, if recrystallisation for altering crystalline morphology and separating IA is needed in any case.

In order to explain the advantages of prior IA reduction, the subsequent Table 6-4 displays the limit temperatures for IA to remain in solution after recrystallization. Thus, if the solid/liquid separation after recrystallization falls below the stated temperatures, IA crystallizes and impurifies rTA.

Table 6-4 Solubility limit temperatures for different  $IA_0$  contents in TA after recrystallization of  $100 g_{TA+LV}/kg_{solvent}$  at 270 °C.

IA <sub>0</sub> content / g <sub>IA</sub> /100 g	Solubility limit / °C
1	81
2	102
3	114
4	122
5	129

The values of the example refer to an initial complete dissolution at 270 °C of a TA/IA mixture with different IA $_0$  contents. This is in line with the fossil purification, during which crude TA is completely dissolved in water at temperatures exceeding 250 °C preferably between 15-30 wt.-% of TA. $_0^{153}$  The solubility temperatures were approximated using the single component solubility data for IA and TA by Sheehan. $_0^{10}$  It is shown that an increasing IA $_0$  content demands for higher temperatures to avoid crystallization of IA. Consequently, for IA $_0$  contents exceeding 2 %, the IA enriched mother liquor must be separated from crystals above 100 °C and 1 bar to avoid crystallization of IA. As a mutual solubility interference between IA and TA can be expected, the limit temperature can be expected to be even higher. Moreover, local IA supersaturation and thus its incorporation could occur during rapid flashing.

In consequence, additional effort must be applied by using rotary pressure filters for separation of IA, comparable to separating p-toluic acid during PTA synthesis which in contrast to IA displays a polymerization critical impurity. However, this could be overcome by reducing IA content in rTA before recrystallization simplifying its purification.

Furthermore, in additional experiments beyond the scope of this thesis, an IA residue of 20 % after recrystallization in water at 205 °C was achieved despite dissolving only 1/3 of TA crystals (2/3 excess) at a residence time of 30 min (+ ~1 hour heat up). This can be explained by crystal aging mechanisms which have also been reported for purification of crude TA from 4-CBA. The sake of completeness, it is stated that a complete dissolution in consecutive experiments led to a 2% IA residue for a TA with 1.35 gra/100g IAo. The consequence, post-precipitation purification of TA does not necessarily demand for complete dissolution if IA content of TA input is sufficiently low to benefit from a 20 % IA residue after recrystallization. Another key point is the fact that IA does not display a critical impurity acting as a chain terminator in polymerization as IA is intentionally added for desired transparency in packaging and avoided for textile applications. Thus, IA does not necessarily have to be

removed if the polymer application demands its addition.<sup>158</sup> Instead, BMR processes must be able to control and adjust IA content (e.g. by mixing TA(1) and TA(2)) but not separate it completely.

As a result, the developed concept extents the possibilities of BMR to control IA content in rTA while sustaining the application of strong sulfuric acid. It additionally promotes an advantageous TA filterability after precipitation, reduces effort for subsequent recrystallization and provides a starting point for the separate recovery of a second recycled co-monomer IA. While final adjustment of crystal morphology is still necessary, eventually this concept can extent the applicability of BMR processes and improve the overall economic efficiency through recovery of another valuable recycled monomer that can replace fossil-based IA.

### 7 Conclusion and Outlook

#### 7.1 Conclusion

In this work, the reactive precipitation of terephthalic acid (TA) as the product recovery step within PET back-to-monomer recycling (BMR) based on alkaline hydrolysis (revolPET®) was investigated. Fundamentally, this precipitation consists of dosing a mineral or organic precipitation acid (PA) into a disodium terephthalate (DST) solution leading to instant crystallization of TA.

In order to crystallize a TA with a larger crystal size, improved filterability and purity, the influence of different operational parameters was analysed. Starting point was an experimental parameter screening in a model reactant system focussing on crystal size and filterability. The most promising parameters were subsequently applied on real depolymerized reactants from PET waste and additionally evaluated regarding their purification potential. Next to the objective of reducing coloured impurities, especially separation of isophthalic acid (IA) was focussed as the control of its concentration in PET synthesis is crucial. Finally, these results obtained in a batch setup were transferred to a continuous operation in continuation of a continuous PET depolymerization step (revolPET®). This development concludes in conceptual procedure for an optimized exploitation of the precipitation step for TA purification and recovery.

#### Batch Precipitation in Model System

The results after batch precipitation show that an increase in process temperature substantially improves TA crystal size and filterability. Although absolute TA solubility hardly changes between 36.5 °C and 90 °C, its relative increase suffices to induce this processability improvement. While these results were obtained using sulfuric acid, this effect was even more obvious upon application of acetic acid as precipitation agent. In accordance with literature data on solubility, acetic acid precipitates TA crystals that are up to 10 times larger in all dimensions than needle crystals after precipitation with any other acid (oxalic, hydrochloric, phosphoric, citric, sulfuric).

Similarly, the filtration times were generally shorter for acetic acid but approximated for sulfuric acid precipitate at higher temperatures. However, weaker acids provide less hydronium ions for protonation of the terephthalate ion which reduces product yield at equimolar addition (~78 %) in comparison to stronger dissociating acids. Nevertheless, this effect is attenuated by low solubility of TA which represents an artificial product removal, advantageously shifting the

#### Conclusion and Outlook

dissociation equilibrium of the PA. Therefore, hyper stoichiometric amounts of acetic acid (e.g.) also lead to higher yield and potentially complete TA recovery despite maintaining an almost constant pH around 4.

## Batch Precipitation in Real System

The behaviour on crystal size and processability was also confirmed for reactants from real depolymerized PET waste fractions originating from post-consumer PET bottles and post production multilayer trays. These reactants additionally contain IA intentionally added to promote packaging transparency by reducing PET crystallinity. It could be shown that an increasing temperature reduced incorporation of IA in the precipitate. An even more pronounced effect was induced during application of acetic acid which reduced IA to 20 % of the original content. With regard to the yellow discolouration of the PET reactants, only elevated temperatures lead to a significant reduction, while differences between PAs were negligible.

Generally, impurities could be reduced by the same parameters which promote larger TA crystals and faster filterability (acetic acid and elevated temperatures). However, the primary degree of purity is defined by the original PET reactant, since operational parameters during precipitation could not restore virgin TA purity.

### Continuous Precipitation in Real System

Finally, the batch precipitation was transferred to continuous operation maintaining the general stirred tank reactor setup. This setup reduced the effective concentration of the reactants and provided growable crystal seeds which were initially provided through a batch precipitation followed by continuous operation. Monitoring the development of the quantiles of the cumulative crystal size distributions showed a steep initial inclination reaching a stationary state after approximately 3-4 times reactor volume exchange. Microscopic images revealed formation of dendrites which significantly improved filterability after sulfuric acid precipitation.

For acetic acid, no significant increase in crystal size was evidenced and likewise filterability remained constant. The reducing effect of acetic acid on incorporation of IA was sustained during continuous precipitation as well while sulfuric acid showed no purification effect.

In consequence of higher yield, crystal size and faster filterability, the subsequent focus was set to sulfuric acid for precipitation. While a longer residence time and a higher dilution promoted crystal purity, a significant effect on crystal size was not witnessed. However, an increase in energy dissipation through higher stirring

#### Conclusion and Outlook

rates at higher reactant concentrations reduced the crystal size at the stationary state whereas at lower stirring rates crystal growth continued not reaching constancy.

In continuation of the applied batch precipitation at start-up, a variation of the crystal seeds was considered which did not affect crystal morphology nor size. Instead, a substantial effect on crystal size and purity was induced by increasing the target pH which simultaneously represents a constant reduction in supersaturation. Thus, at a pH between 3 and 4 and a reduced yield, the dendrites adopted a spherical shape of outward pointing needles. These aggregates possess an improved filterability while on the other side washing efficiency could suffer. However, especially at a pH above 3.5, IA content was reduced to up to 35 % of the initial content at a yield around 96 %, adopting the IA purification of acetic acid (~20 %) to sulfuric acid at a higher yield.

The transfer of this crystal purification effect into a mass balance, infers the consequential accumulation of IA in the residual mother liquor. This raises the opportunity for a separation of this mother liquor and a subsequent recovery of the residual IA enriched TA as a separate product. Thus, next to an improved TA recovery by filtration, its isomeric purity is substantially reduced in addition to the possible separation of an IA enriched TA. This IA enriched TA can possibly open up new economic perspectives for BMR processes by replacing fossil-based IA.

In conclusion, within this work the influencing operating parameters on the precipitation of TA have been identified and studied extensively. As result, a continuously operated two-step precipitation concept is proposed which combines the crystallization of TA showing significantly improved filterability with a significant reduction of incorporated IA. Additionally, this isomer can be recovered in a separate precipitation step. While the morphology of precipitated rTA impedes its direct application ("drop-in readiness"), the advantageous recovery substantially contributes to a universal utilization of rTA from BMR processes in packaging or fibre applications.

## 7.2 Outlook

### **Fundamentals**

Generally, this research work primarily consists of phenomenological findings that are directly applied in process development. Thus, a more fundamental perspective could be investigated regarding the individual crystallization behaviour (nucleation and growth) during precipitation of TA. This also comprises the extension of solubility data for the system IA/TA/water together with the determination of activity-based supersaturations. While this contributes to a more fundamental understanding of the precipitation in model reactant, it could be extended by intentional addition of common impurities and comonomers of PET reactants in order to identify their individual impact on rTA quality.

## Concept Validation

As the proposed two-step concept is partially based on assumptions, future research should confirm the theoretically derived mass balance regarding IA. Additionally, the exploited effect of the pH on reduction of IA should be extended and validated for pH 3.5 and above, since an even greater impurity reduction could be possible. Likewise, reduction on PET reactants with different initial IA contents should be confirmed. Next to this focus on the crystals of the first product, crystallization of the second IA enriched product should be optimized as its different composition could affect its crystallization behaviour.

### Scale-up

Furthermore, a central objective of this research is the provision of an industrially relevant concept, as its motivation is derived from a global recycling challenge. Therefore, the developments regarding precipitation of TA must be transferred and validated in an industrial level (scale-up). Thus, application of a continuous crystallizer cascade should be considered reducing residence time width and possible distribution and heat transfer issues to achieve a constant product quality.

## Recrystallization

Apart from precipitation for product recovery a subsequent recrystallization step can be necessary in order to produce an industry conforming TA being drop-in ready for existing polycondensation plants. While this displays an additional effort, stressing overall process economics, it also inherits a significant advantage, since reaction intermediates of crude oil TA synthesis have already been removed during its purification by hydrogenation. Moreover, separately conducted

### Conclusion and Outlook

experiments indicate, that precipitated TA does not necessarily have to be dissolved completely during recrystallization to cope with drop-in requirements. Thus, future research should also focus on recrystallisation of recycled TA which can additionally influence the precipitation due to potentially different quality requirements for recrystallization.

- [1] PETcore Europe. *PET Market in Europe State of Play 2022*:

  \*\*Production, collection and recycling. https://www.petcore-europe.org/images/news/pdf/PET\_REPORT\_2022\_V4\_compressed.pdf (accessed 2022-06-21).
- [2] Pinter, E.; Welle, F.; Mayrhofer, E.; Pechhacker, A.; Motloch, L.; Lahme, V.; Grant, A.; Tacker, M. *Circularity Study on PET Bottle-To-Bottle Recycling. Sustainability* **2021**, *13* (13), 7370. DOI: 10.3390/su13137370.
- [3] Directive 2019/904 on the reduction of the impact of certain plastic products in the environment: Single Use Plastics Directive, **2019**.
- [4] Nisticò, R. *Polyethylene terephthalate (PET) in the packaging industry. Polym. Test.* **2020**, *90*, 106707. DOI: 10.1016/j.polymertesting.2020.106707.
- [5] Suhaimi, N. A. S.; Muhamad, F.; Abd Razak, N. A.; Zeimaran, E. Recycling of polyethylene terephthalate wastes: A review of technologies, routes, and applications. Polym. Eng. Sci. 2022, 62 (8), 2355–2375. DOI: 10.1002/pen.26017.
- [6] Crippa, M.; Morico, B. PET depolymerization: a novel process for plastic waste chemical recycling. In Catalysis, Green Chemistry and Sustainable Energy; Angelo Basile, Gabriele Centi, Marcello De Falco, Gaetano Iaquaniello, Ed.; Studies in Surface Science and Catalysis; Elsevier, 2020; pp 215–229. DOI: 10.1016/B978-0-444-64337-7.00012-4.
- [7] Gravendeel, M.; Groot, M. de; Slenders, L.; Stevens, B.; Stolk, M.; Wolters, J.; Wolters, A.; Wouters, F. Depolymerization of PET Polymers at Ioniqa Technologies (Case Study). In Industrial Arene Chemistry; Mortier, J., Ed.; Wiley, 2023; pp 2117–2141. DOI: 10.1002/9783527827992.ch67.
- [8] Alvarado Chacon, F.; Brouwer, M. T.; van Thoden Velzen, E. U. Effect of recycled content and rPET quality on the properties of PET bottles, part I: Optical and mechanical properties. Packag. Technol. Sci. 2020, 33 (9), 347–357. DOI: 10.1002/pts.2490.
- [9] Geyer, B.; Lorenz, G.; Kandelbauer, A. Recycling of poly(ethylene terephthalate) A review focusing on chemical methods. Express Polym. Lett. **2016**, 10 (7), 559–586. DOI: 10.3144/expresspolymlett.2016.53.

- [10] Sheehan, R. J., Ed. Ullmann's Encyclopedia of Industrial Chemistry: Terephthalic Acid, Dimethyl Terephthalate and Isophthalic Acid; Wiley-VCH Verlag GmbH & Co. KGaA: Weinheim, Germany, 2012. DOI: 10.1002/14356007.a26 193.pub2.
- [11] Ji, L. N. Study on Preparation Process and Properties of Polyethylene Terephthalate (PET). AMM 2013, 312, 406–410. DOI: 10.4028/www.scientific.net/AMM.312.406.
- [12] Valh, J. V.; Vončina, B.; Lobnik, A.; Zemljič, L. F.; Škodič, L.; Vajnhandl, S. Conversion of polyethylene terephthalate to high-quality terephthalic acid by hydrothermal hydrolysis: the study of process parameters. Text. Res. J. 2020, 90 (13-14), 1446–1461. DOI: 10.1177/0040517519893714.
- [13] Brepohl, E. Continuous back to monomer recycling of PET from composite materials using a twin-screw extruder; ProcessNet Reaction Engineering: Online, 2021.
- [14] Biermann, L.; Brepohl, E.; Eichert, C.; Paschetag, M.; Watts, M.; Scholl, S. *Development of a continuous PET depolymerization process as a basis for a back-to-monomer recycling method. Green Process.*Synth. 2021, 10 (1), 361–373. DOI: 10.1515/gps-2021-0036.
- [15] Franco, R. L. C.; Eichert, C.; Lücking, C.; Biermann, L.; Paschetag, M.; Scholl, S. revolPET®: An Innovative "Back-to-Monomer" Recycling Technology for the Open Loop Value Chain of PET and Polyester Composite Packaging and Textiles. In Manufacturing Driving Circular Economy:Proceedings of the 18th Global Conference on Sustainable Manufacturing, October 5-7, 2022, Berlin, 1st ed. 2023; Kohl, H., Seliger, G., Dietrich, F., Eds.; Lecture Notes in Mechanical Engineering; Springer International Publishing; Imprint Springer, 2023; pp 175–183. DOI: 10.1007/978-3-031-28839-5\_20.
- [16] Tournier, V.; Topham, C. M.; Gilles, A.; David, B.; Folgoas, C.; Moya-Leclair, E.; Kamionka, E.; Desrousseaux, M.-L.; Texier, H.; Gavalda, S.; Cot, M.; Guémard, E.; Dalibey, M.; Nomme, J.; Cioci, G.; Barbe, S.; Chateau, M.; André, I.; Duquesne, S.; Marty, A. An engineered PET depolymerase to break down and recycle plastic bottles. Nature 2020, 580, 216–219. DOI: 10.1038/s41586-020-2149-4.
- [17] Müller, C.; Heck, C. A.; Stephan, L.; Paschetag, M.; Scholl, S. Precipitation of Terephthalic Acid from Alkaline Solution: Influence of Temperature and Precipitation Acid. Ind. Eng. Chem. Res. 2023, 62 (30), 12029–12040. DOI: 10.1021/acs.iecr.2c04451.

- [18] Lee, H. L.; Chiu, C. W.; Lee, T. Engineering terephthalic acid product from recycling of PET bottles waste for downstream operations.

  Chem. Eng. J. Adv. 2021, 5, 100079. DOI: 10.1016/j.ceja.2020.100079.
- [19] Wu, S.-C.; Cheng, Z.-M.; Wang, S.-D.; Shan, X.-L. Recovery of Terephthalic Acid from Alkali Reduction Wastewater by Cooling Crystallization. Chem. Eng. Technol. 2011, 34 (10), 1614–1618. DOI: 10.1002/ceat.201100096.
- [20] Träger M.; Jostmann T. Kristallisation von Terephthalsäure aus wässerigen Hydrolyseprodukten des Dimethylterephthalates. Chem. Ing. Tech. 1997, 69, 493–496.
- [21] Donaldson, P. A. Slurries of terephthalic acid in ethylene glycol: European Patent 0 030 794 (1979).
- [22] Mullin, J. W. Crystallization, 4th edition; Butterworth-Heinemann, 2001. DOI: 10.1016/B978-0-7506-4833-2.X5000-1.
- [23] Myerson, A. S.; Erdemir, D.; Lee, A. Y., Eds. *Handbook of industrial crystallization*, Third edition; Cambridge University Press: Cambridge, **2019.** DOI: 10.1017/9781139026949.
- [24] Mersmann, A. *Crystallization technology handbook*, 2nd ed., rev. and expanded.; Marcel Dekker: New York, **2001.** DOI: 10.1201/9780203908280.
- [25] Bromley, L. A. *Thermodynamic properties of strong electrolytes in aqueous solutions. AIChE J.* **1973**, *19* (2), 313–320. DOI: 10.1002/aic.690190216.
- [26] Joseph F. Zemaitis Jr.; Diane M. Clark; Marshall Rafal; Noel C. Scrivner. *Handbook of Aqueous Electrolyte Thermodynamics: Theory & Application* **1986**.
- [27] Luckas, M.; Krissmann, J. Thermodynamik der Elektrolytlösungen: Eine einheitliche Darstellung der Berechnung komplexer Gleichgewichte; Springer-Verlag: Berlin, Heidelberg, Germany, 2001. DOI: 10.1007/978-3-642-56785-8.
- [28] Ulrich, J.; Heinrich, J. Reaktivkristallisation. Chem. Ing. Tech. 2005, 77 (11), 1759–1772. DOI: 10.1002/cite.200500128.
- [29] Mersmann, A.; Kind, M. Chemical engineering aspects of precipitation from solution. Chem. Eng. Technol. 1988, 11 (1), 264–276. DOI: 10.1002/ceat.270110136.
- [30] Volmer, M.; Weber, A. Keimbildung in übersättigten Gebilden. J. Phys. Chem. 1927 (1), 277–301.

- [31] Becker, R.; Döring, W. Kinetische Behandlung der Keimbildung in übersättigten Dämpfen. Ann. Phys. 1935, 416 (8), 719–752. DOI: 10.1002/andp.19354160806.
- [32] Turnbull, D.; Fisher, J. C. Rate of Nucleation in condensed Systems. J. Chem. Phys. 1959, 17 (1), 71–73.
- [33] Devos, C.; van Gerven, T.; Kuhn, S. *A Review of Experimental Methods for Nucleation Rate Determination in Large-Volume Batch and Microfluidic Crystallization. Cryst. Growth Des.* **2021**, *21* (4), 2541–2565. DOI: 10.1021/acs.cgd.0c01606.
- [34] Xiao, Y.; Wang, J.; Huang, X.; Shi, H.; Zhou, Y.; Zong, S.; Hao, H.; Bao, Y.; Yin, Q. Determination Methods for Crystal Nucleation Kinetics in Solutions. Cryst. Growth Des. 2018, 18 (1), 540–551. DOI: 10.1021/acs.cgd.7b01223.
- [35] Davey, R. J.; Schroeder, S. L. M.; Horst, J. H. ter. *Nucleation of organic crystals--a molecular perspective. Angew Chem Int Ed Engl* **2013**, *52* (8), 2166–2179. DOI: 10.1002/anie.201204824. Published Online: Jan. 10, 2013.
- [36] Kind, M.; Mersmann, A. Methode zur Berechnung der homogenen Keimbildung aus wässerigen Lösungen. Chem. Ing. Tech. 1983, 55 (9), 720–721. DOI: 10.1002/cite.330550914.
- [37] Lewis, A.; Seckler, M.; Kramer, H.; van Rosmalen, G., Eds. *Industrial Crystallization: Fundamentals and Applications*; Cambridge University Press, **2015.** DOI: 10.1017/CBO9781107280427.
- [38] McDonald, M. A.; Salami, H.; Harris, P. R.; Lagerman, C. E.; Yang, X.; Bommarius, A. S.; Grover, M. A.; Rousseau, R. W. Reactive crystallization: a review. React. Chem. Eng. 2021, 6 (3), 364–400. DOI: 10.1039/D0RE00272K.
- [39] Tung, H.-H. Crystallization of organic compounds: An industrial perspective; Wiley: Hoboken N.J., 2009.
- [40] Mersmann, A. Bei welcher Übersättigung soll man kristallisieren? Chem. Ing. Tech. 1992, 64 (11), 991–999. DOI: 10.1002/cite.330641105.
- [41] Franke, J.; Mersmann, A. The Influence of the Operational Conditions on the Precipitation Process. Chem. Eng. Sci. 1995, 50 (11).
- [42] Åslund, B. L.; Rasmuson, Å. K. C. Semibatch reaction crystallization of benzoic acid. AIChE J. 1992, 38 (3), 328–342. DOI: 10.1002/aic.690380303.
- [43] Caro, J. A.; Woldehaimanot, M.; Rasmuson, Å. C. Semibatch reaction crystallization of salicylic acid. Chem. Eng. Res. Des. 2014, 92 (3), 522–533. DOI: 10.1016/j.cherd.2013.09.009.

- [44] Wong, D.; Jaworski, Z.; Nienow, A. W. Barium Sulphate Precipitation in a Double-Feed Semi-Batch Stirred Reactor. Chem. Eng. Res. Des. 2003, 81 (8), 874–880. DOI: 10.1205/026387603322482112.
- [45] Torbacke, M.; Rasmuson, Å. K. C. *Influence of different scales of mixing in reaction crystallization. Chem. Eng. Sci.* **2001**, *56*, 2459–2473.
- [46] Pons-Siepermann, C. A.; Huang, S.; Myerson, A. S. *Purification of nitrophenols using complex-assisted crystallization. CrystEngComm* **2016**, *18* (39), 7487–7493. DOI: 10.1039/C6CE01603K.
- [47] Zhang, G. G. Z.; Grant, D. J. W. Formation of Liquid Inclusions in Adipic Acid Crystals during Recrystallization from Aqueous Solutions. Cryst. Growth Des. 2005, 5 (1), 319–324. DOI: 10.1021/cg049868h.
- [48] Biermann, L. Alkalische Hydrolyse PET-haltiger Verbundmaterialien als Grundlage eines rohstofflichen Recyclingverfahrens; ProcessNet Abfallbehandlung und Wertstoffrückgewinnung: Frankfurt am Main, 2019.
- [49] Brepohl, E.; Paschetag, M.; Scholl, S. *Monomer Recycling as Complementary Technology in a Circular Economy. Chem. Ing. Tech.* **2023.** DOI: 10.1002/cite.202300052.
- [50] Eunomia, Ed., Grant, Andy; Lahme, Vera; Connock, Toby; Lugal, Leyla. *How circular is PET: Case Study*. https://zerowasteeurope.eu/library/how-circular-is-pet/, **2022**.
- [51] Awaja, F.; Pavel, D. Recycling of PET. Eur. Polym. J. 2005, 41 (7), 1453–1477. DOI: 10.1016/j.eurpolymj.2005.02.005.
- [52] Déloye, E.; Haudin, J.-M.; Billon, N. Stretch-Blow Molding of PET Copolymers – Influence of Molecular Architecture. Int. Polym. Process. 2012, 27 (3), 358–369. DOI: 10.3139/217.2549.
- [53] Mohan, T. P.; George, A. P.; Kanny, K. Combined effect of isophthalic acid and polyethylene glycol in polyethylene terephthalate polymer on thermal, mechanical, and gas transport properties. J. Appl. Polym. Sci. 2012, 126 (2), 536–543. DOI: 10.1002/app.36818.
- [54] Damayanti; Wu, H.-S. Strategic Possibility Routes of Recycled PET. Polymers 2021, 13 (9). DOI: 10.3390/polym13091475. Published Online: May. 2, 2021.
- [55] Chanda, M. Chemical aspects of polymer recycling. Adv. Ind. Eng. Polym. Res. **2021**, 4 (3), 133–150. DOI: 10.1016/j.aiepr.2021.06.002.
- [56] Oromiehie, A.; Mamizadeh, A. Recycling PET beverage bottles and improving properties. Polym. Int. **2004**, 53 (6), 728–732. DOI: 10.1002/pi.1389.

- [57] Berg, D.; Schaefer, K.; Koerner, A.; Kaufmann, R.; Tillmann, W.; Moeller, M. Reasons for the Discoloration of Postconsumer Poly(ethylene terephthalate) during Reprocessing. Macro. Materials & Eng. 2016, 301 (12), 1454–1467. DOI: 10.1002/mame.201600313.
- [58] Welle, F. Twenty years of PET bottle to bottle recycling—An overview. Resour. Conserv. Recycl. 2011, 55 (11), 865–875. DOI: 10.1016/j.resconrec.2011.04.009.
- [59] Thiyagarajan, S.; Maaskant-Reilink, E.; Ewing, T. A.; Julsing, M. K.; van Haveren, J. Back-to-monomer recycling of polycondensation polymers: opportunities for chemicals and enzymes. RSC Adv. 2021, 12 (2), 947–970. DOI: 10.1039/d1ra08217e. Published Online: Jan. 5, 2022.
- [60] Biessey, P.; Vogel, J.; Seitz, M.; Quicker, P. Plastic Waste Utilization via Chemical Recycling: Approaches, Limitations, and the Challenges Ahead. Chem. Ing. Tech. 2023, 95 (8), 1199–1214. DOI: 10.1002/cite.202300042.
- [61] Uekert, T.; Singh, A.; DesVeaux, J. S.; Ghosh, T.; Bhatt, A.; Yadav, G.; Afzal, S.; Walzberg, J.; Knauer, K. M.; Nicholson, S. R.; Beckham, G. T.; Carpenter, A. C. Technical, Economic, and Environmental Comparison of Closed-Loop Recycling Technologies for Common Plastics. ACS Sustainable Chem. Eng. 2023, 11 (3), 965–978. DOI: 10.1021/acssuschemeng.2c05497.
- [62] Thomas, S.; Rane, A.; Kanny, K.; Abitha, v. K.; Thomas, M. G., Eds. *Recycling of Polyethylene Terephthalate Bottles*; Elsevier, **2019**.
- [63] Barnard, E.; Rubio Arias, J. J.; Thielemans, W. Chemolytic depolymerisation of PET: a review. Green Chem. 2021, 23 (11), 3765– 3789. DOI: 10.1039/D1GC00887K.
- [64] Tournier, V.; Duquesne, S.; Guillamot, F.; Cramail, H.; Taton, D.; Marty, A.; André, I. Enzymes' Power for Plastics Degradation. Chem. Rev. 2023, 123 (9), 5612–5701. DOI: 10.1021/acs.chemrev.2c00644. Published Online: Mar. 14, 2023.
- [65] K-PET Consulting, S. L. Chemical Recycling The PET Recyclers and the Philosopher's Stone: Barcelona, 2019.
- [66] Al-Sabagh, A. M.; Yehia, F. Z.; Eshaq, G.; Rabie, A. M.; ElMetwally, A. E. Greener routes for recycling of polyethylene terephthalate. Egypt. J. Pet. 2016, 25 (1), 53–64. DOI: 10.1016/j.ejpe.2015.03.001.
- [67] Sinha, V.; Patel, M. R.; Patel, J. V. Pet Waste Management by Chemical Recycling: A Review. J. Polym. Environ. 2010, 18 (1), 8–25. DOI: 10.1007/s10924-008-0106-7.

- [68] Kosmidis, V. A.; Achilias, D. S.; Karayannidis, G. P. Poly(ethylene terephthalate) Recycling and Recovery of Pure Terephthalic Acid. Kinetics of a Phase Transfer Catalyzed Alkaline Hydrolysis. Macromol. Mater. Eng. 2001, 286 (10), 640–647.
- [69] Cosimbescu, L.; Merkel, D. R.; Darsell, J.; Petrossian, G. Simple But Tricky: Investigations of Terephthalic Acid Purity Obtained from Mixed PET Waste. Ind. Eng. Chem. Res. 2021, 60 (35), 12792–12797. DOI: 10.1021/acs.iecr.1c02604.
- [70] Karayannidis, G. P.; Chatziavgoustis, A. P.; Achilias, D. S. Poly(ethylene terephthalate) recycling and recovery of pure terephthalic acid by alkaline hydrolysis. Adv. Polym. Technol. 2002, 21 (4), 250–259. DOI: 10.1002/adv.10029.
- [71] Ramopoulos, V.; Link, G.; Soldatov, S.; Jelonnek, J. *Industrial scale microwave applicator for high temperature alkaline hydrolysis of PET. Int. J. Microw. Wireless Technol.* **2018**, *10* (5-6), 709–716. DOI: 10.1017/S1759078718000727.
- [72] Leipert, L.; Eichert, C.; Peschel, E.; Scholl, S. *Verfahren, Vorrichtung und Verwendung zur Wiederaufarbeitung von Polyalkylenterephthalat*: German Patent DE 10 2018 122 210 A1 (2018).
- [73] Brepohl, E. Continuous back to monomer recycling of PET from composite materials using a twin-screw extruder; AIChE Annual Meeting 2021: Boston (Online), 2021.
- [74] Rezazadeh, A.; Thomsen, K.; Gavala, H. N.; Skiadas, I. V.; Fosbøl, P. L. Solubility and Freezing Points of Disodium Terephthalate in Water–Ethylene Glycol Mixtures. J. Chem. Eng. Data 2021, 66 (5), 2143–2152. DOI: 10.1021/acs.jced.1c00052.
- [75] Lücking, C. Gewinnung hochwertiger Terephthalsäure aus dem Polyester-Recycling; ProcessNet Abfallbehandlung und Wertstoffrückgewinnung: Bamberg, 2022.
- [76] Whitchurch, P. C.; Johnsen, J. A. *The Honeywell UOP ParexTM Process: Fifty Years of Growth for the Petrochemical Industry (Case Study)*. In *Industrial Arene Chemistry*; Mortier, J., Ed.; Wiley, **2023**; pp 297–325.
- [77] Gong, W. H. *BP-Amoco Mid-Century Process for Terephthalic Acid Production (Case Study)*. In *Industrial Arene Chemistry*; Mortier, J., Ed.; Wiley, **2023**; pp 1107–1135.
- [78] Tomás, R. A. F.; Bordado, J. C. M.; Gomes, J. F. P. p-Xylene oxidation to terephthalic acid: a literature review oriented toward process optimization and development. Chem. Rev. 2013, 113 (10), 7421–7469. DOI: 10.1021/cr300298j. Published Online: Jun. 14, 2013.

- [79] Allen, N. S.; Edge, M.; Daniels, J.; Royall, D. Spectroscopic analysis of organic contaminants in terephthalic acid: colour implications in poly(ethylene terephthalate) manufacture. Polym. Degrad. Stab. 1998, 62, 373–383.
- [80] Stahl, S. S.; Alsters, P. L., Eds. *Liquid phase aerobic oxidation* catalysis: *Industrial applications and academic perspectives*; Wiley-VCH Verlag GmbH & Co. KGaA: Weinheim, **2016**.
- [81] Davey, R. J.; Maginn, S. J.; Andrews, S. J.; Buckley, A. M.; Cottier, D.; Dempsay, P.; Rout, J. E.; Stanley, D. R.; Taylor, A. Stabilization of a metastable crystalline phase by twinning. Nature 1993, 366, 248–250. DOI: 10.1038/366248a0.
- [82] Gerasimov, V. P.; Zharikov, N. K.; Korobkov, V. S.; Ovchinnikov, I. V.; Rud, L. V. Phase transition in terephthalic acid crystals from Raman spectra: translated by Plenum Publishing Corporation. J. Appl. Spectrosc. 1981, 34 (2), 308–311.
- [83] Bailey, M.; Brown, C. J. The crystal structure of terephthalic acid. Acta Cryst. 1967, 22, 387–391.
- [84] Sledz, M.; J. Janczak, J.; R. Kubiak, R. New crystalline modification of terephthalic acid. J. Mol. Struct. 2001 (595), 77–82.
- [85] McKinnon, J. J.; Fabbiani, F. P. A.; Spackman, M. A. Comparison of Polymorphic Molecular Crystal Structures through Hirshfeld Surface Analysis. Cryst. Growth Des. 2007, 7 (4), 755–769. DOI: 10.1021/cg060773k.
- [86] Davey, R. J.; Black, S. N.; Logan, D.; Maginn, S. J.; Fairbrother, J. E.; Grant, D. J. Structural and Kinetic Features of Crystal Growth Inhibition: Adipic Acid Growing in the presence of n-Alkanoic Acids. J. Chem. Soc. Faraday Trans. 1992, 88, 3461–3466.
- [87] Raecke, B.; Stein, W.; Schirp, H. *Process for the production of terephthalic acid*: United States Patent 2,794,830 (1957).
- [88] Fan, L.; Zhang, L.; Shen, J.; Wang, S.; Chen, H. *Study on recovery and refining of TA from alkali reduction wastewater. Desalination* **2007**, *206* (1-3), 353–357. DOI: 10.1016/j.desal.2006.03.573.
- [89] Liu, C., Chen, J. The study of the recovery of highly purified terephthalic acid from alkali weight-reduction wastewater. Int. J. Environ. Pollut. **2007**, 29 (4), 484–494.
- [90] Marlena, B.; Sulistyo, H.; Rochmadi, R. Investigation of Crystal Size Distribution in Purification of Terephthalic Acid from Polyester Textile Industry Waste by Reactive Crystallization. Indones. J. Chem. 2023, 23 (3), 742. DOI: 10.22146/ijc.80820.

- [91] Jinichi Yazaki; Kozaburo Sakano; Nobuyuki Funakoshi; Kazuho Tanaka. *Process for recovering terephthalic acid from pulverized product of spent polyethylene terephthalate and system for use in such process*: United States patent 6,580,005 (2000).
- [92] European Chemicals Agency. *ECHA*: *Database on chemicals and regulated substances*. https://echa.europa.eu/de/home (accessed 2023-12-13).
- [93] Cheng, Y.; Huo, L.; Li, X. Solubilities of Isophthalic Acid in Acetic Acid + Water Solvent Mixtures. Chin. J. Chem. Eng. 2013, 21 (7), 754–758. DOI: 10.1016/S1004-9541(13)60520-0.
- [94] Han, N.; Wang, L.; Sun, C.; Fu, R. Determination and Correlation of the Phase Equilibrium of Terephthalic Acid, Water and Acetic Acid Ternary System. Huaxue Gongcheng/Chem. Eng. 2000, 28 (2), 55–58.
- [95] Ma Peisheng; Xia Qing. Determination and Correlation for Solubility of Aromatic Acids in Solvents. Chin. J. Chem. Eng. 2001, 9 (1), 39–44.
- [96] Nanyin Han, Liang Zhu, Lisheng Wang, Ruonong Fu. *Aqueous* solubility of m-phthalic acid, o-phthalic, acid and p-phthalic acid from 298 to 483 K. Sep. Purif. Technol. **1999** (16), 175–180.
- [97] Apelblat, A.; Manzurola, E.; Abo Balal, N. *The solubilities of benzene polycarboxylic acids in water. J. Chem. Thermodyn.* **2006**, *38* (5), 565–571. DOI: 10.1016/j.jct.2005.07.007.
- [98] Takebayashi, Y.; Sue, K.; Yoda, S.; Hakuta, Y.; Furuya, T. Solubility of Terephthalic Acid in Subcritical Water. J. Chem. Eng. Data 2012, 57 (6), 1810–1816. DOI: 10.1021/je300263z.
- [99] Chen, M.; Ma, P. *Solid-Liquid Equilibria of Several Systems*Containing Acetic Acid. J. Chem. Eng. Data **2004**, 49, 756–759. DOI: 10.1021/je034114c.
- [100] Coniglio, M. A.; Fioriglio, C.; Laganà, P. Non-Intentionally Added Substances in PET-Bottled Mineral Water; Springer International Publishing: Cham, 2020. DOI: 10.1007/978-3-030-39134-8.
- [101] Turner, S. R.; Seymour, R. W.; Smith, T. W. Cyclohexanedimethanol Polyesters. In Encyclopedia of polymer science and technology; Mark, F. H., Ed.; Wiley Interscience, 2004. DOI: 10.1002/0471440264.pst257.
- [102] Müller, C.; Franke-Hameke, D. W.; Brepohl, E.; Biermann, L.; Eichert, C.; Scholl, S. *Precipitation of terephthalic acid from post-consumer polyethylene terephthalate waste fractions. Green Process. Synth.* **2025**, *14* (1). DOI: 10.1515/gps-2023-0244.
- [103] European Chemicals Agency, Ed. Guidance of monomers and polymers: Version 3.0, 2023. DOI: 10.2823/933.

- [104] Kaiser, K.; Schmid, M.; Schlummer, M. Recycling of Polymer-Based Multilayer Packaging: A Review. Recycling 2018, 3 (1), 1. DOI: 10.3390/recycling3010001.
- [105] Commission Regulation (EU) No 10/2011 on plastic materials and articles intended to come into contact with food, 2011.
- [106] Kirstein, M.; Lücking, C.; Biermann, L.; Brepohl, E.; Salikov, V.; Eichert, C.; Paschetag, M.; Scholl, S. Monomer Recycling and Repolymerization of Post - Consumer Polyester Textiles. Chem. Ing. Tech. 2023, 95 (8), 1290–1296. DOI: 10.1002/cite.202200197.
- [107] Liu, C., Gao, C., Xia, W., & Cao, P., Ed. *Research of Purifying Terephthalic Acid and Recycling PET*; Institute of Electrical and Electronics Engineers: New Jersey, USA, **2010**.
- [108] Quartinello, F.; Vajnhandl, S.; Volmajer Valh, J.; Farmer, T. J.; Vončina, B.; Lobnik, A.; Herrero Acero, E.; Pellis, A.; Guebitz, G. M. Synergistic chemo-enzymatic hydrolysis of poly(ethylene terephthalate) from textile waste. Microb. Biotechnol. 2017, 10 (6), 1376–1383. DOI: 10.1111/1751-7915.12734. Published Online: Jun. 2, 2017.
- [109] Slapnik, Janez; Kraft, Gregor; Wilhelm, Thomas; Lobnik, Aleksandra. Purification of Recycled Terephthalic Acid and Synthesis of Polyethylene Terephthalate, 2019.
- [110] Biermann, L.; Quast, D.; Brepohl, E.; Eichert, C.; Scholl, S. *Alkali Depolymerization of Poly(ethylene terephthalate) in a Quasi solid solid Kneading Reaction. Chem. Eng. Technol.* **2021**, 44 (12), 2300–2308. DOI: 10.1002/ceat.202100327.
- [111] Biermann, M. Untersuchungen zur kontinuierlichen Kristallisation von Terephthalsäure. Master thesis, Biermann, Michelle: Braunschweig, 2021.
- [112] Biermann, L. Alkalische Depolymerisation von Poly(ethylenterephthalat) als Grundlage eines Monomerrecyclings. Dissertation, Biermann, Lars: Braunschweig, 2023.
- [113] Paschetag, M.; Schneider, H.; Scholl, S. *Life Cycle Assessment of a new Monomer Recycling Process for PET*. In *Recycling of Plastics*; Niessner, N., Ed.; Hanser Publishers, **2022**; pp 212–238.
- [114] Kocks, C.; Görtz, J.; Holtz, A.; Gausmann, M.; Jupke, A. Electrochemical Crystallization Concept for Succinic Acid Reduces Waste Salt Production. Chem. Ing. Tech. 2020, 92 (3), 221–228. DOI: 10.1002/cite.201900088.

- [115] Gausmann, M.; Kocks, C.; Doeker, M.; Eggert, A.; Maßmann, T.; Jupke, A. Recovery of succinic acid by integrated multi-phase electrochemical pH-shift extraction and crystallization. Sep. Purif. Technol. 2020, 240, 116489. DOI: 10.1016/j.seppur.2019.116489.
- [116] Myren, T. H. T.; Stinson, T. A.; Mast, Z. J.; Huntzinger, C. G.; Luca, O. R. Chemical and Electrochemical Recycling of End-Use Poly(ethylene terephthalate) (PET) Plastics in Batch, Microwave and Electrochemical Reactors. Molecules 2020, 25 (12). DOI: 10.3390/molecules25122742. Published Online: Jun. 13, 2020.
- [117] Wynkoop, R.; Norman, O. L.; Norton, R. V. *Terephthalic acid process*: United States Patent 4,093,528 (1977).
- [118] Jacques Thauront; Sylvain Durecu; Jean-Paul Wiaux; Bach-Tuyet Lam. Formation of terephthalic acid by electrochemical acidification of a sodium terephthalate solution: United States Patent 6,312,582 (2000).
- [119] Evans, D.; Ripin, D. H.; Williams, R. *Hans Reich's Collection*. *Bordwell pKa Table*. https://organicchemistrydata.org/hansreich/resources/pka/#ka-water (accessed 2023-01-24).
- [120] Ellingboe, J. L.; Runnels, J. H. Solubilities of Disodium Terephthalate in Aqueous Solutions of Sodium Carbonate and Sodium Bicarbonate. J. Chem. Eng. Data 1966, 11 (2), 185–187. DOI: 10.1021/je60029a017.
- [121] Röthele, S., H. Neuman, M. Heuer. *Die Anwendung der Fraunhofer Beugung unter 1 µm zur Partikelgrössenanalyse von 0.1 µm bis 2000 µm*; Proceedings of the Fourth European Symposium on Particle Characterization (PARTEC), **1989**.
- [122] Aya, N.; Iki, N.; Shimura, T.; Shirai, T., Eds. International Conference on Optical Particle Characterization (OPC 2014); SPIE Proceedings; The international society for optics and photonics: Bellingham, USA, 2014.
- [123] Markert Filtration GmbH, Ed., marsyntex. PPD 3143 Datasheet, 2020.
- [124] BHS-Sonthofen GmbH, Ed. Bedienungsanleitung BHS Labornutsche, **2016**.
- [125] Equipolymers Global GmbH, Ed., Equipolymers Global GmbH. *Sales Specification: Terephthalic Acid Purified*, **2019**.
- [126] Heck, C. A. *Untersuchung zur reaktiven Fällung von Terephthalsäure*. Master thesis, Heck, Carina A.: Braunschweig, **2019**.
- [127] Nývlt, J. Nucleation and Growth Rate in Mass Crystallization. Prog. Cryst. Growth Charact. Mater. 1984, 9, 335–370.

- [128] Mullin, J. W.; Osman, M. M. The nucleation and precipitation of nickel ammonium sulphate crystals from aqueous solution. Cryst. Res. and Technol. 1973, 8 (4), 471–481. DOI: 10.1002/crat.19730080410.
- [129] Kim, W.-S.; Tarbell, J. M. Micromixing Effects on Barium Sulfate Precipitation in an MSMPR Reactor. Chem. Eng. Commun. 1996, 146 (1), 33–56. DOI: 10.1080/00986449608936480.
- [130] Franck, R.; David, R.; Villermaux, J. Crystallization and Precipitation Engineering - II. A Chemical Reaction Engineering Approach to Salicylic Acid Precipitation: Modeling of Batch Kinetics And Application to Continuous Operation. Chem. Eng. Sci. 1988, 43 (1), 69–77.
- [131] Blandin, A. F.; Mangin, D.; Nallet, V.; Klein, J. P.; Bossoutrot, J. M. Kinetics identification of salicylic acid precipitation through experiments in a batch stirred vessel and a T-mixer. Chem. Eng. J. 2001, 81 (1-3), 91–100. DOI: 10.1016/S1385-8947(00)00227-8.
- [132] Ståhl, M.; Rasmuson, Å. C. Towards predictive simulation of single feed semibatch reaction crystallization. Chem. Eng. Sci. 2009, 64 (7), 1559–1576. DOI: 10.1016/j.ces.2008.12.001.
- [133] Ståhl, M.; Åslund, B. L.; Rasmuson, Å. C. Reaction crystallization kinetics of benzoic acid. AIChE J. **2001**, 47 (7), 1544–1560. DOI: 10.1002/aic.690470708.
- [134] Po, H. N.; Senozan, N. M. The Henderson-Hasselbalch Equation: Its History and Limitations. J. Chem. Educ. 2001, 78 (11), 1499–1503.
- [135] Franke-Hameke, D. W. *Untersuchung zur Gewinnung von Terephthalsäure aus depolymerisiertem PET*. Bachelor thesis, Franke-Hameke, Dirk W.: Braunschweig, **2020**.
- [136] Iqbal, M. J.; Ashiq, M. N. Adsorption of dyes from aqueous solutions on activated charcoal. J. Hazard. Mater. 2007, 139 (1), 57–66. DOI: 10.1016/j.jhazmat.2006.06.007.
- [137] Zhu, F.; Johnson, J. A.; Ablin, D. W.; Ernst, G. A. *Efficient* petrochemical processes: Technologies, design and operation; Wiley-AIChE: Hoboken, **2020**.
- [138] Biermann, L.; Brepohl, E.; Eichert, C.; Müller, C.; Salikov, V.; Scholl,
   S. Verfahren zur Herstellung eines Terephthalsäure-Gemisches:
   German Patent 10 2020 123 772 B4 (2020).
- [139] Müller, C.; Brepohl, E.; Biermann, L.; Eichert, C.; Scholl, S. Verfahren zur Gewinnung aromatischer Dicarbonsäuren aus ihren Metallsalzen: German Patent 10 2021 105 970 A1 (2021).
- [140] Gutz, I. G. CurTiPot: pH and Acid-Base Titration Curves: Analysis and Simulation, 4.3.1, 2021. http://www.iq.usp.br/gutz/Curtipot\_.html.

- [141] Müller, C. Terephthalic acid precipitation from real polyethylene terephthalate (PET) waste; ProcessNet Kristallisation: Dortmund, 2022.
- [142] Goedecke, R., Ed. Fluidverfahrenstechnik: Grundlagen, Methodik, Technik, Praxis; Wiley-VCH: Weinheim, 2006.
- [143] Gottwald, S. Optimierung der kontinuierlichen Kristallisation von Terephthalsäure für einen PET Recycling Prozess. Studienarbeit, Gottwald, Saskia: Braunschweig, 2021.
- [144] Schneemann, H. Erweiterte Untersuchungen zur kontinuierlichen Kristallisation von Terephthalsäure für einen PET-Recyclingprozess.

  Bachelor thesis, Schneemann, Henrik: Braunschweig, 2022.
- [145] Jansen, Y. Parameteroptimierung zur kontinuierlichen Fällung von Terephthalsäure aus dem back-to-monomer Recycling von PET.
  Bachelor thesis, Jansen, Yunis: Braunschweig, 2023.
- [146] Kind, M. Grundlagen der Technischen Kristallisation. In Kristallisation in der industriellen Praxis; Hofmann, G., Ed.; Wiley-VCH, 2004; pp 101–113.
- [147] O'Hern, H. A.; Rush, F. E. Effect of Mixing Conditions in Barium Sulfate Precipitation. Ind. Eng. Chem. Fund. 1963, 2 (4), 267–272. DOI: 10.1021/i160008a005.
- [148] Pohorecki, R.; Baldyga, J. The effects of micromixing and the manner of reactor feeding on precipitation in stirred tank reactors. In Tenth International Symposium on Chemical Reaction Engineering; Elsevier, 1988; pp 1949–1954. DOI: 10.1016/b978-0-08-036969-3.50035-x.
- [149] Marcic, F. Einfluss von Saatkristallen auf die kontinuierliche Kristallisation von Terephthalsäure. Studienarbeit, Marcic, Fabian: Braunschweig, 2022.
- [150] Hofmann, G., Ed. Kristallisation in der industriellen Praxis; Wiley-VCH: Weinheim, 2004.
- [151] Alison Lewis; Marcelo Seckler; Herman Kramer; Gerda van Rosmalen. Nucleation. In Industrial Crystallization: Fundamentals and Applications; Lewis, A., Seckler, M., Kramer, H., van Rosmalen, G., Eds.; Cambridge University Press, 2015; pp 71–103. DOI: 10.1017/CBO9781107280427.005.
- [152] Berg, J. M.; Romoser, A.; Banerjee, N.; Zebda, R.; Sayes, C. M. The relationship between pH and zeta potential of ~ 30 nm metal oxide nanoparticle suspensions relevant to in vitro toxicological evaluations. Nanotoxicology 2009, 3 (4), 276–283. DOI: 10.3109/17435390903276941.

- [153] Seosamh O'Meadhra, R.; Lin, R.; Kirk, S. K.; McMurray, B. D. *Crystallization method for production of purified aromatic dicarboxylic acids*: United States Patent 6,689,903 (2004).
- [154] Streich, D. J.; Graziano, D. J.; Grimm, R. J.; Schiller, S. K. *Process for recovery of purified terephthalic acid*: United States Patent 5,175,355 (1992).
- [155] Müller, M. Untersuchungen zur Umkristallisation von Terephthalsäure aus einem Verfahren zum chemischen Recycling von Polyethylenterephthalat. Master thesis, Müller, Moritz: Braunschweig, 2021.
- [156] Wang, Q.; Cheng, Y.; Xu, H.; Wang, L.; Li, X. Aging of Crude Terephthalic Acid Crystals at High Temperatures. Ind. Eng. Chem. Res. 2007, 46 (22), 7367–7377. DOI: 10.1021/ie0616139.
- [157] Brown, P. M.; Marquering, M.; Myerson, A. S. *Purification of terephthalic acid by crystal aging. Ind. Eng. Chem. Res.* **1990**, *29*, 2089–2093.
- [158] Camlibel, N. O. *Polyester: Production, Characterization and Innovative Applications*; IntechOpen: Rijeka, Croatia, **2018**.

# 8 Appendix

# 8.1 Appendix A – General

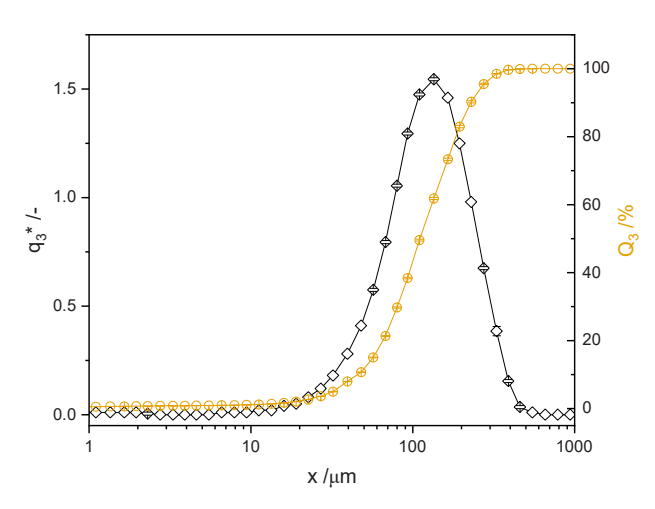


Figure 8-1 Volume related logarithmic density and cumulative crystal size distributions of PTA

# 8.2 Appendix B – Experimental

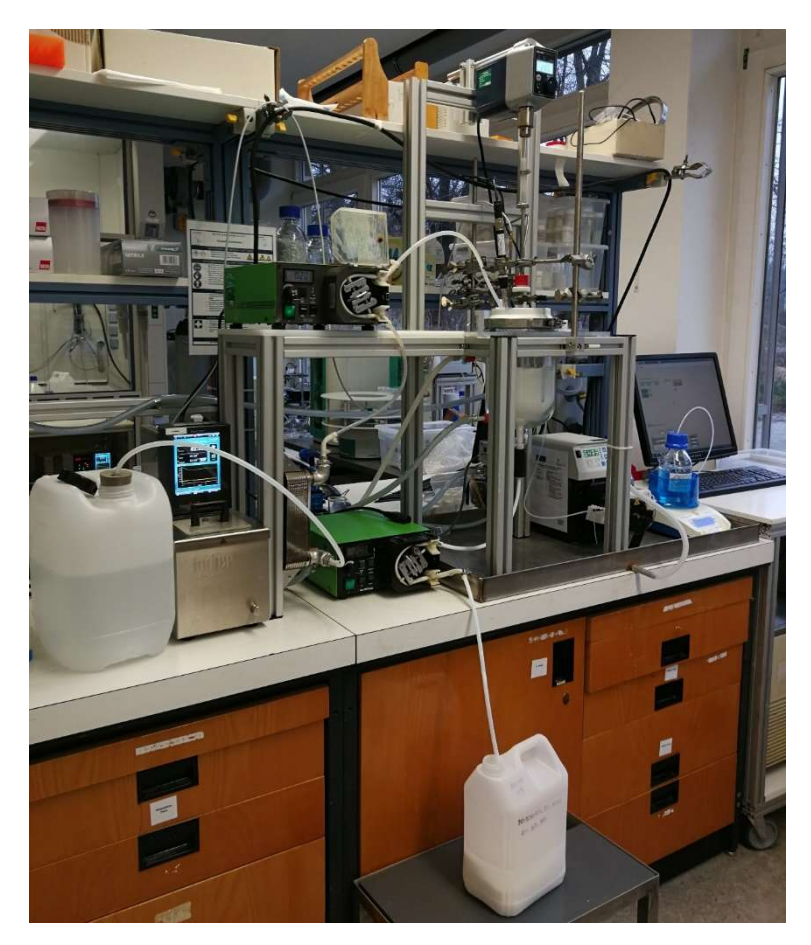


Figure 8-2 Image of experimental setup for continuous operation.

## Appendix

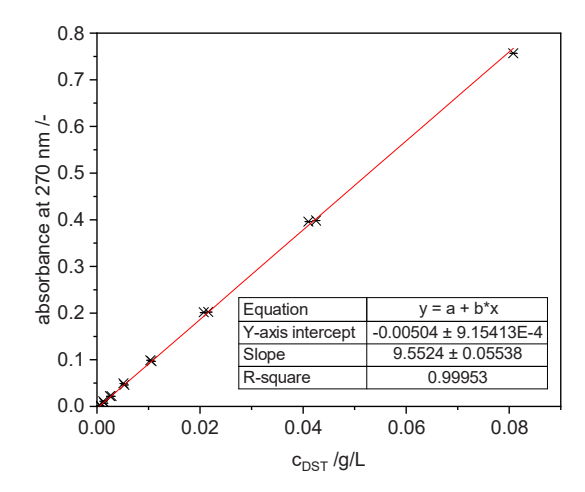


Figure 8-3 Linear fit of absorbance at 270 nm over DST concentration for determination of initial and residual DST content.

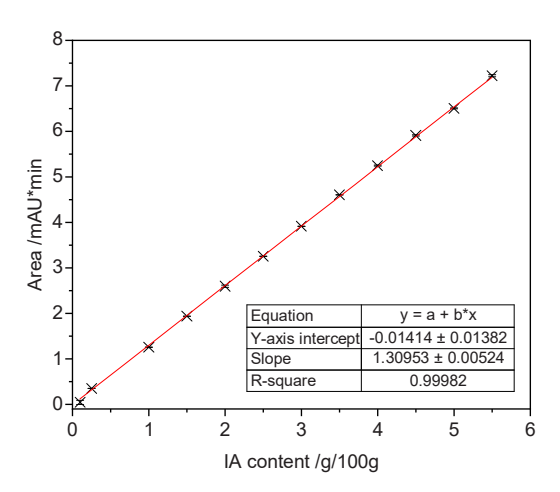


Figure 8-4 Linear fit of chromatogram area (mAU\*min) over IA content for determination of IA content in rTA.

# 8.3 Appendix C – Batch Operation

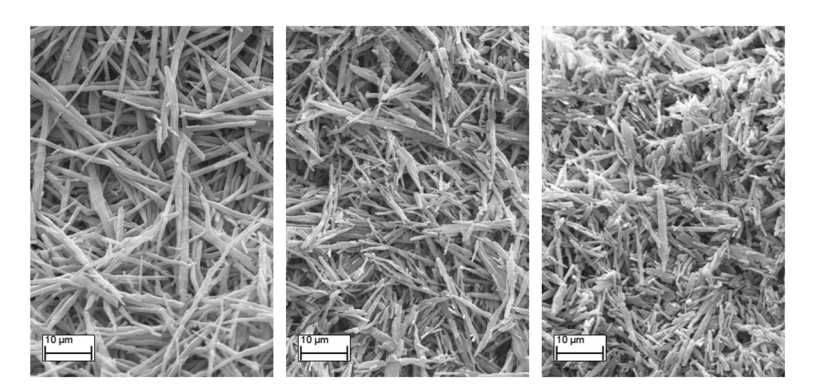


Figure 8-5 SEM images of TA precipitated with sulfuric acid at 45°C. 0.0021  $g_{DST}/g_{total}$  (left), 0.021  $g_{DST}/g_{total}$  (centre) and 0.063  $g_{DST}/g_{total}$  (right).

# Appendix

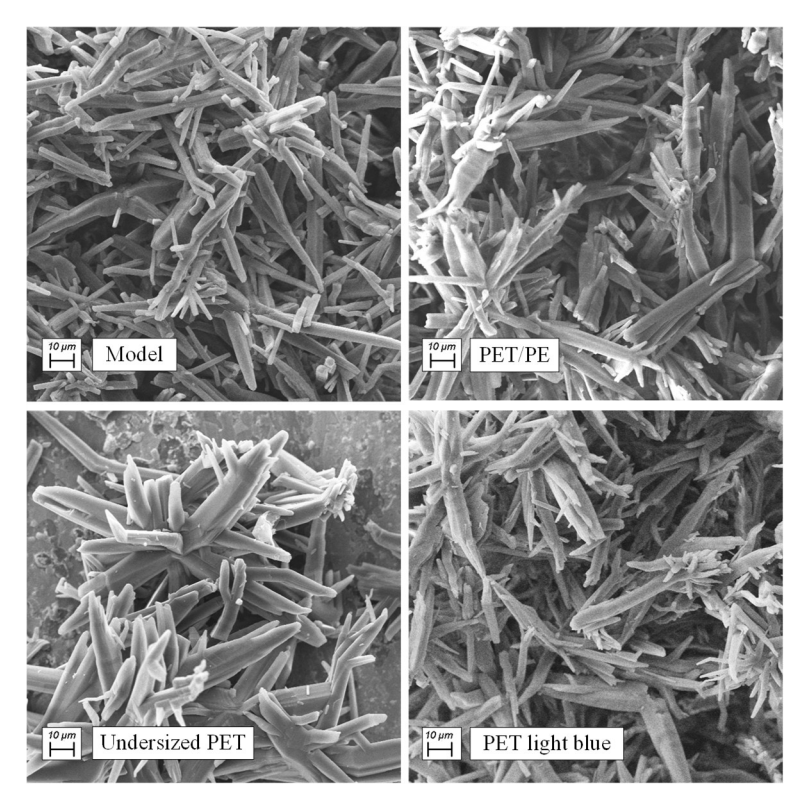


Figure 8-6 SEM images of TA precipitated with acetic acid at 60 °C, adapted from Müller et al..  $^{102}$ 

# 8.4 Appendix D – Continuous Operation

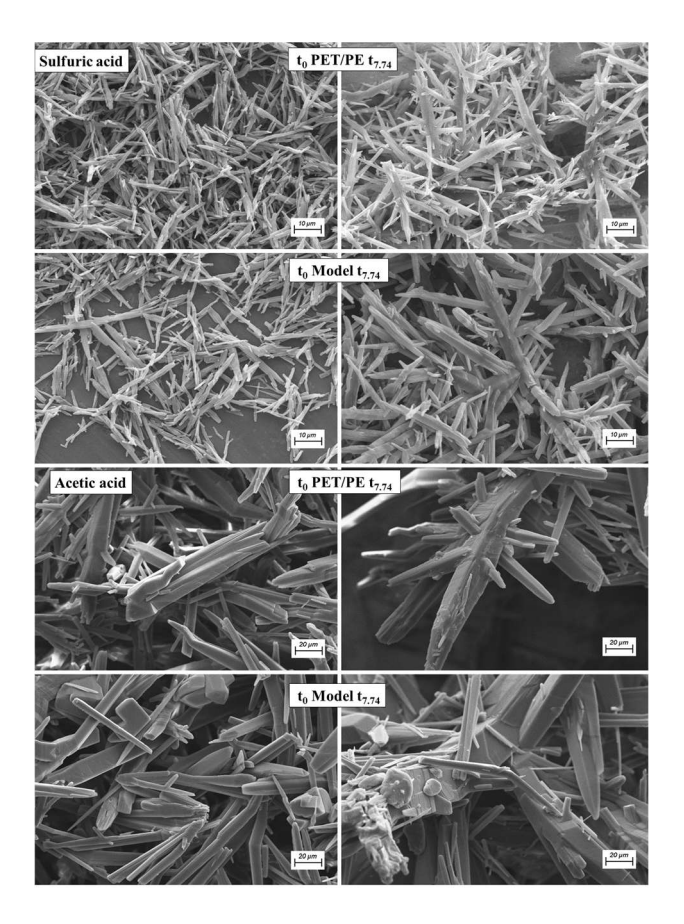


Figure 8-7 SEM images of TA after precipitation with acetic and sulfuric acid at 80° C,  $t_0$  (left) and  $t_{7.74}$  (right) for PET/PE and model reactant.

# Appendix

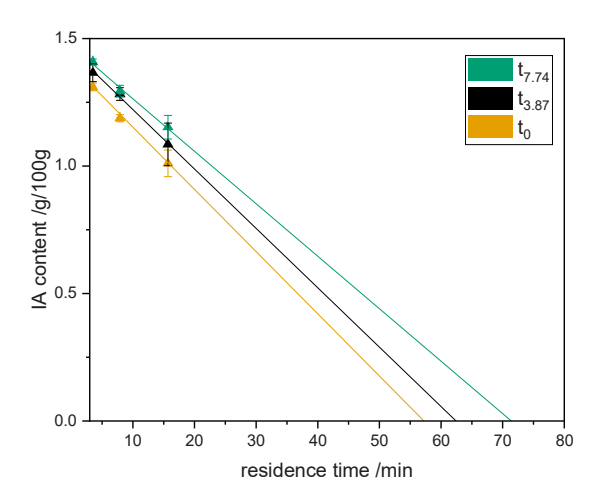


Figure 8-8 IA content of TA over residence time with extrapolated linear fit.

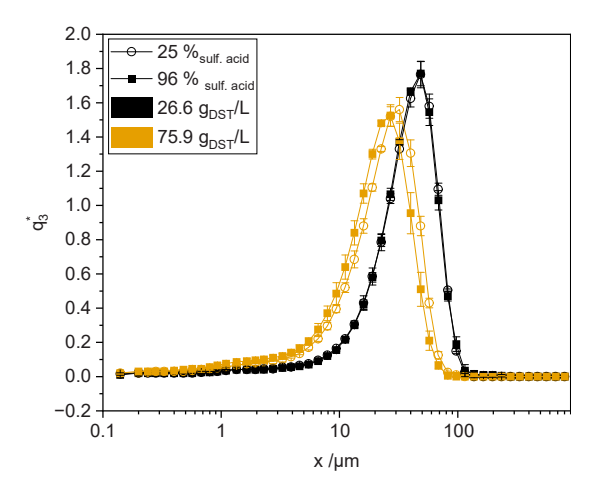


Figure 8-9 PSD of TA after precipitation at 80 °C in PET light blue reactant of different concentrations, t<sub>9</sub> samples.

## Appendix

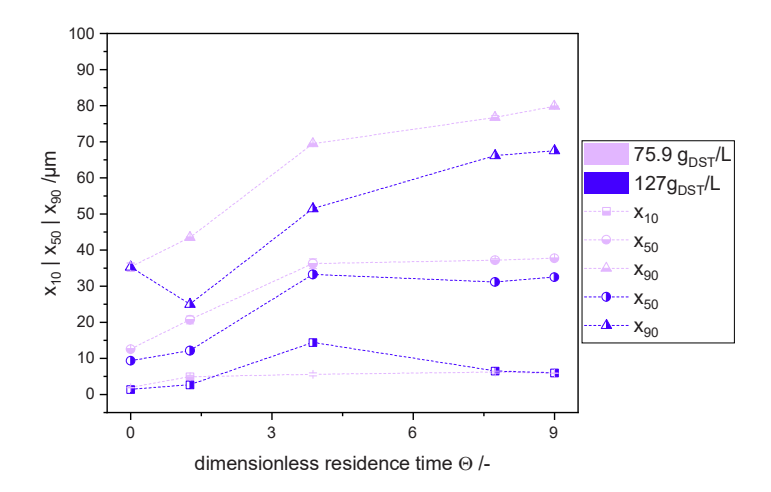


Figure 8-10 Quantile Values of TA after precipitation with 25 % sulfuric acid at 80 °C in PET/PE reactant of different concentrations.

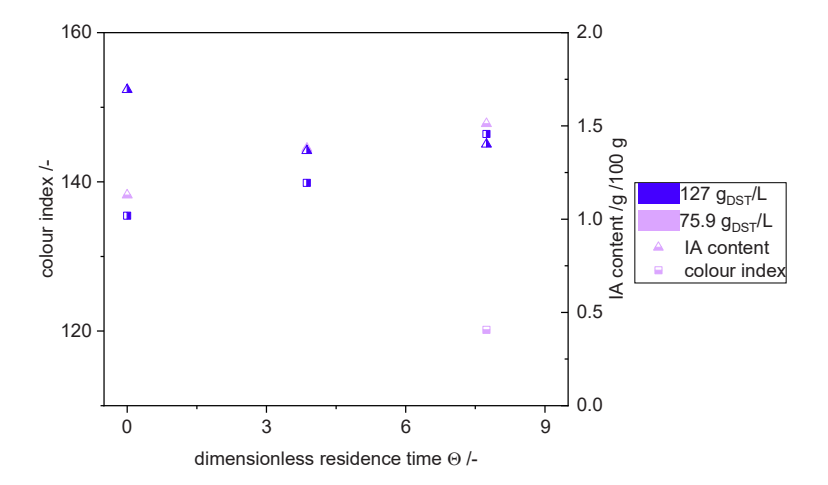


Figure 8-11 Purity of TA after precipitation with 25 % sulfuric acid at 80 °C in PET/PE reactant of different concentrations.

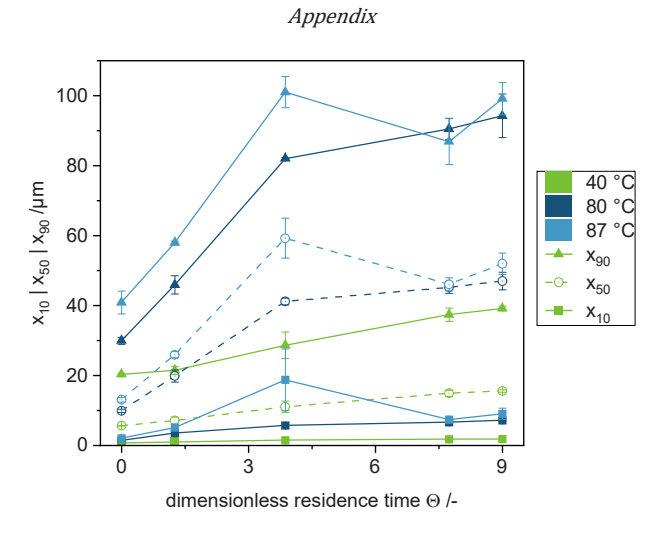


Figure 8-12 Quantile values of TA after precipitation with 25 % sulfuric acid at different temperatures from PET/PE reactant.

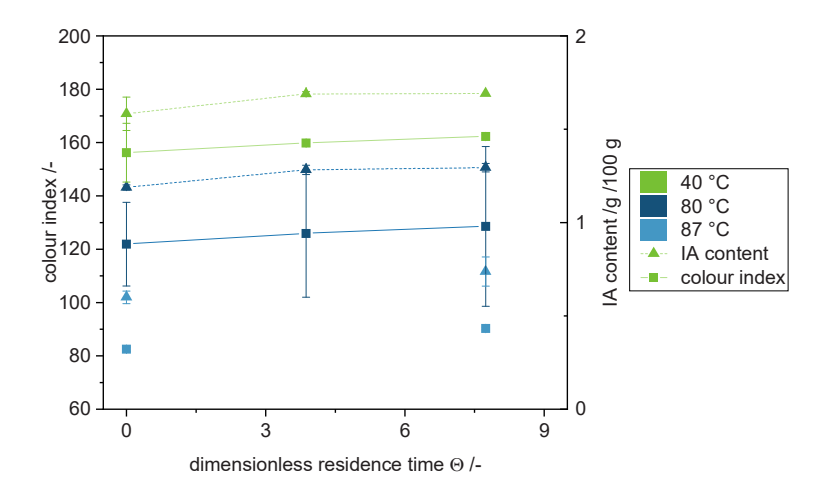


Figure 8-13 IA content and colour index of TA after precipitation with 25 % sulfuric acid at different temperatures from PET/PE reactant.

# 8.4.1 Start-up

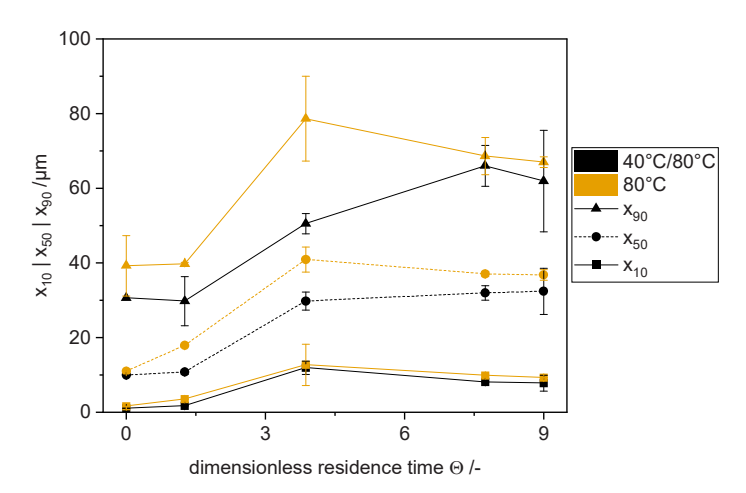


Figure 8-14  $x_{3,10}, x_{3,50}$  and  $x_{3,90}$  quantiles of TA after precipitation with sulfuric acid with different initial precipitation temperatures, lines are shown to guide the eye.

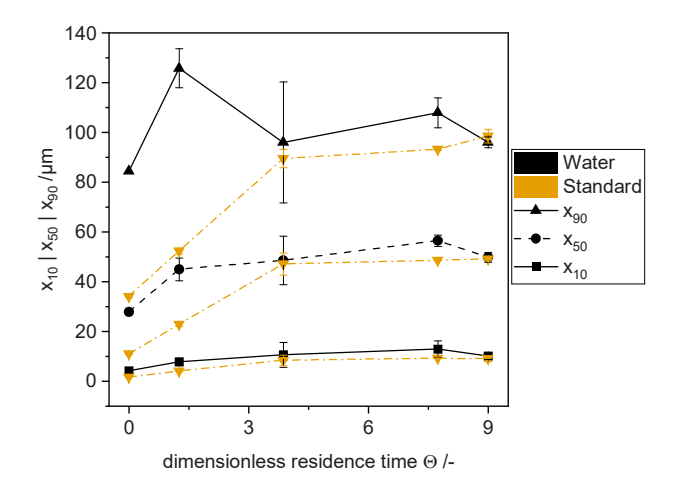


Figure 8-15  $x_{3,10}, x_{3,50}$  and  $x_{3,90}$  quantiles of TA after precipitation with sulfuric acid at 80 °C with different initial reactor content, lines are shown to guide the eye.

# 8.4.2 pH Variation

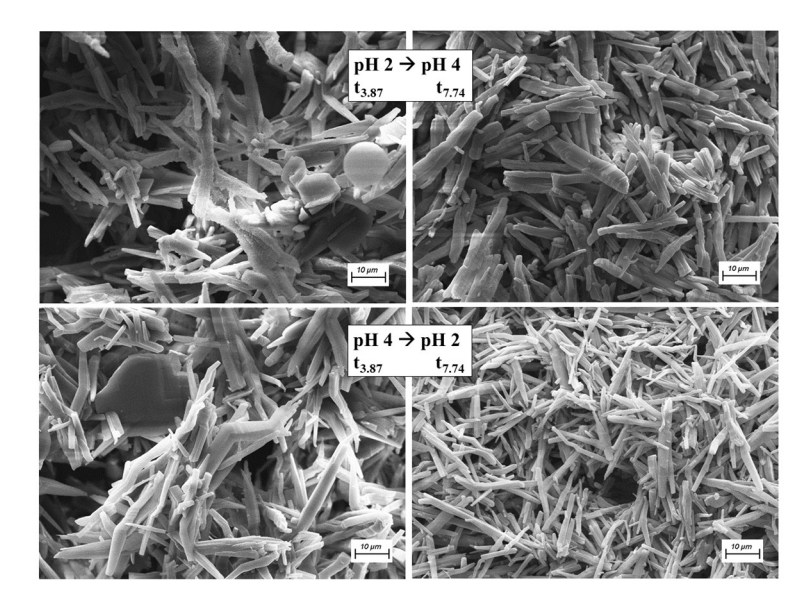


Figure 8-16 SEM images of TA from for PET/PE reactant after precipitation with sulfuric acid at 80 °C, after pH variation,  $t_{3.87}$  (left) and  $t_{7.74}$  (right).

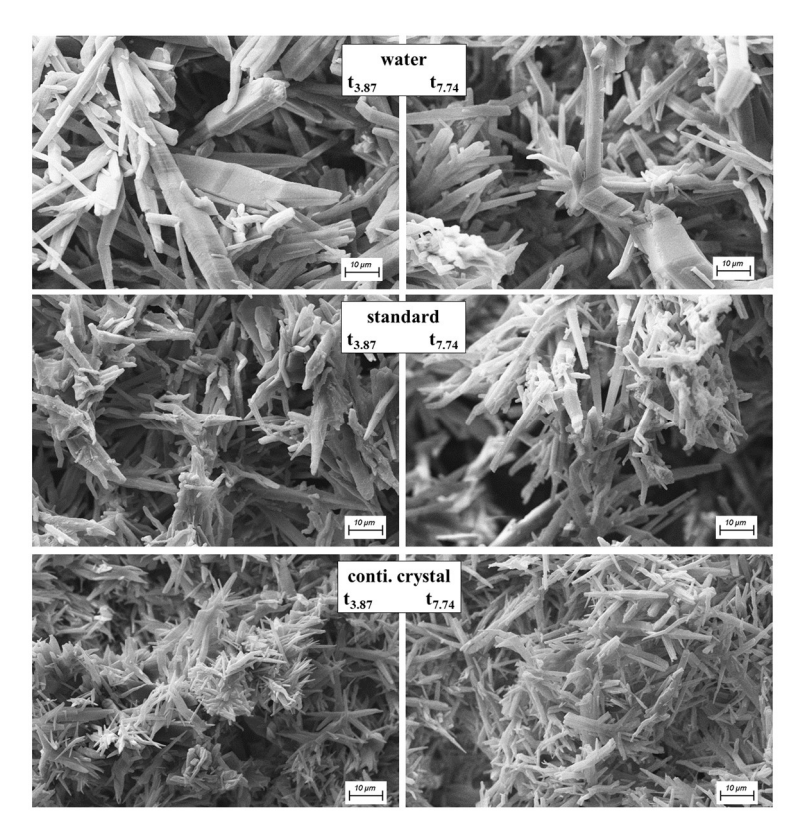


Figure 8-17 SEM images of TA from for PET/PE reactant after precipitation at pH 3.5 with sulfuric acid at 80 °C, start-up variation,  $t_{3.87}$  (left) and  $t_{7.74}$  (right).

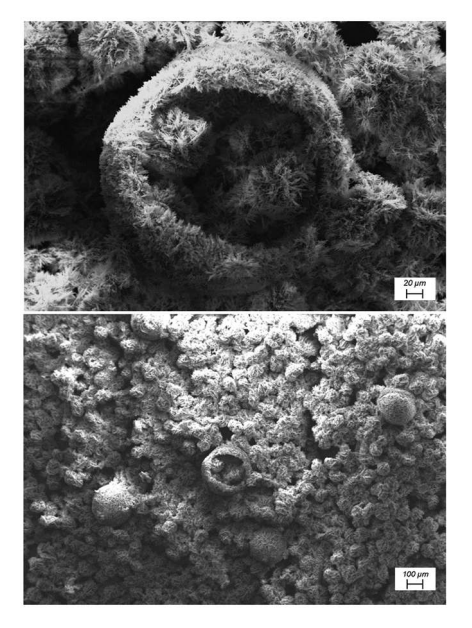


Figure 8-18 SEM images of TA aggregate inside, after precipitation with sulfuric acid at 80 °C, pH 3.5.

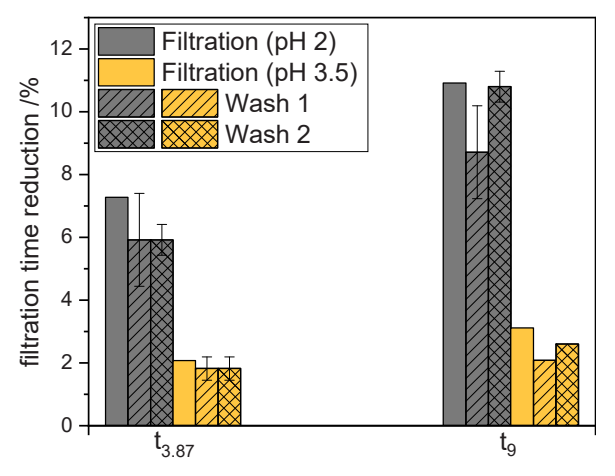


Figure 8-19 Filtration time reduction (Equation 6-1) after precipitation with sulfuric acid at 80 °C, pH 2 and pH 3.5 (with rounded morphology).

# 8.4.3 Precipitation Concept

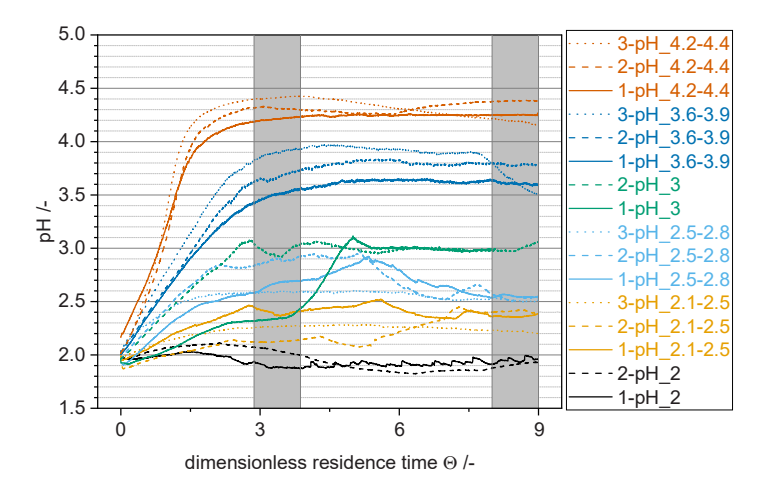


Figure 8-20 pH courses over dimensionless residence time for precipitation with sulfuric acid at 80 °C with pH variation, grey bars represent duration of "one dimensionless residence time" for calculation of pH average.

$$m_{TA0} = m_{TA1} + m_{TA2} 8-1$$

$$m_{TA0} \cdot IA_0 = m_{TA1} \cdot IA_1 + m_{TA2} \cdot IA_2$$
 8-2

$$IA_{residue} = 0.35 \dots 0.45 \cdot IA_0$$
 8-3

$$m_{TA1} = yield \cdot m_{TA0}$$
  
 $m_{TA2} = (1 - yield) \cdot m_{TA0}$  8-4

# Appendix

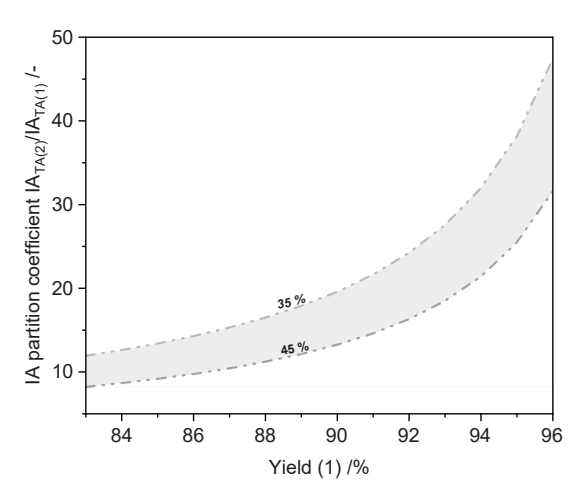


Figure 8-21 Partition coefficient of IA content between TA(1) and TA(2) over yield of the first precipitation step.

## List of Publications

### **Publications**

Müller, Clemens; Heck, Carina A.; Stephan, Luca; Paschetag, Mandy; Scholl, Stephan (2023): Precipitation of Terephthalic Acid from Alkaline Solution: Influence of Temperature and Precipitation Acid. Ind. Eng. Chem. Res 62(30), Article: acs.iecr.2c04451, S. 12029–12040,

DOI: 10.1021/acs.jecr.2c04451.

Müller, Clemens; Franke-Hameke, Dirk W.; Brepohl, Esther; Biermann, Lars; Eichert, Carsten; Scholl, Stephan (2024): Precipitation of Terephthalic Acid from post-consumer polyethylene terephthalate waste fractions. Green Processing and Synthesis. 14(1), pp. 20230244, DOI: /10.1515/gps-2023-0244

### Patents

Patent WO 2022/033735 A1, Process for the preparation of a mixture of recycled terephthalic acid and isophthalic acid, Inventors: Biermann, Lars; Brepohl, Esther; Eichert, Carsten; Müller, Clemens; Salikov, Vitalij; Scholl, Stephan, Assignee: RITTEC Umwelttechnik GmbH

Patent DE 10 2021 105 970 A1, Process for the recovery of aromatic dicarboxylic acids from their metal salts. Inventors: Biermann, Lars; Brepohl, Esther; Eichert, Carsten; Müller, Clemens; Scholl, Stephan: Assignee: Rittec Umwelttechnik GmbH

Patent DE 10 2023 134 489.7 (pending), Process for obtaining aromatic dicarboxylic acids, Inventors: Eichert, Carsten; Müller, Clemens; Scholl, Stephan; Assignee: Rittec 8.0 Umwelttechnik GmbH

# Conference Contributions

Müller, C., Heck, C., Eichert, C., Scholl, S.: Precipitation of terephthalic acid after alkaline hydrolysis of polyethylene terephthalate (PET), Annual Meeting of DECHEMA-Specialist group on Crystallisation, Online, 17.03.-19.03.2021 (Poster)

Müller, C., Franke-Hameke, D., Eichert, C., Scholl, S.: Terephthalic acid precipitation from real polyethylene terephthalate (PET) waste, Annual Meeting of DECHEMA-Specialist group on Crystallisation, Dortmund, Germany, 16.03.-18.03.2022 (Talk)

**Müller, C., Biermann, M., Eichert, C., Scholl, S.:** Continuous precipitation of terephthalic acid from real polyethylene terephthalate (PET) waste, Annual Meeting of DECHEMA-Specialist group on Crystallisation, Frankfurt am Main, Germany, 09.03.-10.03.2023 (Talk)

Müller, C., Biermann, M., Eichert, C., Scholl, S.: Continuous precipitation of terephthalic acid from real polyethylene terephthalate (PET) waste, International Symposium on Industrial Crystallization (ISIC), Glasgow, United Kingdom, 05.09.-08.09.2023 (Talk)

## Student contributions

Final theses and student research projects

**Heck, Carina A.:** *Investigations on the Reactive Precipitation of Terephthalic Acid*, Master Thesis, Technische Universität Braunschweig, 2019.

**Schulze, Luisa.:** Recrystallization of precipitated Terephthalic Acid under elevated Temperature and Pressure, Bachelor Thesis, Technische Universität Braunschweig, 2019.

**Franke-Hameke, Dirk W.:** Investigations on the Recovery of Terephthalic Acid from depolymerized PET, Bachelor Thesis, Technische Universität Braunschweig, 2020.

**Nguyen, Thi Y. T.:** Analysis and Evaluation of Production Processes of crude-oil-based purified Terephthalic Acid, Student Research Project, Technische Universität Braunschweig, 2020.

Alijanzadeh, Roshan A.: Determination of comparative Data of Terephthalic Acid Production Processes for Life Cycle Assessment by flow chart simulation, Student Research Project, Technische Universität Braunschweig, 2020.

#### Student contributions

**Biermann, Michelle:** Investigations on the Continuous Crystallization of Terephthalic Acid, Master Thesis, Technische Universität Braunschweig, 2021.

**Müller, Moritz:** Investigations on the Recrystallization of Terephthalic Acid from a chemical Recycling Process of Polyethylene Terephthalate, Master Thesis, Technische Universität Braunschweig, 2021.

**Gottwald, Saskia E.:** Optimization of the Continuous Crystallization of Terephthalic Acid for a PET Recycling Process, Student Research Project, Technische Universität Braunschweig, 2021.

**Schneemann, Henrik:** Extended Investigations into the Continuous Crystallization of Terephthalic Acid for a PET-Recycling Process, Bachelor Thesis, Technische Universität Braunschweig, 2022.

Marcic, Fabian: Influence of Seed Crystals in the Continuous Crystallization of Terephthalic Acid, Student Research Project, Technische Universität Braunschweig, 2022.

**Jansen, Yunis:** Parameter Optimization for the Continuous Crystallization of Terephthalic acid in a Back-to-Monomer Recycling Process for PET, Bachelor Thesis Technische Universität Braunschweig, 2023.

Wilkening, Marius: Flash Crystallization of Terephthalic Acid from a Back-to-Monomer Recycling Process for PET, Bachelor Thesis, Technische Universität Braunschweig, 2023.

### Student Research Assistants

**Biermann, Michelle:** Batch precipitation on model reactants, general analytical and preparatory tasks, support of research projects, 2018-2020.

**Stephan, Luca:** Batch and continuous precipitation on model and PET reactants, Recrystallization experiments, general analytical and preparatory tasks, Data analysis and programming, development and validation of analytical procedures, support of research projects, 2020-2024.

Franke-Hameke, Dirk W: Batch precipitation experiments on real PET

### Student contributions

reactants and analysis, support of research projects, 2020-2021.

Klinke, Tim: Support of research projects, 2022.

**Tiedemann, Jonte:** Batch precipitation experiments on real PET reactants and analysis, pressure precipitation experiments, general support of tasks in research projects, 2022.

**Jansen, Yunis:** Batch and continuous precipitation experiments on real PET reactants and analysis, general support of tasks in research projects, 2022-2023.

**Wilkening, Marius:** Batch precipitation experiments on real PET reactants and analysis, recrystallization experiments, general support of tasks in research projects, *2022-2023*.